ACS NANO

www.acsnano.org

REVIEW

Impact of Surface Enhanced Raman Spectroscopy in Catalysis

Andrei Stefancu, Javier Aizpurua, Ivano Alessandri, Ilko Bald, Jeremy J. Baumberg, Lucas V. Besteiro, Phillip Christopher, Miguel Correa-Duarte, Bart de Nijs, Angela Demetriadou, Renee R. Frontiera, Tomohiro Fukushima, Naomi J. Halas, Prashant K. Jain, Zee Hwan Kim, Dmitry Kurouski, Holger Lange, Jian-Feng Li, Luis M. Liz-Marzán, Ivan T. Lucas, Alfred J. Meixner, Kei Murakoshi, Peter Nordlander, William J. Peveler, Raul Quesada-Cabrera, Emilie Ringe, George C. Schatz, Sebastian Schlücker, Zachary D. Schultz, Emily Xi Tan, Zhong-Qun Tian, Lingzhi Wang, Bert M. Weckhuysen, Wei Xie, Xing Yi Ling, Jinlong Zhang, Zhigang Zhao, Ru-Yu Zhou, and Emiliano Cortés*

Cite This: https://doi.org/10.1021/acsnano.4c06192

Read Online

ACCESS | Metrics & More | Article Recommendations

ABSTRACT: **Catalysis stands as an indispensable cornerstone of modern society, underpinning the production of over 80% of manufactured goods and driving over 90% of industrial chemical processes. As the demand for more efficient and sustainable processes grows, better catalysts are needed. Understanding the working principles of catalysts is key, and over the last 50 years, surface-enhanced Raman Spectroscopy (SERS) has become essential. Discovered in 1974, SERS has evolved into a mature and powerful analytical tool, transforming the way in which we detect molecules across disciplines. In catalysis, SERS has enabled insights into dynamic surface phenomena, facilitating the monitoring of the catalyst structure, adsorbate interactions, and reaction kinetics at very high spatial and temporal resolutions. This review explores the achievements as well as the future potential of SERS in the field of catalysis and energy conversion, thereby highlighting its role in advancing these critical areas of research.**

KEYWORDS: *Surface Enhanced Raman Scattering, SERS, Electrocatalysis, Photocatalysis, Thermocatalysis, Plasmonic Catalysis, Energy Conversion, Energy Storage*

1. INTRODUCTION

Marking its 50th anniversary since its discovery in 1974,[1] Surface-enhanced Raman spectroscopy (SERS) has emerged as a powerful analytical method for understanding natural phenomena at the metal-molecule interface but has also found applications in various aspects of life and materials sciences.[2−8] Initially observed as an enhancement phenomenon in which Raman scattering occurred from molecules adsorbed onto roughened metal electrodes, SERS has evolved significantly over the past few decades. The early 2000s saw the development of nanostructured substrates, such as colloidal nanoparticles and lithographically nanostructured surfaces, leading to a large enhancement in Raman signal intensities. This breakthrough facilitated applications across diverse disciplines, ranging from life sciences to natural sciences including materials science.

In chemistry, SERS enabled molecular detection, enabling ultrasensitive analysis of trace substances, and facilitating the study of molecular structures and interactions at surfaces.[9] In biology, SERS found utility in label-free detection of biomolecules, aiding in diagnostics,[10,11] drug discovery, and

Received: May 10, 2024
Revised: September 18, 2024
Accepted: September 20, 2024

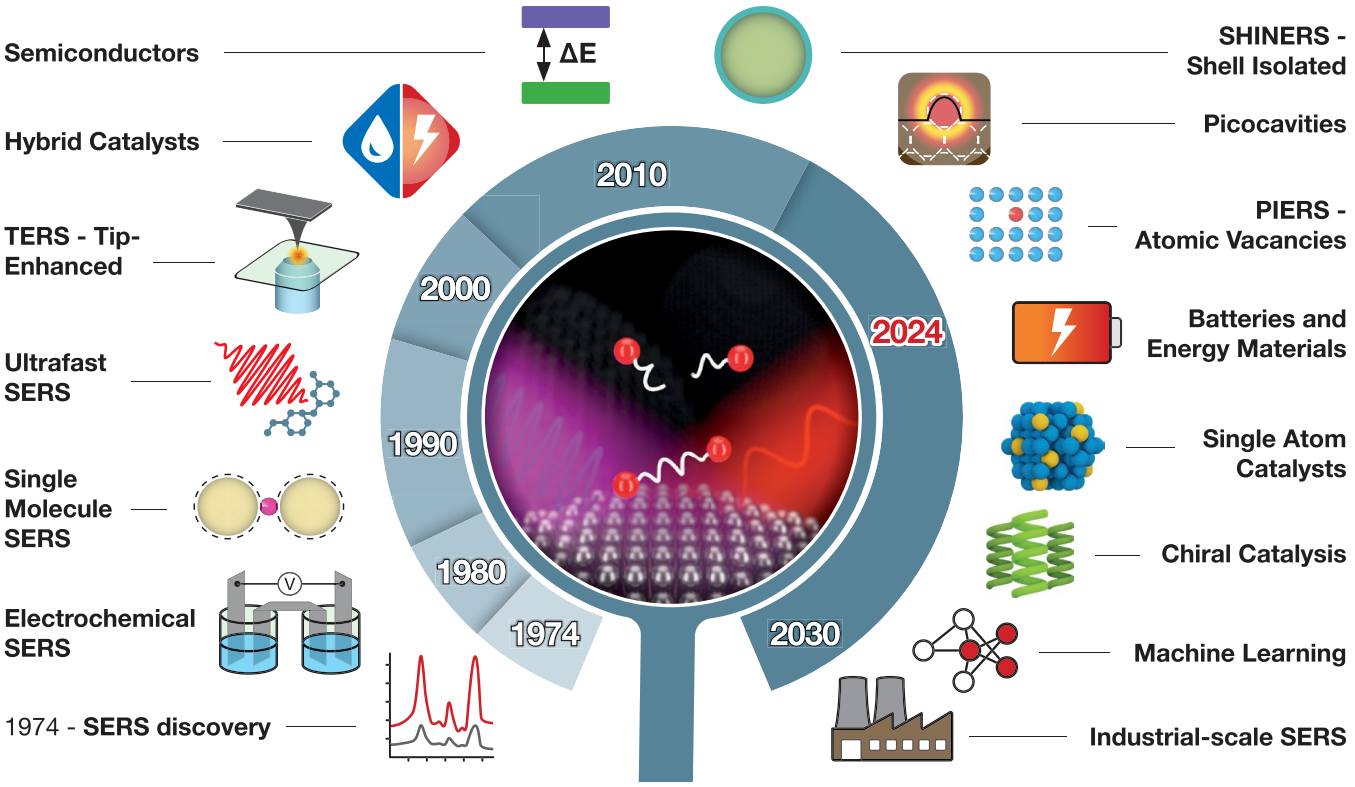

Figure 1. Progress of surface-enhanced Raman spectroscopy for monitoring catalytic processes. Since the discovery of SERS in 1974, numerous important techniques and materials have been developed for its application in catalysis. Notably, the past 20 years have witnessed rapid advancements in the field, with many emerging areas and topics promising further advancements in the integration of SERS for real-time monitoring of energy conversion processes. In this Figure, we summarize a selection of the most important milestones and developments of SERS in the field of catalysis over the last 50 years.

understanding cellular processes. In physics, SERS provided insights into plasmonics and nanophotonics, enhancing our understanding of light-matter interactions on the nanoscale. Across applications, SERS sensing has been demonstrated for a wide variety of analytes, including pollutants, toxins, and drugs, with high sensitivity and specificity. It also has advanced drug delivery systems by characterizing nanocarriers and monitoring drug release kinetics. Moreover, in energy research, SERS has contributed to the development of efficient photovoltaic devices and photocatalysts for energy conversion processes. Overall, SERS continues to drive many scientific and technological innovations across disciplines, offering high capabilities for molecular analysis—including single-molecule and single-particle detection - and related surface characterization.

While numerous comprehensive and outstanding reviews[12−14] delve into the fundamentals of SERS and its application across various fields,[15−20] this focus review article concentrates on the distinctive and significant opportunities that SERS presents to the field of catalysis and energy conversion (Figure 1). Catalysts are ubiquitous in today's society, being involved in the production of over 80% of all manufactured products and over 90% of all industrial chemical products.[21] Catalysts are also key in transitioning toward a more sustainable and circular chemistry because they minimize waste production and maximize the selective transformation of feedstock molecules into the fuels, chemicals, and materials of the future, thereby reducing the energy and material demands, as well as the burden on the environment.[22−25]

Notwithstanding, big gaps remain in our understanding of the working principles of catalysts, especially when they are studied in their real working environment. Today it is widely recognized that the structure and composition of heterogeneous catalysts is not fixed, but changes dynamically *during* a chemical reaction, influencing the overall activity, selectivity and stability of the catalyst.[26,27] At the nanometer scale, the catalytic activity is influenced by a plethora of dynamic phenomena such as molecular adsorption/desorption, surface reconstruction, alloying-dealloying processes, as well as active surface poisoning and activation.[28−32] Many efforts have been made to tackle these challenges, by taking "snapshots" of catalysts in situ and operando, much like a high-speed camera captures a fast transient event.[33−35] For example, X-ray absorption spectroscopy (XAS), small-angle X-ray scattering (SAXS) or X-ray absorption near edge spectroscopy (XANES) can capture under operando conditions the electronic, compositional and structural properties of solid catalysts, but they usually require synchrotron radiation to achieve a sufficiently high time and spatial resolution.[36,37] Likewise, electron microscopy can uncover the structural features that drive for example the efficient energy conversion of catalyst materials.[38−40] On the other hand, spectroscopies making use of visible or infrared light, such as Raman or IR spectroscopy offer a high molecular specificity and can identify with high spatial and temporal resolution the adsorbed species, interadsorbate interactions, local environment, or metal oxide species.[41,42] Different methods to couple these experimental techniques, including optical methods (e.g., UV−vis, fluorescence, and luminescence spectroscopy), X-ray absorption techniques, such as X-ray absorption spectroscopy (XAS)) and X-ray diffraction and scattering methods (X-ray diffraction (XRD), small-angle X-ray

https://doi.org/10.1021/acsnano.4c06192
ACS Nano XXXX, XXX, XXX−XXX

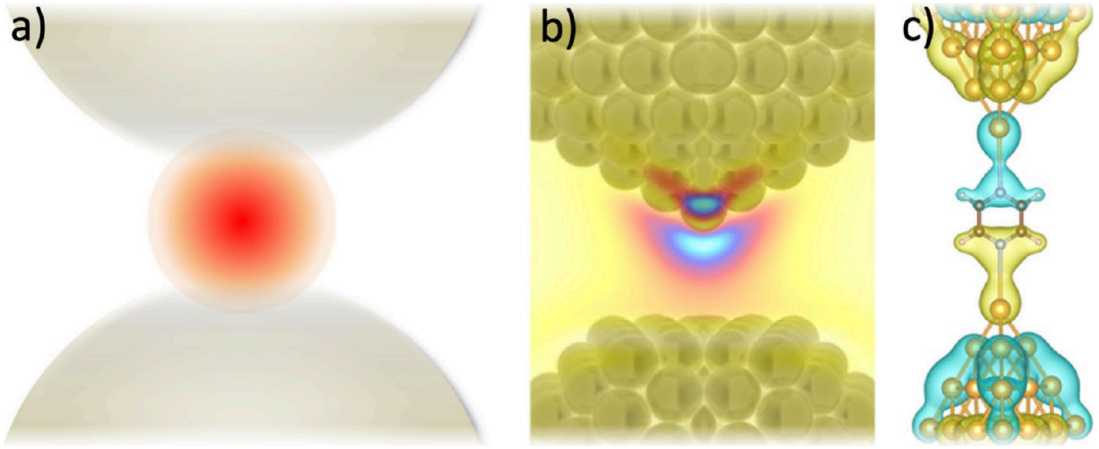

Figure 2. Computational modeling of plasmonic nanocavities and molecules. a) Two metallic nanostructures at close proximity form a strong field enhancement in the gap between them. b) A picocavity made of a single atomic protrusion from one of the metallic nanostructures leads to stronger and spatially inhomogeneous field enhancement. c) The molecular orbitals of a molecule within a plasmonic gap.

scattering (SAXS), and wide-angle X-ray scattering (XAXS), have been implemented to gain an exhaustive and often very detailed view of catalysts under operando conditions.[36]

In this context, the benefits of SERS in the various fields of catalysis, such as thermal, photocatalysis, electrocatalysis, and photoelectro catalysis cannot be understated. After all, in the original SERS paper, Raman spectroscopy was used to monitor the structure of the electrical double layer on Ag electrodes and adsorbate−adsorbate interactions.[3] For SERS, subwavelength metal nanoparticles (NPs) are employed, which focus light below the diffraction limit due to the collective oscillations of their free electrons, a process called localized surface plasmon resonance (LSPR). Consequently, the generated high local electro-magnetic (EM) fields enhance the inelastically Raman scattered light by factors of $\sim 10^6$ or more. This level of sensitivity makes it possible to detect reagents, reaction intermediates and products, with high molecular specificity and with subsecond time resolution.[30,43] Even monitoring a chemical reaction at the single molecule level has been possible in specific cases due to the capabilities of SERS.[44] Since the LSPR is a surface-confined effect, SERS signals decrease sharply as the distance between the molecule and the surface of the NPs increases, scaling generally with r^{-12} for a single NP. As a result, the acquired molecular and chemical information has a high spatial localization. Furthermore, SERS peaks in the low wavenumber region allow the monitoring of dynamical adsorbate−metal catalyst bonding and the transient formation of surface metal oxide species.[30,41] These features of SERS have facilitated, for example, tracking atomic defects and their impact in catalysis.[45] A further advantage of SERS over other in situ or in operando spectroscopies, which often goes unmentioned, is its adaptability and accessibility. X-ray spectroscopies often require high brilliance sources (such as synchrotron radiation sources) for which there is competition for measurement time through beamline applications. On the other hand, SERS requires relatively simple experimental equipment that can be easily adapted to fit different catalytic reactors. Recent developments in the synthesis of metal nanomaterials with chiral geometries and enhanced optical activity can yield selective detection of intermediates in asymmetric catalysis, by either using SERS or its derivative surface-enhanced Raman optical activity (SEROA).[46]

In this Focus Review, we offer an overview of both past accomplishments and prospects regarding the utilization of SERS as an analytical tool to advance our understanding across various domains related to energy conversion, extending beyond the field of classical heterogeneous catalysis (see Figure 1). Encompassing a spectrum of length scales, from atomic to single-molecule levels, as well as ensembles and devices, we focus on the analysis of kinetics, thermodynamics, and current SERS advancements toward examining chemical reactivity and the dynamics and functionality of energy conversion materials, thereby not being limited to the fields of thermal, electro-catalysis, photocatalysis, and photoelectro catalysis. Hence, we explore in the last section of this Review the potential of emerging scientifical and technological innovations in the fields of machine learning, chiral catalysis, batteries, and other energy-related aspects to advance significantly with the help of SERS. We anticipate that this comprehensive exploration will act as a true "catalyst" itself for the emergence of applications and discoveries in SERS within the wide field of energy conversion, thereby spurring the necessary discoveries to make our daily life operations more sustainable and circular. Moreover, we do hope that scientists currently less familiar with the SERS method will feel encouraged to make use of its wide variety of possibilities, thereby exploring science and technologies in the broad field of catalysis and energy conversion.

2. THEORETICAL MODELING OF PLASMONS, SERS, AND CATALYTIC REACTIONS

Although metallic surfaces generate strong evanescent fields at metal-dielectric interfaces (Figure 2a), which amplify the Raman signal of molecules, plasmonic nanoantennas can further significantly boost the electromagnetic field enhancement. Such plasmonic nanoantennas, particularly those with nanosized gaps, enable the detection of SERS signals, even from single molecules. Plasmonic nanoantennas, particularly those with nanosized gaps, significantly boost electromagnetic field enhancement, enabling the detection of SERS signals,[18] even from single molecules.[19,47,48] As an example, picocavities, made from single gold atoms protruding in a plasmonic gap (see Figure 2b), produce inhomogeneous fields and can probe specific molecular bonds within a single molecule.[49] The applications of picocavities in SERS and catalysis are highlighted in Section 3 of the review. The field enhancement of such

https://doi.org/10.1021/acsnano.4c06192
ACS Nano XXXX, XXX, XXX−XXX

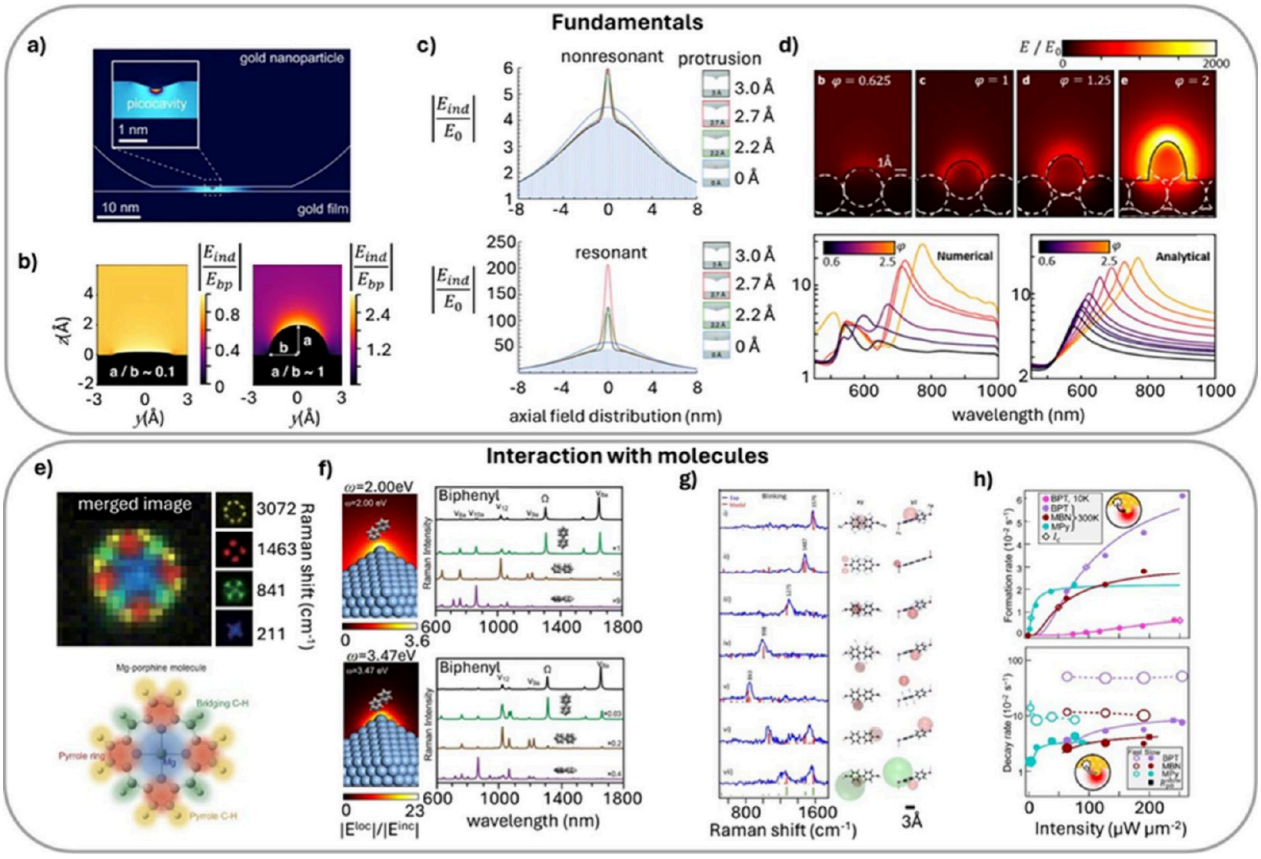

Figure 3. Optical properties of picocavities. a) Atomic protrusions inside plasmonic nanogaps provide subnanometric field localization (picocavities), enabling single molecule sensing. Figure adapted with permission from ref 49. Copyright 2016 American Association for the Advancement of Science. b) Atomic scale features provide lightning rod effects which act as a field multiplier with possible mode volumes below 1 nm. Figure adapted with permission under a Creative Commons CC BY-NC license from ref 72. Copyright 2018 American Chemical Society. c) Such small features possess resonances based on the aspect ratio of the protrusion. Figure adapted with permission from ref 73. Copyright 2017 Royal Society of Chemistry. d) Griffiths et al. demonstrated the resulting significant wavelength dependence of picocavities. Figure adapted with permission from ref 75. Copyright 2021 American Chemical Society. e) Hyper resolved single molecule mapping using "scanning Raman picoscopy". Figure adapted with permission under a Creative Commons CC BY license from ref 83. Copyright 2019 National Academy of Science. f) The submolecular scale fields from picocavities drop rapidly with distance and, as a result, SERS signals depend highly on the position and orientation of nearby molecules probed. Figure adapted with permission under a Creative Commons CC BY-NC license from ref 85. Copyright 2021 Wiley. g) Example of the strong dependence observed in vibrational spectra on the adatom position with respect to the molecule in nanocavities. Figure adapted with permission from ref 86. Copyright 2018 American Chemical Society. h) Systematic investigation of the formation and destruction rates show that the energy barrier can be optically suppressed and is highly dependent on molecular functional tip. Figure adapted with permission under a Creative Commons CC BY-NC license from ref 87. Copyright 2022 American Association for the Advancement of Science.

nanogaps is typically calculated using classical numerical methods that solve Maxwell's equations, where typically metals have a local linear response and sharp boundaries.

However, small plasmonic nanogaps deviate from the classical picture. For example, electrons can spill out of the metal boundary by ∼0.5−1 nm, creating a "fuzzy" boundary, and plasmonic nonlocality emerges due to the electron Coulomb repulsion.[50] For the precise understanding and modeling of these nonclassical effects, first-principles calculations based on time-dependent density functional theory (TDDFT) have been employed (Figure 2c), including both jellium and ab initio atomistic descriptions. Although jellium descriptions are well suited to address the optical response of the free electron gas in the metals (usually Na and Al), ab initio atomistic descriptions further address the strong influence of d-electrons for Au and Ag.[51] First-principles calculations are computationally expensive and are therefore limited to nanostructures of a few tenths of a nanometer. Hence, various methods have been developed to capture behavior derived from the quantum nature of the electrons in the bulk and at interfaces, namely, (i) dynamical screening, (ii) electron spill-out, (iii) Landau damping, and (iv) atomistic effects. These approaches include early hydrodynamical descriptions,[52,53] more advanced generalized nonlocal optical response (GNOR) models,[54] and quantum hydrodynamic descriptions.[55] A notable example is the surface response formalism,[56] which incorporates quantum surface-response corrections in classical Maxwell's equations, through the effective Feibelman parameters. These capture the position of the charge centroid and its surface damping for a given metal-dielectric interface at each excitation energy. Other effective methods bring together quantum mechanical and classical descriptions to model the electron spill-out and tunnelling across a plasmonic gap.[57] All these methods bring quantum mechanical information into classical plasmonic calculations, using empirical elements, and show that the quantum nature of electrons in metals tends to reduce the field enhancement in

https://doi.org/10.1021/acsnano.4c06192
ACS Nano XXXX, XXX, XXX−XXX

plasmonic gaps, without significantly distorting the spatial profile of the field enhancement.[58]

Despite these complexities, molecules placed in plasmonic nanogaps experience extreme field enhancement, thereby amplifying their Raman signal and allowing for low concentration analyte detection, even reaching the single molecule limit.[59] The Raman signal enhancement near a metallic interface of physisorbed molecular species is related to the product of the intensities of the local field enhancements at the incident wavelength and the outgoing wavelength (Stokes or anti-Stokes). Frequently, this product neglects the difference between incoming and outgoing wavelengths and approximates the enhancement factor as the fourth power of the local field. This local field factor can be as high as several orders of magnitude (up to ~1000) in extreme plasmonic gaps. On the other hand, chemical binding with a metallic surface involves electron and orbital sharing with gold atoms, altering the molecule's Raman signal with usually new Raman vibrational modes emerging, compared to the same molecule in solution or in vacuum. Additionally, the inhomogeneous illumination of the molecule from an evanescent plasmonic field, and in particular from pico-cavities, can also lead to the emergence of new Raman lines, due to the influence of the surface selection rules.[49]

The Raman tensor of a molecule provides basic information about its vibrational fingerprints. This tensor can be calculated with TDDFT, which considers the atomistic structure of the molecule and its electronic structure. To consider the molecule's Raman tensor, i.e. the chemical effects arising from binding to the metal interface, one can attach several metal atoms (typically gold or silver) to the TDDFT modeling of the molecule.[60] Small silver clusters of just 20 atoms also provide a realistic description of plasmonic states that extrapolates smoothly with cluster size for the electrodynamic behavior of 20 nm nanoparticles.[61] Resonance Raman calculations at the plasmon frequency of such clusters can be used to generate SERS enhancements in adsorbed molecules that include both electromagnetic and chemical enhancements. The Raman tensor (with or without metal binding) of a molecule, together with the effective mode volume of the nanocavity, are key elements in the description of surface-enhanced Raman scattering as an optomechanical process,[62,63] which allows for addressing nonlinear Raman signals under sufficiently strong illumination.[64]

In principle, one can use the molecule's SERS signal to track photocatalytic reactions. The theoretical description of plasmon-driven photocatalysis has primarily been provided using electronic structure methods applied to structures that include a metal particle or surface interacting with the reacting molecules. A key consideration is the alignment between the Fermi energy of the metal and energy levels in the molecules leading to dissociation (or other reactions) after electron transfer because this determines which plasmon excitation energies will promote reaction.[65] Another approach has involved the use of real-time TDDFT or tight-binding (DFTB) calculations to directly simulate plasmon excitation leading to electron transfer and reaction in a system consisting of a metal cluster with hundreds of atoms plus one or many adsorbed molecules.[66] This approach has recently been adapted to calculate SERS spectra,[67] which means that the same method can be used for both SERS and photocatalysis.

Of particular interest is the determination of Raman spectra for transient intermediates in time-resolved photocatalysis experiments. Ideally this would involve measurements using SE-FSRS (surface enhanced femtosecond stimulated Raman scattering)[68] where subpicosecond time-resolved observations are accessible. The electrodynamic theory of SE-FSRS has been developed,[69] but so far no experimental results have been reported.

3. FUNDAMENTALS OF PICOCAVITIES AND THEIR INTERACTION WITH MOLECULES

SERS substrates are composed of nanostructured metals that give rise to highly localized plasmonic hot-spots. Since SERS signal strengths scale favorably with field enhancements (approximately as $|E|^4$),[70] significant contributions to SERS spectra arise from these small regions. This can lead to poor reproducibility in signal intensity but also enables few or single molecule sensing, even in ensembles of molecules, where otherwise their dynamics would be averaged out. As already pointed out in the previous Section, the most extreme examples of these regions are atomic scale protrusions in metal surfaces (adatoms).[71] The protrusions generate subnanometric hotspots termed picocavities,[49,72,73] which can provide additional field enhancements up to $|E^2| \approx 10^2$ on top of the preexisting field confinement (Figure 3a).[49,72,74] The enhancements consist of a broad nonresonant contribution (arising from "lightning rod" effects, Figure 3b,c), and a strong resonant contribution (dependent on aspect ratio, Figure 3c,d).[72,74,75] An analytical description within classical electromagnetism of these optical properties has been introduced[74] (Figure 3d), which agrees with quantum-corrected and ab initio models reasonably faithfully.[76,77] Such atomic features are also credited with facilitating hyper-resolved single molecule mapping in scanning tunneling microscopy,[73,78−80] and tip-enhanced Raman scattering (TERS), covered in Section 5 of the review, which enables single molecule investigations (Figure 3e).[81−83] The submolecular size of these mode volumes means the orientation and position of nearby molecules greatly influence the vibrational spectra in SERS measurements, and the strong field gradients even allow otherwise Raman inactive modes to become predominant (Figure 3f,g).[49,84,85]

In plasmonic nanogaps (e.g., such as that of the "nanoparticle-on-mirror", NPoM[88]) containing molecular monolayers with widths <5 nm and thus very strong initial field enhancements, picocavity formation is identified by the stochastic appearance of transient but intense lines in the SERS spectrum.[49,89] These can coincide with existing lines but also appear at new vibrational energies, either as a result of shifts in energy arising from interactions with the adatom or from Raman inactive/weak modes now probed by the picocavity. The energy and strength of these new Raman lines are highly dependent on the relative position of the adatom with respect to the molecule (Figure 3g).[49,84,86] Using analyte molecules with distinct functional groups on each end allows identification of the adatom approach direction. For BPT-CN (4′-mercapto-[1,1′-biphenyl]-4-carbonitrile) as the spacer molecule the adatom is found to originate from the thiolated side in 80% of instances, and indicates a strong influence from the local chemistry.[90] Monitoring the picocavity formation rates at varying laser powers and for different spacer molecules, Lin and Hu et al. showed that energy barriers for formation and destruction of picocavities are optically suppressed, and dependent on the molecular spacer functional groups (Figure 3h).[87] Combining this method with large picocavity data sets (isolated through machine learning) allows for estimates of relative adatom positions (with respect to the molecule), and reveals how an atomic monolayer of Pd can suppress picocavity formation on either side.[91]

https://doi.org/10.1021/acsnano.4c06192
ACS Nano XXXX, XXX, XXX−XXX

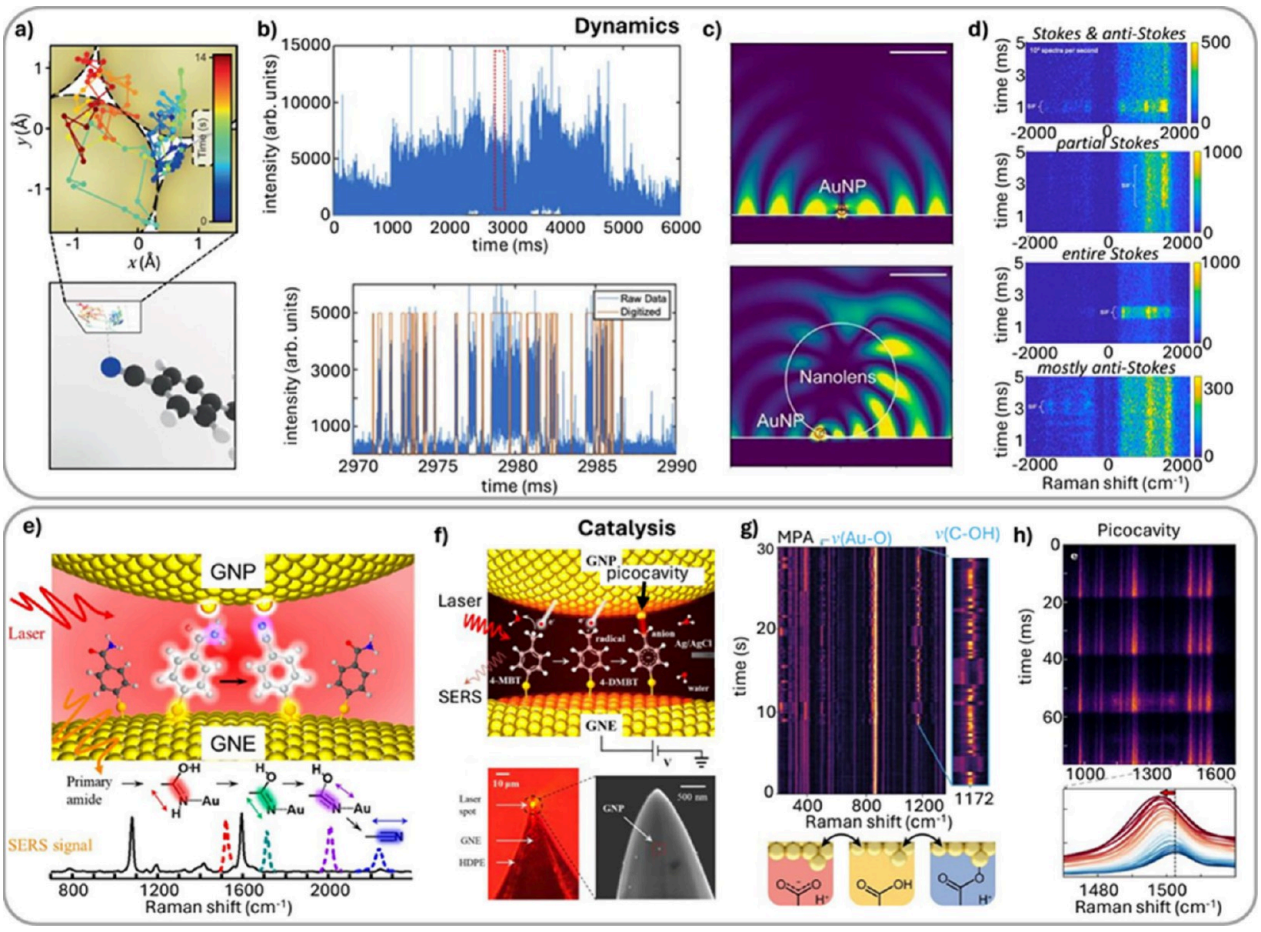

Figure 4. Picocavity dynamics and catalysis. a) Using picocavity spectra and density functional theory (DFT) modeling, the combined motion of molecules and adatoms can be reconstructed. Figure adapted with permission under a Creative Commons CC BY-NC license from ref 89. Copyright 2021, Springer Nature. b) High-speed measurements reveal fast dynamics with the fastest intensity fluctuations attributed to molecule-in-hotspot effects and "slower" (>10 μs) processes to surface atom movements. Figure adapted with permission from ref 97. Copyright 2023 American Chemical Society. c) Using nanolenses on NPoM geometries allows for μs regime spectra to be collected, revealing strong shifts in picocavity SERS peaks. Figure adapted with permission from ref 99. Copyright 2020 National Academy of Science. d) Schmidt et al. showed fast SERS intensity fluctuations that exhibit either: both Stokes and anti-Stokes, partial Stokes, entire Stokes, or mostly anti-Stokes intensity fluctuations. Figure adapted with permission from ref 100. Copyright 2023 American Chemical Society. e) Picocavity-assisted dehydrogenation of primary amide. Figure adapted with permission from ref 101. Copyright 2022 American Chemical Society. f) Dehydrogenation of aromatic methyl groups using picocavities. Figure adapted with permission under a Creative Commons CC BY license from ref 102. Copyright 2023 Royal Society of Chemistry. g) Tracking single carboxylic acid functional group (de)protonation and interfacial binding dynamics. Figure adapted with permission under a Creative Commons CC BY-NC license from ref 103. Copyright 2021 American Association for the Advancement of Science. h) Weakening of molecular bonds in intense optical fields of picocavities. Figure adapted with permission under a Creative Commons CC BY-NC license from ref 104. Copyright 2023 Springer Nature.

In the results above, picocavity formation is enhanced by light illumination but only stochastically. Thus, there is interest in reproducibly creating them on demand. There are also chemical routes toward forming adatoms using, e.g., N-heterocyclic carbenes (NHCs).[92] These compounds form complex bonds with a single metal atom, pulling them from a smooth surface.[93] SERS experiments on "NHC roughened" nanoparticles show strong signal modulation with orientation of the NHC controlled through the ligands.[94] It will be of interest to compare how these adatoms behave in carefully constructed nanogaps (such as NPoMs) and how their properties compare to those of optically induced picocavities. Other interesting routes toward possible picocavity formation and stabilization might come though electromigration, as this too can control the migration of metal atoms at the interface.[95] A more detailed chemical intuition toward the explanation of these combined observations is provided by Kim et al.[96]

Atomic-Scale Dynamics of Picocavities. The intense local fields around adatoms can promote charging, diffusion, conformational changes, and photo/electro-chemistry of the neighboring molecules.[97,98] These changes give rise to the observed shifts and intensity fluctuations in the associated picocavity lines and can be used to reveal how molecules interact with the metal surface. For example, Griffiths et al. showed that, by comparing shifts in picocavity peaks with extensive DFT modeling, a 3D reconstruction can be made of how BPT-CN interacts with an adatom, at 0.1 s temporal resolution (Figure 4a).[89] However, subsequent studies showed that much faster dynamics also occur in the picocavity and on the nanoparticle surface, meaning high-speed acquisition is required for full characterization of the dynamics (Figure 4b).[97−100] Although it remains challenging to pinpoint the origin of specific spectral fluctuations, by comparing dry and aqueous hotspots, Lindquist et al. were able to assign highest-speed fluctuations (<10 μs) to

https://doi.org/10.1021/acsnano.4c06192
ACS Nano XXXX, XXX, XXX−XXX

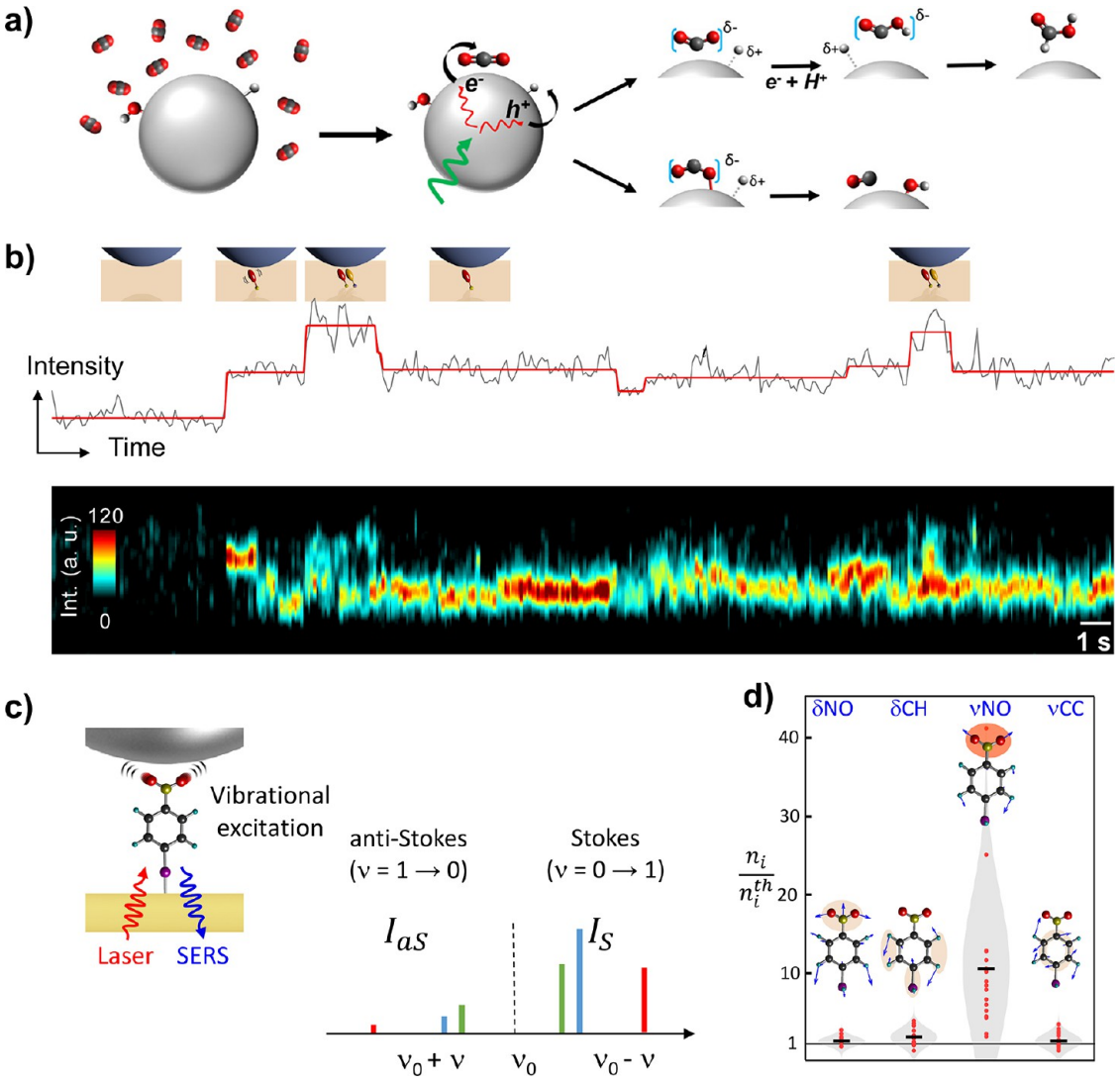

Figure 5. Monitoring single-molecule reaction events and vibrational activation by surface-enhanced Raman scattering. a) Proposed pathway for CO_2 photoreduction on Ag nanoparticles under plasmonic excitation as deduced from SM-SERS probing. C, O, and H atoms are colored gray, red, and white, respectively. Adapted with permission from ref 113. Copyright 2018 American Chemical Society. b) SM-SERS trajectory of 4,4′-dimercapto-azobenzene (DMAB) product from 4-nitrobenzenethiol, showing discrete single-molecule reaction events. Reprinted with permission from ref 120. Copyright 2016 American Chemical Society. c) Evaluation of molecular vibrational excitation through analysis of anti-Stokes and Stokes SERS peak intensities. d) The vibrational occupation number (n) for four vibrational modes of 4-nitrobenzenethiol in a hotspot, plotted relative to thermal reference (n^{th}), showing the selective nonthermal excitation of the symmetric N−O stretching (νNO) mode. Adapted with permission from ref 122. Copyright 2023 American Chemical Society.

molecule-in-hotspot effects while adatom rearrangements accounted for longer fluctuations (10 μs − 1 s).[97] Kamp et al. showed that adding a nanolens onto NPoM geometries improved in- and out-coupling efficiencies, enabling picocavity SERS spectra to be collected in the μs regime, thereby revealing strong submillisecond vibrational shifts (Figure 4c).[99] Schmidt et al. showed that such fast picocavity events can be detected in aggregates of nanoparticles as well, with typical events lasting between 10^{-5}−10^{-2} s (note that maximum durations are limited by number of frames).[100] They reported how SERS intensity fluctuations occur with various distributions across the SERS spectra: in Figure 4d (from top to bottom): (i) both Stokes and anti-Stokes (an inelastic light scattering processes where either a phonon is generated (Stokes) or absorbed (anti-Stokes), resulting in a red- or blue shift, respectively), (ii) only partial Stokes, (iii) entire Stokes, and (iv) only anti-Stokes. These varying enhancement mechanisms suggest a range of dynamics can occur at these time scales such as molecular motion and reconstruction in the metal surface, with the authors suggesting the latter to be the most likely contributor.

Picocavities in Catalysis. The atomic protrusions that give rise to picocavities are also important features in heterogeneous catalysis. Undercoordinated adatoms on metal surfaces are important binding sites. An example was reported by Björk et al. where adatoms were shown to facilitate the initial dehydrogenation and subsequent C−C bond formation in cyclodehydrogenation reactions.[105] Single gold atoms are also extensively studied as single atom catalysts (SACs), though often in combination with various nonmetallic supports.[106,107] As such, picocavities will offer a powerful tool because they directly report on molecule-metal interactions at the single molecule level. Moreover, the high temporal resolution allows reaction intermediates to be tracked and allows for the characterization of complex surface binding dynamics. Picocavities can thus offer

https://doi.org/10.1021/acsnano.4c06192
ACS Nano XXXX, XXX, XXX−XXX

potentially valuable insights into reaction pathways, rate limiting steps, and how undesirable byproducts are formed and the mechanistic working of molecular catalysts.[108] Early examples of studies monitoring such catalytic processes using picocavities are the tautomeric switching of individual molecules optically tracked on an atomic level using STM;[109] the dehydrogenation of primary amides and aromatic methyl groups (Figure 4e,f respectively);[101,102] and the hopping between protonation, deprotonation and surface bound states for individual carboxylic acid groups (Figure 4g).[103] Finally, picocavities exhibit strong optomechanical coupling to molecules, often observed as unusually intense anti-Stokes peaks with a nonlinear power dependence.[49,110] Jakob et al. showed how in intense optical fields, molecular bonds are weakened due to a 'giant opto-mechanical spring effect' (Figure 4h).[104] This brings opto-mechanics in the nanoscale regime enabling different avenues toward molecular technologies and light assisted chemistry. These can include directed catalysis through optically weakened molecular bonds, single molecules acting as opto-mechanical switches, and molecular scale memristive devices where states of individual molecules can be optically read out.

4. SINGLE-MOLECULE PROBING OF CATALYTIC MECHANISMS

SERS Probing for Single-Molecule-Level Elucidation of Elementary Steps and Intermediates of Catalytic and Photocatalytic Reactions. In this section, we pick up from the concept of picocavities and single-molecule and single particle SERS and discuss the unparalleled capabilities of SERS for tracking single-molecule reaction dynamics and elucidating the plasmon-driven reaction mechanisms. Heterogeneous catalysis involves numerous elementary reaction steps and various intermediates, presenting a challenge for ensemble-level spectroscopy in resolving these components. Single-molecule SERS (SM-SERS)[111,112] allows the formation and disappearance of individual, unlabeled molecules to be tracked in real time from their vibrational spectra. This enables the elucidation of fleeting intermediates and determination of elementary steps in the catalytic pathway, information that is often obscured in ensemble-averaged kinetic measurements. The use of Ag nanoparticle aggregates provides Raman enhancement factors on the order of 10^9, large enough to allow the single-adsorbate-molecule sensitivity required for such mechanistic elucidation of catalytic reactions.[113] Using SM-SERS, Jain and co-workers[113] have been able to capture discrete reaction events in CO_2 photoreduction on Ag nanoparticles under plasmonic excitation (Figure 5a). Some of the discrete SERS spectra acquired from individual aggregates captured a critical intermediate in CO_2 photoreduction: the $HOCO^{\bullet}$ radical formed by $1e^-$, $1H^+$ transfer to adsorbed CO_2. The HOCO· radical is further transformed either into CO or into HCOOH, which is also detected. By in situ SERS spectroscopy in a CO_2-saturated liquid water medium and automated assignment of SM-SERS spectra in 500-frame movies from single hotspots, a comprehensive catalog of adsorbates, intermediates, and products was determined from thousands of single-molecule events.[30,114] Detected species include butanol, which is a liquid hydrocarbon, and oxalic acid, which is an intermediate in natural photosynthesis. The SERS probing approach is applicable to a wide range of catalytic reactions beyond plasmon-induced CO_2 reduction, owing to the ubiquity of Raman scattering as a molecular fingerprint that obviates the need for labeling. For instance, in situ SERS probing has been used to elucidate the dynamics of the oxygen evolving complex (OEC) of Photosystem II in the course of water oxidation[115] and to probe the plasmon-induced oxidation of ethylene on Ag nanoparticles, where an unusual photocondensation to form graphene fragments has been observed.[116]

SM-SERS has been successfully validated, including the statistical confirmation of the single-molecule origin of SERS signals,[117,118] quantification of signal enhancement,[119] and real-space visualization[120] of electromagnetic hotspots for SM-SERS. These studies indicate that a signal enhancement of 10^8-10^9 is sufficient[120,121] for recording SM-SERS spectra of both on- and off-resonant[121] organic molecules, and such an enhancement can readily be attained with plasmonic gap structures featuring a ~1 nm gap distance. However, a significant challenge in studying catalytic mechanisms arises from the spectrotemporal fluctuations of SM-SERS that are unrelated to the chemical reaction itself. These fluctuations stem from molecular diffusion,[98] reorientation, and dynamic metal−molecule charge transfer. Despite these challenges, recent work by Choi et al.[120] has demonstrated that, for plasmon-assisted chemical reactions occurring at well-defined hotspots, the temporal dynamics and statistics of discrete jumps (or steps) in SM-SERS trajectories (Figure 5b) of products accurately reflect single-molecule reaction events. This validation underscores the utility of SM-SERS for studying catalytic reaction kinetics with a single-molecule resolution. Further advancements in hotspot design, precise placement (or immobilization) of reactants, and utilization of vibrational markers hold promise in mitigating some of the limitations associated with SM-SERS. Consequently, these improvements may expand the utility of SM-SERS in catalysis research.

Quantifying Nonthermal and Thermal Activation in Plasmonic Catalysis through SERS. In plasmon-induced or plasmon-enhanced catalytic reactions, a significant amount of energy can be transferred from the photoexcited nanoparticle to an adsorbate; the assessment of the transferred energy may offer valuable insights into nonthermal and thermal mechanisms of adsorbate activation. The ratio (ρ) of the intensity of the anti-Stokes (I_{aS}) SERS peak to that of the Stokes (I_S) peak (Figure 5c) for an adsorbate vibrational mode, $\rho = I_{aS}/I_S$, can provide such information,[122] because:

$$\rho = A \cdot \left(\frac{\nu_0 + \nu}{\nu_0 - \nu}\right)^3 \cdot \frac{n}{n+1} \tag{4.1}$$

where ν_0 and ν are the frequencies of the excitation light and the molecular vibration, respectively. The parameter A accounts for the unequal enhancements of the Stokes and anti-Stokes peaks by the plasmon-induced near-field.[123] With a properly calibrated A, the measured ρ allows determination of the vibrational occupation number, n, which represents the average number of vibrational quanta that an adsorbate in a hotspot possesses. Boerigter et al.[124] observed wavelength-dependent ρ for methylene blue on silver nanoparticles, which was interpreted as a signature of direct charge transfer. Keller et al.[125] conducted ultrafast time-resolved ρ-measurements on 4-nitrobenzenethiol (NBT) adsorbed onto gold nanostructures, observing subpicosecond buildup of a vibrationally excited population. The time scale of the excitation rules out photothermal heating being responsible for adsorbate activation. Shin et al.[122] measured ρ of NBT in plasmonic gap structures, observing a highly mode-specific vibrational excitation (Figure 5d), which could be explained by hot-electron mediated energy transfer from the

https://doi.org/10.1021/acsnano.4c06192
ACS Nano XXXX, XXX, XXX−XXX

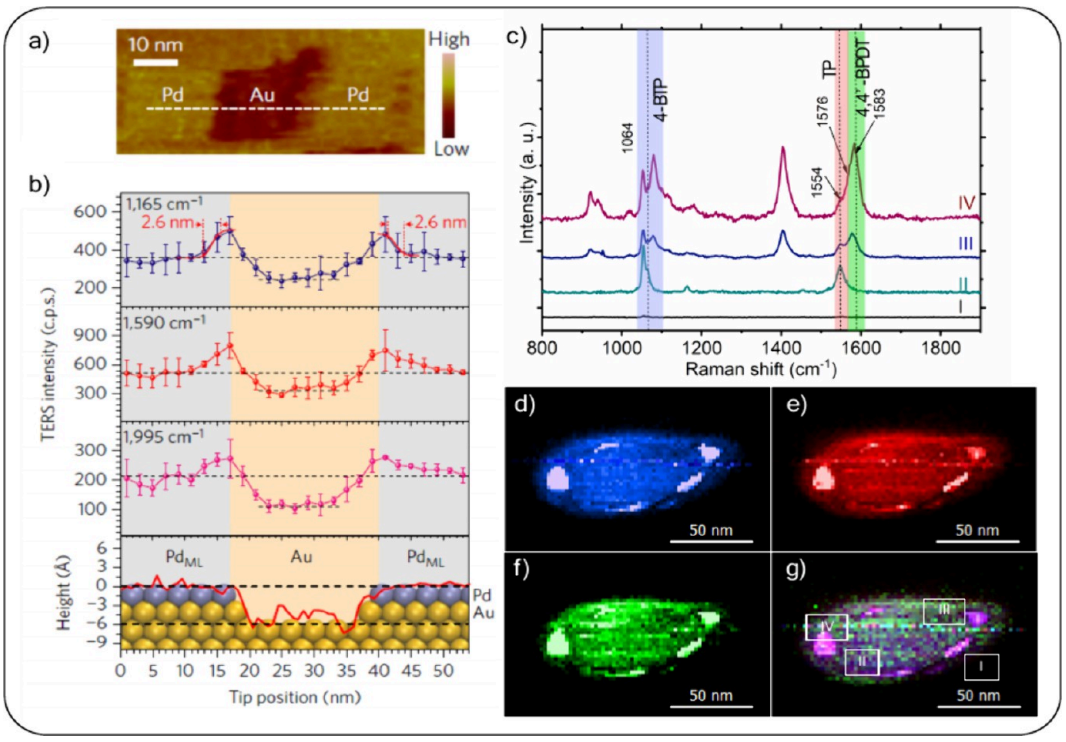

Figure 6. Experimental evidence of Angstrom spatial resolution of TERS. a) Large-scale STM topographic image of a submonolayer coverage of Pd on Au (111) with adsorbed phenyl isocyanide (PIC). b) Plots of intensities of 1165, 1590, and 1995 cm^{-1} of PIC at different surface sites. Error bars indicate standard deviation for the three measurements.[154] Panels a)−b) adapted with permission from ref 155. Copyright 2017 Springer Nature. c) TERS spectra acquired from different locations of a Ni@Au bimetallic nanostructure, revealing the presence of intact 4-BTP (1554 cm^{-1}), in addition to the formation of TP (1575 cm^{-1}) and 4,4′-BPDT (1583 cm^{-1}) on Ni@Au NPs. d)−f) TERS maps for the distribution of 4-BTP (d), TP (e), and 4,4′-BPDT (f). g) An overlay TERS map of all chemical maps. Panels c)−g) adapted with permission from ref 150. Copyright 2023 Royal Society of Chemistry.

plasmonic nanostructure to adsorbates in the gap. The authors of this study further deduced that the excitation rate is as large as 10^{10} s^{-1}, with an incident light intensity of ~100 kW/cm^2 at 633 nm.

The same method can also be utilized to probe the vibrational temperature of the adsorbate.[126−128] Park et al.[127] employed the self-referencing method to calibrate the bias A in eq 4.1, and quantified the extent of local photothermal heating of small organic molecules adsorbed on plasmon-excited nanoparticle aggregates. A closely related approach comprises determining the local electronic temperature of metal from the anti-Stokes continuum emission of hotspots.[129] Here, the continuum emission spectra are fit to the energy distribution of electron−hole pairs to obtain the local temperature of metal.

Further refinement of this method may provide a complete description of the vibrational quantum state distribution of reactants, thereby revealing the detailed mechanism of metal−molecule energy transfer in catalysis.

5. TIP-ENHANCED RAMAN SCATTERING (TERS) FOR VISUALIZING VIBRATIONAL ACTIVATION AND CHEMICAL REACTIONS ON A MOLECULAR SCALE

Similar to picocavities, discussed in Section 3, TERS is an excellent tool to study plasmon-driven reactions at the single molecule level and visualize the dynamics of single chemical bonds in adsorbed molecules. TERS is capable of both quantifying reaction rates and yield, as well as providing information about the catalytic properties of different surface sites of analyzed materials including edges, corners, vacancies and adatoms.[130−132] Therefore, TERS is the perfect tool for investigating the mechanisms of plasmon-driven chemical reactions that were discussed in the previous Section 4, such as direct hot electron transfer or thermal/nonthermal vibrational activation. One example of a plasmon catalyzed chemical reaction demonstrated both by SERS and TERS was the dimerization of p-nitrothiophenol (pNTP) to 4,4-dimercaptoazobenzene (DMAB) on Ag, Au, and Cu surfaces.[133−137] At low concentration of pNTP when dimerization is not possible, the dissociation of pNTP to TP indicates an intramolecular reaction, which usually requires UV light, whereas on a gold nanoparticle the activation barrier is lowered such that the reaction can take place under 632.8 nm irradiation.[138] For surface-bound molecules, hot electrons created by nonradiative plasmon decay, can indeed be shifted by a low bias voltage applied between substrate and tip into the molecule.[139,140]

TERS was used to investigated plasmon-driven redox conversion of 4-mercapto-phenyl-methanol (4-MPM) and 4-mercaptobenzoic acid (4-MBA) on mono and bimetallic nanostrucutres (Figure 6).[141] Li and Kurouski found that Au@Pt NPs could oxidize 4-MPM to 4-MBA, whereas Au@Pd NPs enabled the reduction of 4-MBA to 4-MPM. Such redox reactions could not be observed on Au NPs, which instead caused the decarboxylation of both 4-MBA and 4-MPM into thiophenol. These findings demonstrated that Pt determines oxidation, whereas Pd determines the reduction properties in bimetallic nanostructures. Using TERS, Kurouski and El-Khoury groups observed ionization of 4-nitrobenzenethiol to 4-nitrobenzothiolate (4-NBT^-) on the surface of Au NPs.[18] This conclusion was made by an observation of the shift of 1335

https://doi.org/10.1021/acsnano.4c06192
ACS Nano XXXX, XXX, XXX−XXX

cm^{-1} vibration of 4-NBT to 1305 cm^{-1} of 4-NBT^{-}.[18] Gogotsi's group used TERS to analyze single-layer and few-layer flakes of $Ti_3C_2T_x$ MXene deposited on a gold substrate.[142] The researchers found that the intensity of TERS responses from the single- and few-layer flakes of $Ti_3C_2T_x$ could be used to track early stages of degradation, well before significant morphological changes appear. Using STM-TERS at ultrahigh vacuum, in combination with cryogenic temperatures, submolecular resolution could be achieved. Hou and Jiang were able to probe weak molecule−substrate interactions and conformations of molecular analytes on metallic surfaces.[143−147] Jeong and co-workers employed TERS to investigate defects in α- and β-domains and edges of single-crystalline WS_2 nanosheets.[148,149] The researchers observed shifts of A1g and D modes on the W- and S-edges of the α-domains, respectively. Patil and Kurouski investigated the extent to which Ni-based bimetallic nanostructures could be used to perform dimerization of aromatic halides.[150] They fabricated Ni@Au NPs that were able to dimerize molecular analytes forming BPDT. Using TERS, the researchers demonstrated that the highest yield of BPDT was observed on Ni nanoislands on the surface of these bimetallic nanostructures.

Over the past decade, substantial advances have been made in electrochemical TERS (EC-TERS). Kurouski and co-workers showed that TERS could be used to monitor redox reactions of nile blue (NB) on an indium tin oxide coverslip.[151] The researchers recorded EC-TER spectra consecutively as a function of the potential in cyclic voltammetry, showing a reversible intensity decrease of the vibronic peaks in the fingerprint region upon protonation of NB, in a reduction and oxidation cycle. Recently, Ren et al. have used EC-TERS to study the electrochemical reduction process of 4-nitrophenyl isocyanide (4-NPIC) on a well-defined Pd/Au(III) single crystal surface and observed a negatively charged intermediate which cannot be clearly identified by SERS.[152] The reduction of the nitro group leads to a cathodic current peak in the potential scan from 0.6 V to −0.675 V. The reaction could directly be observed by monitoring the disappearance of the C−NO_2 vibrational mode in subsequent TERS spectra recorded at −0.66 V and at −0.71 V. Furthermore, the vibrational mode of −NO_2 at 1333 cm^{-1} gradually shifted to smaller wavenumbers and lost intensity in the spectra recorded at −0.36 V to −0.66 V whereas the C═C bond at 1596 cm^{-1} shifted to lower wave numbers, associated with an intensity decrease while at the same time a peak reappeared at 1614 cm^{-1}. Theoretically calculated TERS spectra showed that the voltage dependence of these specific bands is associated with negatively charged 4-$NPIC^{-}$ intermediates on the Au_6Pd_2 metal cluster.

In a recent proof-of-concept study, Zenobi et al. have shown the plasmon induced photochemical $[4\pi_s - 4\pi_s]$-cycloaddition of π-stacked anthracene pair.[153] In this example, the tip plays a 2-fold role: (i) precise control of plasmon-mediated polymerization and (ii) via enhanced Raman scattering to monitor in situ the photocatalytic process for exploring the reaction mechanism. The sample consisted of a self-assembled monolayer of anthracene-trimer units of three anthracene molecules arranged in a star-like fashion arranged and connected at their ends by a triptycene core forming in the center of the trimer. The trimers were regularly arranged in a hexagonal pattern in the monolayer, in such a way that the anthracene blades of the trimers could interact face-to-face. The photochemical $[4\pi_s - 4\pi_s]$-cycloaddition of the π-stacked anthracene units were triggered when the junction of the tip and the substrate was illuminated with 633 nm (ca. 1.96 eV) radiation. To carry out the plasmon-induced reaction, the tip was held at a fixed position over the anthracene-trimer monolayer using tunneling current feedback, whereas the junction was illuminated for 120 s under continuous laser illumination and the progress of the polymerization was monitored by continuously recording TERS spectra. The spectra clearly revealed the 2D polymerization because typical anthracene breathing modes at 1425/1445 cm^{-1} disappeared, accompanied by the appearance and increase of the newly formed CC-stretching modes between adjacent anthracenes. DFT calculations suggested that the cycloaddition of two π-stacked anthracene units is plasmon-induced and occurs when the plasmon energy matches the lowest unoccupied molecular orbital (LUMO) of the monomer such that the hot electrons can be inelastically transferred from the gold surface to the anthracene units, although they were only weakly interacting with the gold atoms. The authors estimated the diameter of the area with the strongest plasmon enhancement in the gap to about 10 nm with about 50 trimers. By connecting adjacent trimers, a two-dimensional polymer a two-dimensional network could be formed.

Advantages of using tip-enhanced spectroscopy in combination with chemical reactions are the possibility to apply very locally a specific stimulus such as an electric charge, extremely high electrical fields, pressure, temperature, or mechanical forces and directly observe spectroscopically the molecular changes induced by this external perturbation without ensemble averaging. Similarly, the combination of the optical tip with ultrashort laser pulses is a field to explore for ultrahigh time resolution. Also, the use of an illuminated probe tip in a liquid or in a diluted gas in combination with high resolution optical detection is an avenue to explore. However, these techniques require additional specialized instrumentation, which is currently being developed and is still far from routine applications. Specifically, plasmonic scanning probes used in TERS have a relatively short lifetime. This requires the continuous fabrication of such scanning probes by etching metallic wires (STM-TERS) or by evaporation of plasmonic metals on commercially available silicon tips (AFM-TERS). Furthermore, during TERS imaging, scanning probes can easily adsorb molecular analytes from the sample, which results in their contamination. Although such contaminations could be easily detected via "tip-on" vs "tip-off" experiment, they drastically complicate TERS experiments. Finally, TERS suffers from fluctuations in the intensities and often frequencies of vibrational bands. Such fluctuations may complicate unambiguous interpretation of vibrational spectra and, consequently, experimental results. Therefore, computational simulations based on DFT are often required to fully understand the molecular origin of chemical transformations that are detected by using TERS.

6. TRACKING REACTION KINETICS WITH SERS

In this Section, we take a step back from the single-molecule and single-particle SERS techniques discussed in the previous three Sections and focus on tracking chemical reaction kinetics and pathways in ensembles of molecules, a situation closer to real-life applications. SERS has been used to monitor reaction kinetics by determining changes in the reactant or product concentrations over time. The direct chemical fingerprint detected through Raman scattering identifies reactants, intermediates, and products over time. SERS enables detection at concentrations below the limits of spontaneous Raman. SERS provides extremely high sensitivity down to the single-molecule level,

https://doi.org/10.1021/acsnano.4c06192
ACS Nano XXXX, XXX, XXX−XXX

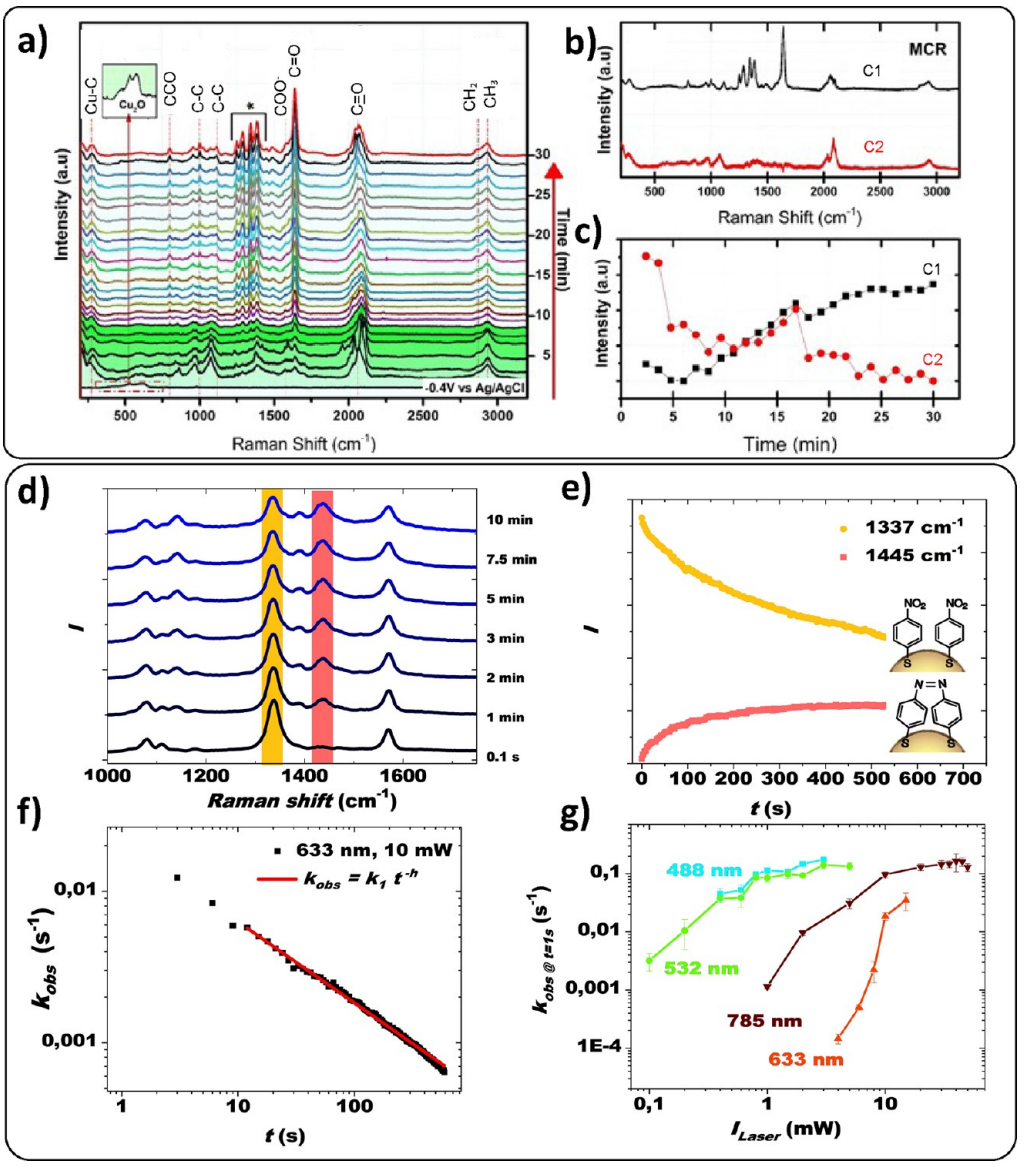

Figure 7. Quantifying reaction kinetics by surface-enhanced Raman scattering. a) Illustration of vibrational modes used to determine intermediate species in the reduction of CO_2 on Cu_2O over Ag nanostructures. b) The spectral changes could be modeled by 2 components (C1 and C2) using multivariate curve resolution (MCR). c) C2 is observed to be initially present and decays as C1 increases over the reaction. Panels a)−c) adapted with permission from ref 157. Copyright 2023, American Chemical Society. d) Raman spectra of NTP on AuNPs recorded with a 633 nm laser and a laser power of 10 mW with 1 s of integration time after different illumination times. The yellow bar marks the NO_2 stretching vibration at 1337 cm^{-1} of NTP, and the red bar marks the ag mode of DMAB at 1445 cm^{-1}. e) Raman signal intensity of the two bands marked in panel a plotted as a function of the illumination time. f) Observed reaction rates determined from the fractal kinetics equation (see the text of this section) fitted with a power-law function. g) Observed reaction rates at 1 s are plotted as a function of the laser power for different laser wavelengths. Error bars are given from the standard deviation of three to five independent measurements. Panels d)−g) adapted with permission from ref 175. Copyright 2019 American Chemical Society.

but the physical effects that provide the high sensitivity also make it challenging to directly correlate the signal intensity and molecular concentration. The variance in the SERS signal intensity arises from the convolution of the number and orientation of molecules in varying enhancement regions on the nanoparticles. Experiments that assess field enhancement along with the surface reactions can help elucidate these complex phenomena.[156] Nevertheless, the SERS signals can be attributed to specific molecular species, including short-lived intermediates, existing on the nanoparticle surface. Hence, SERS is often used to monitor chemical changes occurring over time, often with resolution of milliseconds to seconds. The time dependent change in SERS signals attributed to a particular molecular species can then be used to determine (phenomenological) rate constants. A detailed analysis of time-dependent signals can give access to reaction orders and accurate information about the reaction mechanisms.

Reaction Monitoring. The increased sensitivity provided by SERS has been used to monitor the reaction kinetics in heterogeneous catalysis. Electrified metal interfaces are commonly used for reactions such as carbon dioxide[157−159] and nitrate reduction,[160] and have been investigated on SERS active metals. Modern instrumentation enables SERS to monitor these reactions on relevant time scales, which provides insight

https://doi.org/10.1021/acsnano.4c06192
ACS Nano XXXX, XXX, XXX−XXX

into the chemical species and intermediates governing reactions. For example, in the CO_2 reduction reaction different adsorbed CO species were observed on a Cu_2O layer deposited over silver nanostructures (Figure 7a).[157] The SERS spectrum was modeled by 2 components using multivariate curve resolution where C1 and C2 correlated with C_2 and CO species, respectively (Figure 7b–c). The SERS signal showed these adsorbed CO species evolving along with the observation of C–O and C–C functional groups that correlated with intermediates along the reaction pathway to produce acetate. Blocking surface sites with an alkylthiol altered the observed SERS kinetics, indicating that lateral surface interactions were important for the C_2 product formation mechanism.

An interesting approach proposed more than 25 years ago was to deposit thin films of catalytically active metals (e.g., rhodium, platinum, and palladium) over SERS active surfaces (e.g., roughened silver), such that the Raman signals of the reactants, intermediates, and products can be enhanced during the reaction.[161,162] This "SERS borrowing" approach continues to be used today. In a study of the oxygen reduction reaction (ORR), the mode attributed to peroxide intermediates (*OOH) binding to the surface was observed at smaller Raman shift as the amount of Ni increased in a PtNi alloy catalyst deposited over gold nanoparticles.[163]

In other implementations, SERS has been combined with other catalysts to monitor the reactions. Intermediates in the nitrogen reduction reaction were also observed on porous palladium–silver nanoparticles to optimize electrolysis of N_2 to form ammonia.[164] To further capitalize on the enhanced Raman signal for reaction monitoring, SERS active gold bowties were lithographically printed onto the surface of core/shell SiO_2/TiO_2 oxide beads to monitor the degradation of species on the bead surface.[165] An interesting observation of this study is that the visible laser used for SERS also accelerates the degradation of molecules on the bead surface, suggesting an additional plasmonic mechanism associated with the chemical activity. The use of SERS for reaction monitoring invariably involves plasmon excitation, which may influence reactions in unexpected ways.

Kinetics in Plasmonic Catalysis. The field is of plasmonic catalysis is very well studied because the signal-enhancing material is at the same time acting as catalytically active material making it straightforward to initiate a reaction by the same laser as used for SERS to follow the progress of a reaction.[166] The oxidation of aminothiophenol (ATP) and the reduction of nitrothiophenol (NTP) to dimercaptoazobenzene (DMAB) have been well studied (Figure 7d,e).[166] Apart from the formation of DMAB, the kinetics of other plasmon-induced reactions have been characterized by SERS, e.g., the transformation of thiophenol derivatives (with functional groups such as carboxylic acid, boronic acid and halogens),[167–170] the hydrodehalogenation of brominated adenine and guanine,[171] or the dimerization of benzamine.[172]

Many studies have focused on the identification of products and critical reaction conditions that are required for a transformation; however, kinetic studies can quantify reactivity by determining rate constants.[173] The accurate determination of rate constants is however not trivial due to the heterogeneity of the SERS substrates and the fact that in plasmonic catalysis the signal enhancement is convoluted with the catalytic activity, i.e., the catalytic activity must be assumed to be higher in the SERS hot-spots than at the less signal-enhancing regions. Fractal kinetics are one approach that provides a quantitative description of reaction rates.[174] In this approach, a time-dependent experimental rate constant is introduced, taking into account that reactions proceed faster in highly enhancing regions (hot-spots), while they are slower in other regions of the SERS substrate: $k_{obs} = k \cdot t^{-h}$, with h being the fractal dimension of the system (Figure 7f,g).[175]

Quantitative rate constants also enable deduction of the underlying reaction mechanisms. In plasmonic photocatalysis, the question persists whether plasmon-induced heating or charge transfer is driving a chemical process.[176] The determination of rate constants helps to distinguish between these mechanisms by recording excitation-power-dependent rate constants. A linear increase of rate constants with excitation power points toward nonthermal reaction pathways, while a superlinear increase indicates significant thermal contributions.[177] Nevertheless, it is necessary to analyze power-dependencies carefully, and it is likely that in many reactions both hot charge transfer and temperature play a role for the reaction and the reaction kinetics.[178] The molecular temperature can also be directly measured by SERS from the ratio of the anti-Stokes to Stokes intensities, and recently it was shown that the molecular temperature exceeds the nanoparticle temperature significantly due to nonthermal transient hot charge transfer.[122] From temperature-dependent rate constants, activation energies can be determined, which were shown to depend significantly on the excitation wavelength and power as well as the strength of hole scavengers, although these have not been probed by SERS yet.[179]

The strength of SERS to detect intermediates by carefully tracking the time evolution of transient signals relies on conditions, where only very low concentrations of reactants or single reaction sites are probed, because otherwise transient signals get averaged out.[180,181] Ideally, single-molecule conditions are applied, which have been demonstrated for the case of NTP reduction in the gaps of NPoM arrangements, as discussed in Section 3 of this Review.[120] The authors showed that plasmon-induced reactions of single molecules can be followed in real time and that relevant intermediates can be identified by SERS. In another example, the detailed reaction mechanism of a plasmon-induced dehydration of an aromatic primary amide was investigated at the single-molecule level using nanoparticles on an Au electrode and the role of picocavities for the SERS signal generation was emphasized.[101]

7. ULTRAFAST SERS AND CATALYSIS

If the previous section focused on chemical reaction kinetics on the millisecond to second time scale, here we delve deeper and discuss the applications of SERS in monitoring molecular vibrations in the picosecond and subpicosecond time scale. During catalytic reactions, molecular change proceeds on picosecond to subpicosecond time scales of electron and nuclear motion, making ultrafast measurements crucial for fundamental understanding of molecular reactivity.[182–184] Ultrafast SERS measurements, including those making use of both spontaneous and stimulated Raman probing, are insightful in that they can directly track charge transfer and energy transfer between the catalytic material and proximal adsorbates.[185–187]

On the picosecond time scale, photoinduced reactions can be tracked by spontaneous surface-enhanced Raman probing following photoexcitation. This approach, which typically involves a femtosecond photoexcitation pulse and a picosecond spontaneous Raman probing pulse, has been used to examine multiple facets of photocatalysis. In the context of plasmon-

https://doi.org/10.1021/acsnano.4c06192
ACS Nano XXXX, XXX, XXX–XXX

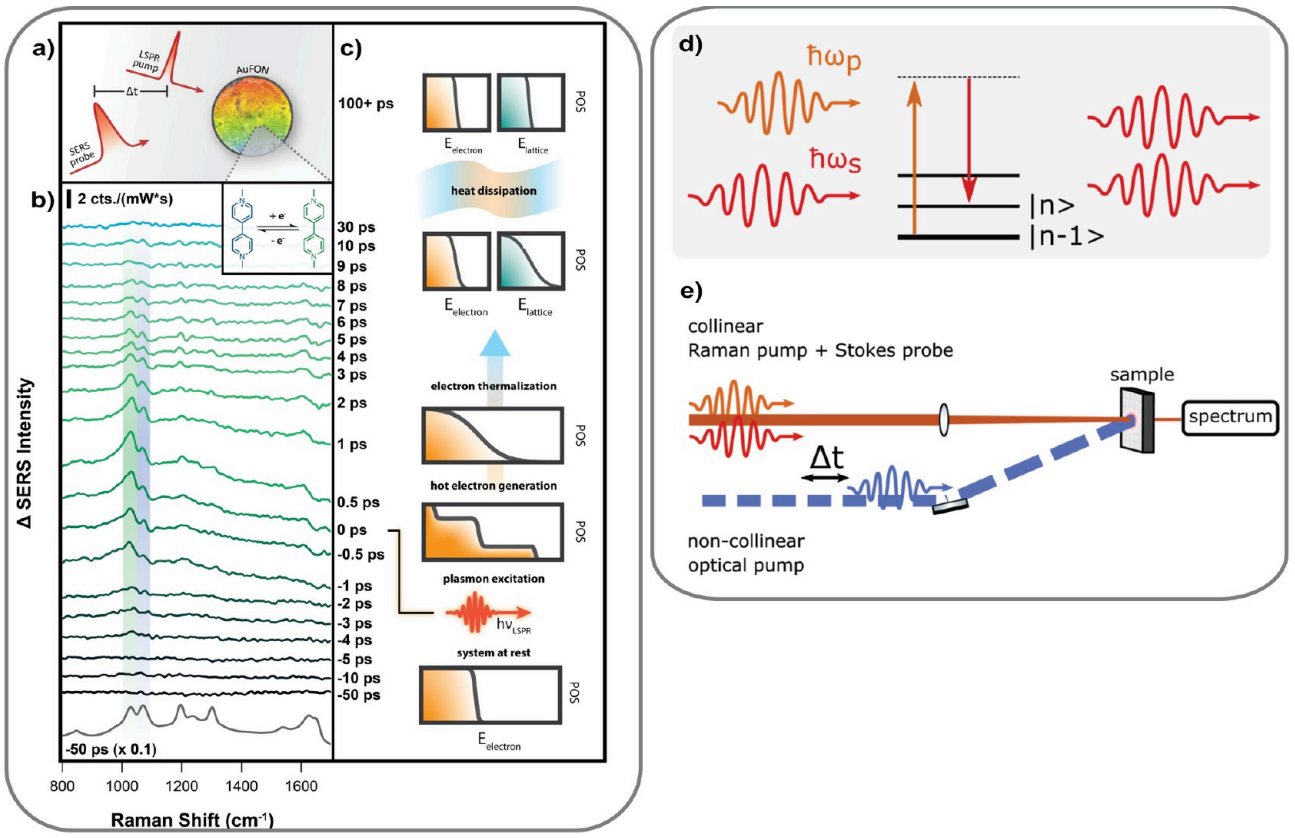

Figure 8. Ultrafast SERS probing of catalysis. a) Schematic depiction and common gold film over nanosphere (FON) substrates used. b) Ultrafast SERS probing of plasmon-to-molecule charge transfer in methyl viologen. c) Depiction of relevant time scales for ultrafast plasmon-molecule dynamics. d) Jabłonski diagram of SRS. The vibration of the molecule is coherently driven by the energy difference between pump (p) and Stokes (s) photons, leading to the stimulated emission of Stokes photons. For a broadband pump pulse, the energy difference condition is fulfilled for a broad range of vibrational states. e) Typical pump−probe configuration: the reaction is initiated by an optical pump pulse and probed after a delay Δt by the coinciding Raman pump and Stokes pulses. Panels a)−c) reprinted with permission under a Creative Commons CC BY-NC license from ref 188. Copyright 2023 National Academy of Sciences.

driven catalysis, this technique was used to successfully monitor gold-nanoparticle-to-molecule electron transfer, proving that some plasmon-derived electrons have reduction potentials in excess of 310 mV (Figure 8a−c).[188] This work also showed that some of the reduced species survive for tens of minutes on the gold surface, suggesting that select regions of a heterogeneous catalytic surface can stabilize charge-transferred species.

Ultrafast SERS can easily be combined with Raman thermometry to separate electron and energy transfer contributions to reaction rate enhancements in, e.g., plasmon-molecule systems. Raman thermometry involves probing both Stokes and anti-Stokes scattering,[122,189,190] which combined with the time resolution afforded by pump−probe measurements, can track how the ultrafast processes vibrationally excite molecular species. This approach was first used to quantify the extent of energy transfer in plasmonic systems, showing that even with exceedingly high photoexcitation powers, the transferred energy was relatively modest compared to many catalytic processes, indicating that heating is not a major contributor to plasmonic photocatalysis.[125] In more recent work, ultrafast SERS thermometry was used to find that intermolecular energy transfer between surface adsorbates is a significant channel for molecular cooling, suggesting that catalysis may actually be more efficient at low surface coverage.[191]

To access intermediate details of proceeding reactions, a higher time resolution may be necessary. Then, stimulated Raman techniques are useful for tracking, e.g., plasmon-molecule interactions.[192] Provided high photon densities, the Raman scattered light retains coherence, and several techniques can be applied: in coherent anti-Stokes Raman scattering (CARS), a pump pulse and a Stokes pulse are mixed. If the energy difference between pump and Stokes photons equals the energy of a normal mode (reaction coordinate), coherent emission at the anti-Stokes energy is induced when mixed with a second pump photon (Figure 8d). In stimulated Raman scattering (SRS), a high intensity pump pulse is combined with a Stokes probe pulse such that the energy difference between the photons corresponds to the energy of a normal mode: $w_p - w_s = w_n$ (1). The use of a second laser pulse to stimulate the interaction leads to orders of magnitude higher signals, as compared to spontaneous Raman scattering. For femtosecond stimulated Raman scattering (FSRS), the pump pulse is broadband and of femtosecond duration such that (1) is fulfilled for the complete spectrum, which is thus accessible. To then monitor chemical reactions on sub−picosecond time scales, a three-pulse configuration is applied. A first pump pulse initiates the (photo)chemical reaction and the Raman pump and Stokes probe pulses arrive simultaneously at a specific delay, probing the progress of the reaction (cf. Figure 8).

https://doi.org/10.1021/acsnano.4c06192
ACS Nano XXXX, XXX, XXX−XXX

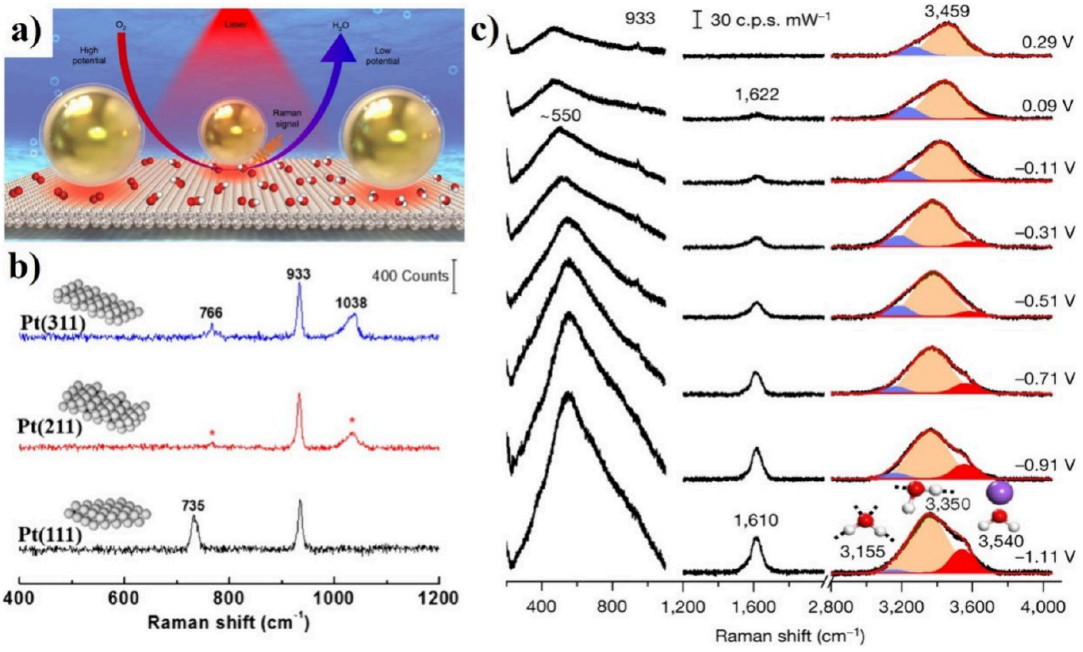

Figure 9. Shell-isolated nanoparticles for probing electrochemical reactions. a) Model of shell-isolated nanoparticles (Au@SiO_2 NPs, SHINs) at a Pt(111) surface and the mechanism of the ORR process revealed by the EC-SHINERS method. Reprinted with permission from ref 213. Copyright 2018, The Author(s), under exclusive license to Springer Nature Limited. b) SHINERS of different Pt(hkl) surfaces in 0.1 M $HClO_4$ solution held at a 0.8 V potential. Reprinted with permission from ref 214. Copyright 2020, American Chemical Society. c) In situ Raman spectra of interfacial water on a Pd(111) electrode in a 0.1 M $NaClO_4$ solution (pH 11). Reprinted with permission from ref 218. Copyright 2021, The Author(s), under exclusive license to Springer Nature Limited.

The improvement of the sensitivity of Raman spectroscopy by surface enhancement can also be applied to the coherent Raman scattering techniques CARS and SRS, resulting in surface-enhanced coherent anti-Stokes Raman spectroscopy and surface-enhanced femtosecond stimulated Raman spectroscopy.[68,193] These techniques can reach single molecule sensitivity,[194] including 2014 work on time-resolved CARS with vibrational coherences monitored on a subpicosecond time scale.[195] Recently, a report of time-resolved impulsive stimulated Raman spectroscopy (ISRS) showed that it is possible to extract dynamical information on a coupled molecular-plasmonic system with ~100 fs time resolution.[196] This work examined *trans*-1,2-bis(4-pyridyl)ethylene and found evidence of a short-lived charge transfer. Future efforts will undoubtedly apply similar surface-enhanced CARS, FSRS, and ISRS techniques to the mechanistic studies of plasmonic photocatalysis.

8. MONITORING NANOSCALE (ELECTRO)CHEMICAL REACTIVITY WITH SERS

SERS and SHINERS in Electrocatalytic Interfaces and Processes. Electrochemical surface-enhanced Raman spectroscopy (EC-SERS)[197] has become one of the mainstream spectroelectrochemical methods, enabling the detection of electrocatalyst evolution, validation of active sites, and recognition of adsorbed intermediate species at electrified interfaces on specific nanostructured metal surfaces. Since a strong SERS effect is often observed on roughened coinage metal surfaces such as gold, silver, and copper, the core−shell nanoparticles-enhanced Raman spectroscopy, by coating transition metals or metal oxides with high electrocatalytic activity outside, was developed and commonly referred to as a borrowing strategy.[198] Owning to its outstanding surface sensitivity and selectivity, EC-SERS has widespread use in various interfacial electrochemical processes.

To move beyond the restriction of coinage metals and specific morphology, shell-isolated nanoparticle-enhanced Raman spectroscopy (SHINERS) was invented in 2010.[199] In this strategy, an ultrathin but compact and pinhole-free silica shell is coated over the Au or Ag core, termed as SHINs. The inner core acts as a Raman signal amplifier by generating a strong electromagnetic field. The silica shell avoids direct contact between the core and the external chemical environments, enabling direct acquisition of signals free from interference. According to practical requirements, appropriate shell materials can be selected (SiO_2, TiO_2, Al_2O_3, CeO_2, MOF, Graphene, etc.) for better stability and the shape or size of the core can be tuned for greater enhancement. By simply dispersing SHINs on substrates, electrochemical processes can be probed in situ on basically any subject. In EC-SHINERS studies, the enhanced Raman signals principally originate from the hotspots between two SHINs or between the SHINs and the substrate. The SHINERS-satellite strategy was then developed for the in situ characterization of nanocatalysts.[200] The practical nanocatalysts are assembled over the surface of SHINs, and the Raman signals of the catalytic particle surfaces are greatly enhanced. EC-SHINERS made it possible to study electrochemical processes on surfaces, such as single crystal surfaces[201] and practical nanocatalysts, further enriching our knowledge of atomic scale mechanism research on interfacial electrochemical processes.[202−205]

In Situ Monitoring of Electrochemical Reactions and Intermediates. With the progress of EC-SERS and EC-SHINERS, many original achievements were obtained, giving a full picture of interfacial electrochemical processes under practical conditions. Unraveling the identity of the intermediate species is paramount for elucidating the mechanisms underlying

https://doi.org/10.1021/acsnano.4c06192
ACS Nano XXXX, XXX, XXX−XXX

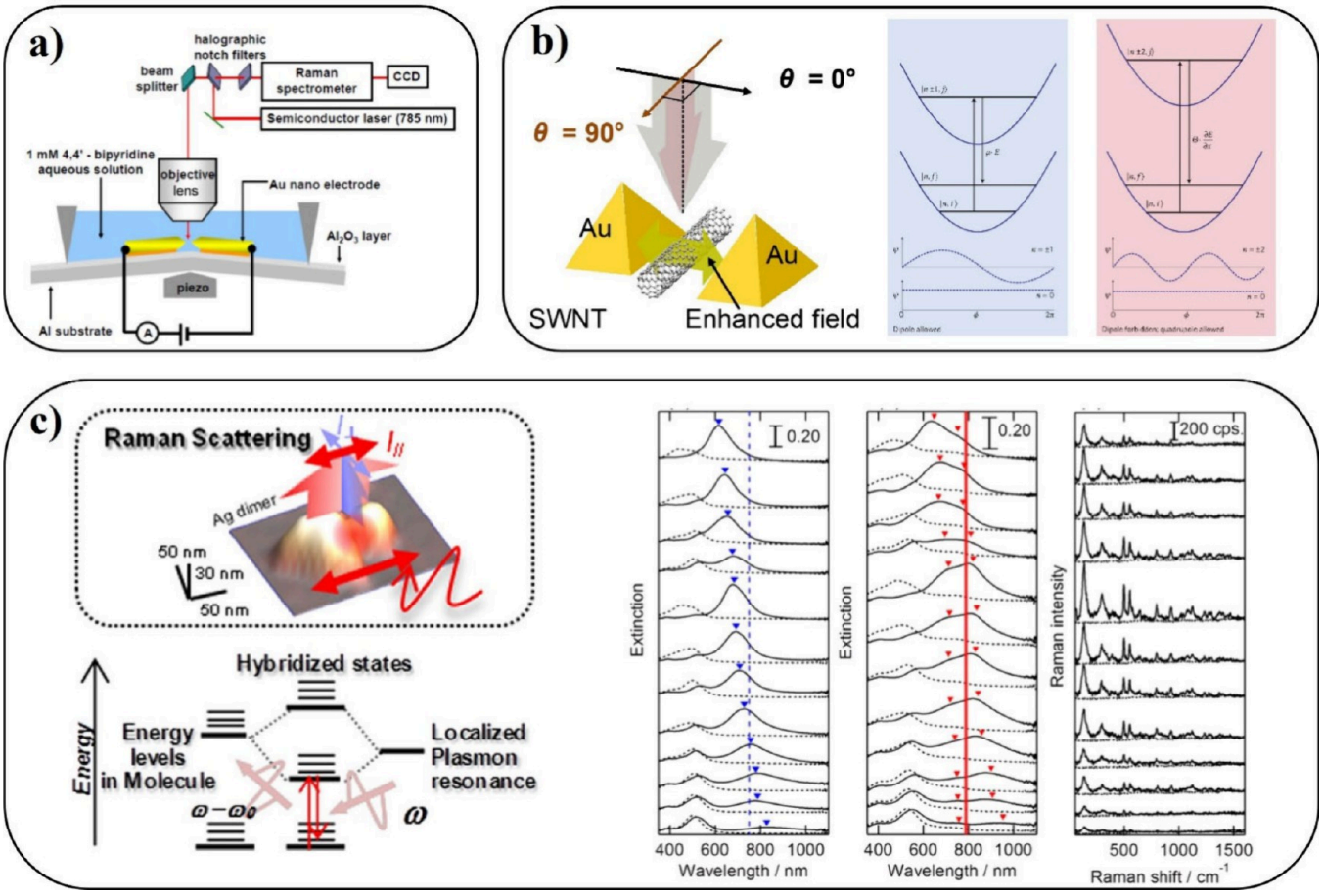

Figure 10. Surface-enhanced Raman scattering in plasmon-driven electrochemical systems. a) Enhanced Raman scattering in the mechanically controllable break junction. Reprinted with permission from ref 233. Copyright 2013, American Chemical Society. b) Selection-rule breakdown in a highly localized electric field. Reprinted with permission from ref 234. Copyright 2019, Springer Nature Limited. c) Raman enhancement of polariton formation. Reprinted with permission from ref 242. Copyright 2014, American Chemical Society.

electrocatalytic reactions. The borrowing-SERS strategy has been applied to study the key intermediates during oxygen reduction reaction (ORR),[206,207] hydrogen oxidation reaction (HOR),[163,208] hydrogen evolution reaction (HER),[209,210] and oxygen evolution reaction (OER),[211] by constructing well-structured Au core-transition metal (Pt, Pd, etc.) shell electrocatalysts. EC-SERS can also be utilized to elucidate the complex structure and chemistry underlying interfacial processes in lithium-based batteries. Xu et al. explored Li_2O_2 desorption from the electrode surface with SERS.[212] They highlighted the essential role of Li_2O_2* desorption in sustaining electrochemical ORR processes in Li−O_2 batteries by facilitating dynamic equilibrium, which dictates electrode potentials and ORR product concentrations with guaranteed stability.

EC-SHINERS, especially Au@SiO_2 nanoparticles, have been extensively applied to single crystals and model catalysts with atomically flat and well-defined surfaces. Schematically depicted in Figure 9a, Dong et al. studied the ORR process, which plays a vital role in proton exchange membrane fuel cells (PEMFCs), on low-index Pt single crystal surfaces.[213] They observed distinct spectral evidence of the ORR intermediates under acid and alkaline conditions. In acidic environments, distinct Raman peaks indicated the presence of different intermediates on different facets. The *OOH at 732 cm^{-1} was obtained on Pt(111), whereas only *OH at 1080 cm^{-1} was observed on Pt(110) and Pt(100). Moreover, in alkaline conditions, similar ORR pathways were suggested across these surfaces, with a notable Raman peak at 1150 cm^{-1} corresponding to O_2^- species. They further extended the investigation on high-index Pt single crystal surfaces,[214] elucidating that the augmented adsorption energy on Pt(311) hampers the dissociation of OOH* and compromises its ORR performance, shown in Figure 9b.

EC-SERS offers a distinctive advantage in elucidating intermediate species and probing the adsorbates with exceptional sensitivity and resolution in intricate electrochemical processes, such as CO_2 reduction on Cu, Cu-based electrolytes, and other electrocatalysts.[215,216] The electrochemical reduction of CO_2 or CO gas holds promise for realizing the carbon cycle on a local scale with the ability to effectively convert greenhouse gases into high-value products. However, the reaction pathways and reaction intermediates are complex and depend on the nature of catalysts and practical reaction environments. Chernyshova and co-workers elucidated the initial step in CO_2 electroreduction, revealing the first intermediate on copper as a carboxylate anion *CO_2^-, coordinated via a C−O bond.[217] Utilizing operando SERS, the research suggested that the conversion of η^2(C, O)−CO_2^- to CO and formate involves specific electronic interactions and is influenced by the electrostatics with hydrated Na^+ and Cu atoms, highlighting its significance in enhancing the selectivity, activity, and efficiency of CO_2 electroreduction.

https://doi.org/10.1021/acsnano.4c06192
ACS Nano XXXX, XXX, XXX−XXX

The different structures of water molecules at electrolyte−electrode interfaces have fascinated but confounded researchers for many years. EC-SERS and EC-SHINERS play significant roles in probing structural changes of the electrochemical interfaces.[201] Integrating advanced ab initio molecular dynamics (AIMD) simulations with EC-SHINERS, Wang and co-workers studied the dynamic structure of interfacial water molecules and its implications for HER.[218] As shown in Figure 9c, the interfacial water was divided into three configurations, which are four-coordinated hydrogen-bonded water (4-HB·H_2O) from 3100 to 3300 cm^{-1}, two-coordinated hydrogen-bonded water (2-HB·H_2O) from 3300 to 3500 cm^{-1}, and Na^+ ion hydrated water (Na·H_2O) at around 3540 cm^{-1}. Their findings highlight that Na·H_2O aligns its vibrational dipole moments more parallel to the electric field than the other two configurations. This alignment predisposes Na·H_2O toward a more ordered structure. The enhancement of the peak at 550 cm^{-1} at negative potentials, attributed to the vibrational mode of water, also confirmed the ordering of interfacial water. Additionally, Na·H_2O exhibits a shorter Pd−H distance, facilitating electron charge transfer and boosting the water dissociation efficiency.

Probing Electrified Interfaces at the Nanoscale and Single-Molecule Level. Successful SERS or SHINERS monitoring of the reaction intermediates was developed by studies on the electrode−electrolyte interfacial design based on fundamental principles. In principle, the enhancement of the Raman scattering of molecules can be induced by the electromagnetic effect[219,220] and the charge transfer (CT) effect.[12,221−224] The degree of CT interaction can be also controlled by the electrochemical potential.[223,225] Therefore, understanding the charge-transfer interaction, which can also be understood as the strong light-matter interaction at the electrified interface, can be an important factor for the electrochemical SERS studies. CT interaction can be often found in the pyridine-based molecules from a historical point of view.[3,4] Osawa et al. discussed by comparing the SERS and surface-enhanced infrared spectroscopy. These CT effects can be discussed along with the observation of reaction intermediates, but can also originate from the CT interaction, due to strong and enhanced SERS signals.[226,227] A small number of the molecules can be also observed from polarized SERS spectroscopy.[228] Polarized Raman spectroscopy can also be utilized to depolarize the SERS signals, originating from the strong light-matter interaction at the electrified interface.[229] In addition, CT-based strong light matter interaction can be also used for the optical trapping of the small molecules at an electrified interface.[230−232]

This strong light-matter interaction can also be observed as a nondiagonal interaction from SERS. Strong light confinement environments can be created from the electrode surface by mechanically controllable break junction methods. Strong SERS signals were observed from the exotic Raman enhancement with the nondiagonal Raman excitation. These exotic enhancements can be used to create light-matter interactions (Figure 10a).[233] The strong localization of the plasmonic fields can be used for the breakdown of the selection rule in SERS. For example, carbon nanotubes were localized between plasmonic nanostructures, showing a strong dependence on the radial breathing mode in their Raman spectra. From theoretical and experimental analyses, it was concluded that a strong electric field gradient can be utilized for the selection-rule breakdown in SERS under strong light-matter interaction (Figure 10b).[234] The strong light-matter interaction can be utilized for the nonzero wavevector based on the observation of nominally forbidden Raman bands. These results can be also utilized for the generation of the energy distribution of holes and electrons in the graphene structure.[235]

The strong light-matter interaction has recently been conceptualized as polaritonic chemistry.[236] Interestingly, similar concepts have been proposed by electromagnetic theory.[4] The understanding of the origin of the light-matter interaction via Raman spectroscopy can be informative for evaluating the polaritonic character in future studies such as modification of chemical reactivity[237,238] and charge transport.[239−241] The understanding of the polariton character from Raman spectroscopy can be useful for understanding strong coupling. Nagasawa et al. reported the Raman enhancement of polariton formation. Dye molecules were used for the electronic strong coupling state due to their high oscillator strength. The maximum Raman enhancement was obtained at the resonant energy between the hybrid states and the excitation (Figure 10c).[242] The Raman enhancement in the strong coupling regime allows us to observe the vibrational structure in the new hybridized molecule states.[243] The utilization of the polariton can be also important for the detection of Raman enhancement and understanding of the electronic structure under polariton formation.

SERS technology markedly advanced detection sensitivity and product selectivity, which are pivotal in examining electrified interfaces. The advent of SHINERS and molecule polaritons has expanded research opportunities into electrochemical reactions at both the nanoscale and single-molecule levels. These methodologies yield important insights into reaction mechanisms, providing more precise control over the targeted electrochemical reactions.

9. HYBRID NANOPARTICLE CATALYSTS FOR SERS

In this section, we continue the idea introduced in the previous Section through SHINERS, that of using different materials which combine the plasmonic properties of the coinage metals with the catalytic properties of the transition metals of groups 8−10. The advantages of exploiting SERS for label-free monitoring of surface-catalyzed reactions are obvious: surface selectivity and chemical specificity with molecular information about bonding and interactions combined with high sensitivity. However, merging SERS with heterogeneous catalysis was not as straightforward as it may seem today. Both usually employ metals; however, they are typically different classes of metals: SERS largely relies on the physical, in particular optical, properties of the coinage metals of group 11 (Cu, Ag, Au), whereas heterogeneous catalysis relies on the chemical properties of transition metals of groups 8 to 10 (Fe/Co/Ni, Ru/Rh, and Os/Ir/Pt). This initial dilemma stimulated ideas on how to introduce SERS as a powerful vibrational spectroscopic technique into heterogeneous catalysis, an important field in chemistry. Historically, achieving this for solid SERS substrates by overlayer deposition strategies was introduced by Weaver[244−246] and continued by Tian with the strategy of borrowing SERS activity.[247,248]

We summarize in this section the development of strategies for colloidal SERS: the design of hybrid nanoparticle catalysts that integrate both plasmonic and catalytic properties into a single bifunctional nanoparticle entity. To maintain a clear focus, we restrict ourselves 2-fold: (i) Focus on hybrid systems where there is either a chemical and/or a physical interaction between the plasmonic and the catalytic component. (ii) Focus on SERS as a passive spectator of chemical processes, i.e., light has

https://doi.org/10.1021/acsnano.4c06192
ACS Nano XXXX, XXX, XXX−XXX

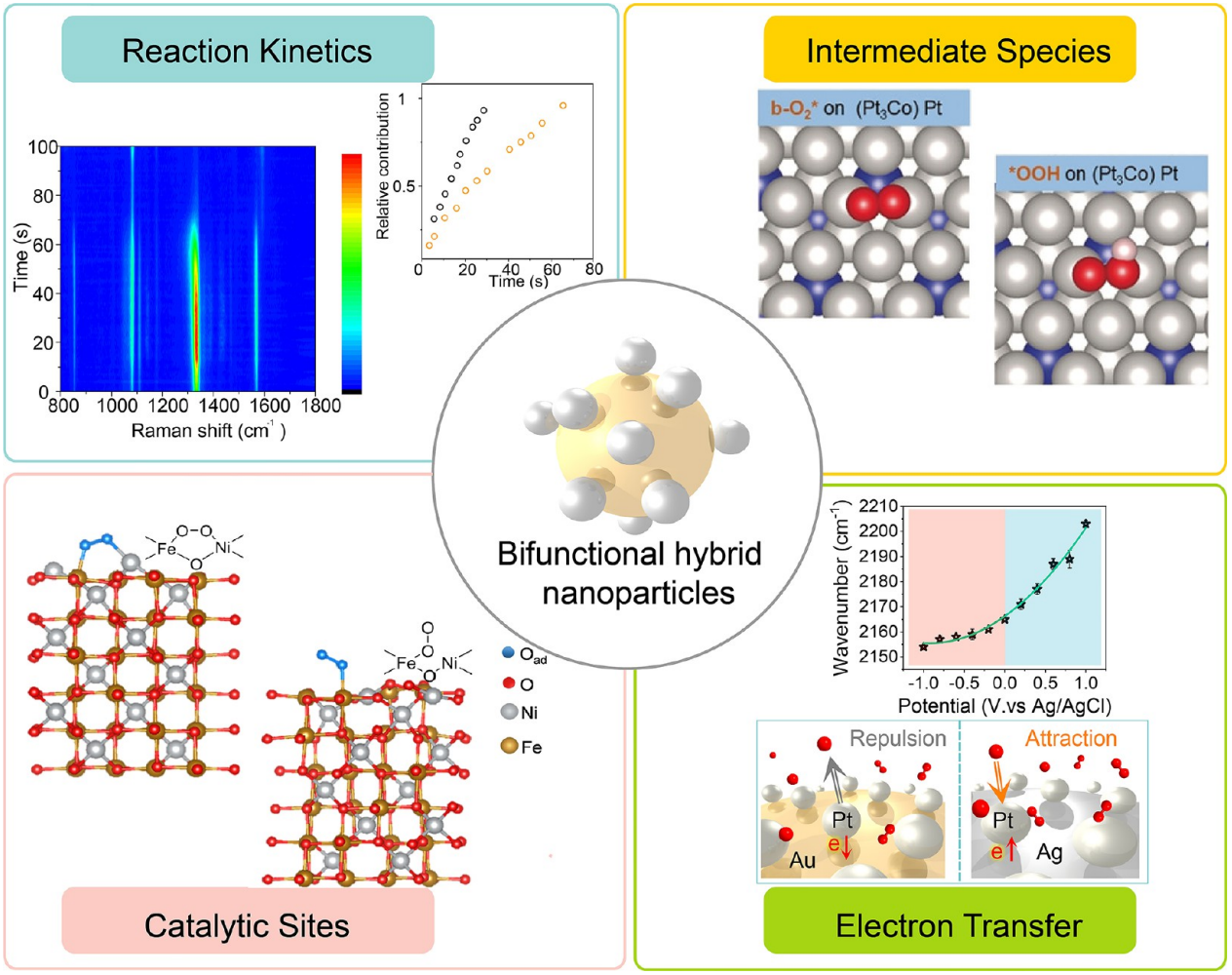

Figure 11. Surface-enhanced Raman scattering in hybrid catalysts. Four facets of bifunctional hybrid nanoparticles as hybrid catalysts for label-free SERS.

exclusively a passive role for interrogating the chemistry using SERS and does not itself actively promote it. In contrast, in plasmon-induced chemistry hot carriers such as hot electrons and hot holes are included as "reactive species" that are actively created by light.[249]

What can be learned from applying hybrid catalysts in combination with SERS? Figure 11 shows an overview of four aspects that are covered in this perspective: reaction kinetics, intermediate species, catalytic sites, and electron transfer.

Kinetic studies are helpful in evaluating the catalytic activity of nanoparticles (NPs). This is based on the hypothesis that the higher the chemical reactivity of a catalyst, the faster the reaction kinetics. A widely used model reaction for assessing the catalytic performance of metal NPs is the reduction of 4-nitrothiophenol (4-NTP) to 4-aminothiophenol (4-ATP) since it can easily be monitored by UV/vis absorption spectroscopy.[250] However, only a color change from yellowish to transparent is observable. In contrast, label-free SERS with the power of vibrational Raman scattering can provide much richer chemical information about functional groups and their interaction with the surface of the catalyst. Replacing oxygen by sulfur for chemisorption to the surface of the hybrid catalyst enabled label-free SERS monitoring of the 4-NTP to 4-ATP reduction. The report on label-free SERS monitoring of the 4-NTP to 4-ATP conversion employed Au/Pt/Au nanoraspberries as a hybrid NP catalyst: Au core and protuberances for SERS and a Pt shell for catalysis.[251] Due to the direct contact between Au core, Pt shell, and Au protuberances, there is both a chemical interaction between the two metals (charge transfer) and a physical interaction between gold core and protuberances, in which the large plasmonically active gold core borrows plasmonic activity to the small gold protuberance with low intrinsic plasmonic activity (plasmonic coupling). In this proof-of-concept study, both the educt (4-NTP) and product (4-ATP) were characterized by SERS. At low concentrations of the reducing agent sodium boron hydride (NaBH4), the formation of the photoproduct dimercaptoazobenzene (DMAB) by reductive coupling can be observed. However, with increasing $NaBH_4$ concentration, the rate of the 4-NTP to 4-ATP conversion is increased such that the formation of the photoproduct is minimized. In the next step, to avoid the formation of the photoproduct DMAB, a different design was employed for the hybrid nanocatalyst: Au/Au superstructures comprising a large Au core that is isolated by a thin dielectric silica shell.[252] After the thiol functionalization of the silica shell with MPTMS, small Au satellites were assembled onto the core. Thus, the chemical interaction between core and satellites was minimized, while the physical interaction via plasmonic coupling still exists and is required for obtaining high SERS enhancements for 4-NTP/4-ATP chemisorbed on the small satellites. Control experiments

https://doi.org/10.1021/acsnano.4c06192
ACS Nano XXXX, XXX, XXX−XXX

demonstrated that this electric insulation of the catalytically active satellites from the plasmonically active core avoids formation of the photoproduct DMAB. The 4-NTP to 4-ATP reduction kinetics occurred on a time scale of 1−3 h and thus could be conveniently observed in conventional cuvette experiments. Smaller 5 nm Au satellites led to faster reaction kinetics compared with larger 10 nm Au satellites due to their larger catalytic activity. In contrast, the reduction kinetics for Au/Pt/Au nanoraspberries from the proof-of-concept study[251] was too fast to be observed in conventional cuvette experiments due to the exceptional catalytic activity of the Pt shell. Continuous (or stopped) flow methods are routine methods in chemical reaction kinetics on the macroscale. Applying them to kinetic SERS monitoring of the 4-NTP to 4-ATP reduction required some adaptations. To this end, a microfluidic reactor for rapid mixing of the reactants 4-NTP@Au/Pt/Au protuberances and $NaBH_4$ with the ability for subsequent label-free kinetic SERS monitoring using confocal Raman microscopy was designed and built.[253] In addition to increasing the temporal resolution down to the millisecond regime, this microfluidic approach has two advantages: (i) it avoids the formation of the photoproduct by quickly removing the reactants out of the laser spot of the confocal Raman microscope, and (ii) it enables the recording of SERS spectra at defined reaction times with a high signal-to-noise ratio since measurement times are only limited by the available amount of reactants.

The concept of core/satellite superstructures as hybrid catalysts for SERS[252,253] was soon recognized to be generic because the catalytic activity can easily be modified and controlled by using other metal NPs as satellites. This is highly relevant because it avoids the former intrinsic limitation of SERS to plasmonically active coinage metals Ag, Au, and Cu. It also soon became clear that it is necessary to go beyond the 4-NTP to 4-ATP model reaction for additionally demonstrating the variety of molecules and reactions that can be studied by hybrid NP catalysts and SERS. Many important reactions are catalyzed by transition metals, such as Pt and Pd. The Pd-catalyzed Suzuki-Miyaura reaction, a C−C cross-coupling reaction, is such an important reaction in metallorganic chemistry and therefore was a nice example for being studied with SERS.[254]

The identification of reaction intermediates is important, because it is a necessary requirement for resolving the underlying reaction mechanism. The examples in this paragraph are reactions that are highly important in the field of chemical energy conversion: water splitting for hydrogen production (oxygen and hydrogen evolution reaction, HER/OER) and the inverse process of using hydrogen as a fuel in fuel cells (oxygen reduction reaction, ORR). An early study on identifying intermediates in water splitting by SERS used the following hybrid catalyst: a monolayer of anatase TiO_2 nanoplates decorated with Pt cocatalyst nanoparticles and silver nanoparticles protected by a thin layer of alumina prepared by atomic layer deposition to prevent charge transfer between Ag and the reaction system. Peroxo, hydroperoxo, and hydroxo surface intermediate species could be identified by SERS.[255] Subsequent studies by other groups adopted the core/satellite approach introduced above, again by using a shell-isolated core and catalytically active satellites.[209] Specifically, small 2.5 nm RuNP satellites were assembled on a large 55 nm Au core, enabling label-free SERS detection of adsorbed hydrogen (*H) and adsorbed OH species (*OH). The inverse reaction of water formation in fuel cells, specifically ORR, was also studied by SERS. Again, the hybrid catalyst was a core/satellite system comprising small catalytically active Pt_3Co satellites.[256] Bridge adsorbed oxygen (b-O_2*) and *OOH reactant intermediates on Pt sites were both directly detected in acidic and basic solutions, while adsorbed *OH was detected on Co sites in a basic solution. Two other important reactions, in which satellite hybrid NP catalysts were employed, are highlighted here. The first one is CO oxidation. By using a plasmonically active gold core and either monometallic Pd or bimetallic PtFe as satellites in conjunction with SERS, active species, such as surface oxides, superoxide/peroxides, and Pd−C/Pt−C bonds were directly observed.[257] The last example is the Ni-catalyzed Ullmann cross coupling reaction, for which the intermediate dehalogenated aryl compound was detected by SERS using gold core/NiNP satellites as hybrid NP catalyst.[258]

Due to its surface selectivity, SERS enables not only the detection of intermediate species but also the identification of catalytic sites. In this section, we highlight three types of reactions: OER[259] and ORR,[260] which were studied by SERS using the core/satellite hybrid NP catalyst approach, as well as the 4-NTP model reaction that was studied by SERS using conventional core/shell NP.[261] In OER, by using Ni_3FeO_x NPs as catalytically active satellites, a dual Fe and Ni site was identified by SERS as the catalytic site.[259] In ORR, by employing small AuCu bimetallic NPs as catalytically active satellites in conjunction with a large gold core, ordered sites were found to be more beneficial due to their lower affinity to adsorbed OH.[260] Finally, in the 4-NTP to 4-ATP conversion, single Pd atoms were identified as the catalytic site on an Au core with a TiO_2 shell.[261]

In the section on kinetic studies, the chemical interaction between the two metals was mentioned; however, no experimental evidence or even quantitative results were presented. This is the topic of the fourth aspect highlighted here: electron transfer (cf. Figure 11). Generally speaking, the electronic structure of the catalyst is very important. In hybrid NP-based catalysis, there is the opportunity to combine two or more metals into a single entity with properties different from those of the isolated metal NPs. In the examples of core/satellite hybrid NP catalysts discussed above, the core was intentionally isolated from the satellites by a thin dielectric shell for a clear separation of labor: the small satellites are responsible for catalytic activity, while a large plasmonically active core is required for SERS detection. The thin dielectric shell avoids chemical interactions between the two and prevents molecules from being adsorbed on the core. We highlight here that the chemical interaction between the core and the satellites indeed provides many opportunities. Upon contact between the satellites and the core, contact electrification occurs, which shifts the Fermi level, in particular, that of the catalytically active satellites. Thus, contact electrification as a purely physical phenomenon directly leads to an altered chemical reactivity. The concept of contact electrification-controlled chemical reactivity was demonstrated for Au core/Pd satellites using the C−N triple bond stretching vibration of an isocyanide as a potential-sensitive vibrational probe in conjunction with electrochemical SERS as a reference method.[262] Two different core/satellite particle systems were employed: a gold core with a thin silica shell and either gold or silver NP satellites. Both types are characterized by SERS and XPS experiments as well as supporting DFT calculations, indicating the transfer of electrons from Pt to Au and from Ag to Pt. This charge transfer leads to different overall catalytic activities in HER, where protons must approach the catalyst surface for reduction to hydrogen: in the

https://doi.org/10.1021/acsnano.4c06192
ACS Nano XXXX, XXX, XXX−XXX

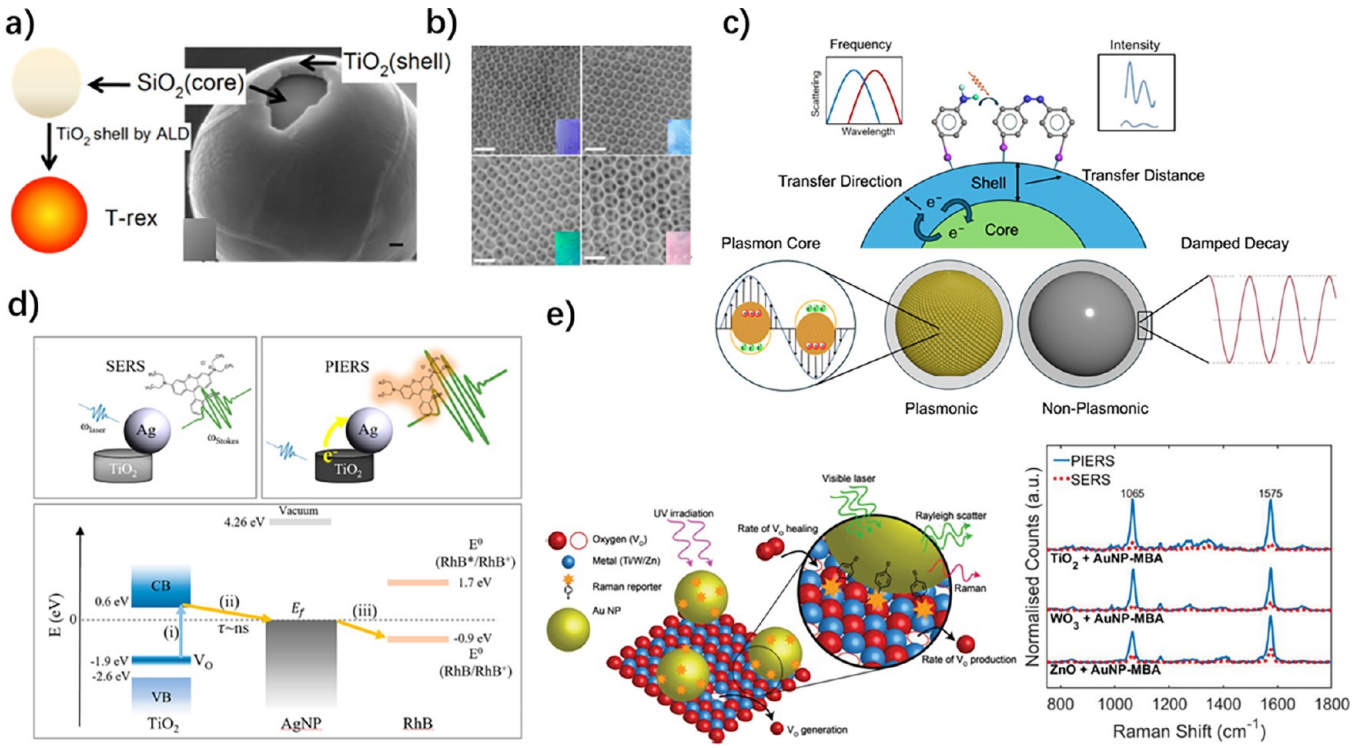

Figure 12. Surface-enhanced Raman scattering in semiconductor catalysts. Nonplasmonic resonant SERS substrates based on a) core/shell SiO_2@TiO_2, adapted with permission from ref 270. Copyright 2013 American Chemical Society and b) an inverse opal TiO_2 photonic microarray, image adapted with permission from ref 274. Copyright 2014 American Chemical Society. c) Monitoring the transfer direction and distance of photoinduced carriers through the core/shell structured nonplasmonic substrate. d) Hybrid plasmonic-metal oxide substrates are combined with preirradiation to further enhance Raman signals from adsorbed molecules, and a mechanism for enhancement has been elucidated to be reliant on the concentration of oxygen vacancies in the metal oxide. Adapted with permission from ref 299. Copyright 2023 American Chemical Society. e) PIERS can be used to monitor the formation and catalytic utility of oxygen vacancies by monitoring enhancement. Adapted with permission under a Creative Commons CC BY license from ref 296. Copyright 2019 Wiley.

case of the Ag core/Pt satellite particle, the HER activity is increased due to the higher electrostatic attraction of the protons, while for the Au core/Pt satellite particle, the opposite is observed.

In summary, the combination of core/satellite hybrid NP catalysts in conjunction with SERS as a powerful analytical technique offers kinetic monitoring of surface-catalyzed reactions and the identification of intermediates and catalytic sites. Contact electrification adds another dimension of control over the catalytic reactivity by tuning the Fermi level of the metal catalyst.

10. SERS IN DIELECTRIC/SEMICONDUCTOR PHOTOCATALYSTS

Expanding on the previous Section of hybrid catalysts, here we focus exclusively on dielectric and semiconductor materials, without a plasmonic metal. Dielectrics and semiconductors play a fundamental role in photocatalytic processes, where they can act either as supports for metallic centers, directly as catalysts, or both. Obtaining direct information about the processes occurring on the surface of photocatalysts and studying their structure and evolution under real operating conditions is extremely important for understanding the reaction mechanisms and enabling rational design of catalysts. Surface-enhanced Raman spectroscopy can be very useful in this regard and is the subject of intense research activity.[186,263,264] However, the use of plasmonic metals can significantly perturb the reactivity of the investigated system because of the generation of hot electrons and localized heat resulting from ohmic losses, which can produce undesired byproducts or alter the course of the reaction.[264,265] Dielectrics or semiconductors can overcome these limitations, especially if the enhancement of the Raman signal is achieved through the exploitation of phenomena such as total reflection, multiple scattering, and morphological optical resonances (Mie modes), which have the overall effect of multiplying the optical path length of light and, consequently, the number of Raman photons, without concentrating the electromagnetic field directly on the target molecules.[266] An example of these systems is represented by the so-called "T-rex," which are core/shell structures of SiO_2/TiO_2 or hollow TiO_2 nanoshells that have allowed monitoring the progress of different reactions,[267−269] included the photodegradation of organic pollutants (Figure 12).[270] The main advantage of these systems is that they can be prepared as individual microspheres with sizes commensurate with the beam size of a Raman microscope. Thus, it is possible to draw a quantitative comparison between the photodegradation processes of different molecules using the same colloidal platform and study the behavior of a reaction in multiple photocatalytic cycles, exploiting the possibility of cleaning the TiO_2 surface through UV-ozone cleaning or thermal treatment. T-rex structures also enable the detection of adsorbed gases (N_2, CO_2, CO, O_2, NO_x, etc.) on the titania surface with extreme sensitivity[271] and can be used for multimodal detection of chemical reaction products, using them as active substrates for MALDI-MS and Raman, without the need for organic ionization matrices.[272] Another

https://doi.org/10.1021/acsnano.4c06192
ACS Nano XXXX, XXX, XXX−XXX

example of dielectric substrates used for multimodal monitoring of catalytic reactions is represented by SiO_2/ZrO_2 core/shell structures (ZORRO).[273] These microresonators present WGM modes that can be directly observed in the spectral output of a Raman measurement. The high sensitivity of WGM modes to the presence of adsorbed molecules on the surface has allowed monitoring of the effectiveness of functionalization processes and the anchoring of azo-dyes inside molecular receptors, with sensitivity in the order of attomoles. In perspective, these strategies, which combine Raman molecular identification with optical sensing, could enable precise characterization of active sites and accurate quantification of catalytic turnover under real operating conditions. Over the last 15 years, there have been several extensions of this type of active nonmetallic SERS substrates based on the effective trapping of light in optical cavities or photonic crystals, in the form of inverse macroporous opals,[274,275] yolk−shell structures of $Fe_3O_4@CeO_2$,[276] ZnO spheres,[277] Si NWs,[278] and even chiral carbon nanotubes loaded with TiO_2.[279] Tittl and co-workers[280] recently demonstrated the use of TiO_2 metasurfaces for all-dielectric SERS, which could advance the investigation of photocatalytic reactions. On the other hand, systems based on graphene, graphene oxide and other 2D materials,[266,281] MXenes,[282] MOFs,[283] and sub-stoichiometric oxides, such as $W_{18}O_{49}$,[284] are more commonly used to promote charge transfer-based SERS.

Moreover, Raman spectroscopy is also an important tool to access information regarding oxygen species adsorbed on the surface of a photocatalyst, such as superoxides, peroxides, and hydroxyl groups, which often play a fundamental role in photo-oxidation reactions.[285] For example, multiple scattering surfaces of TiO_2 have been recently exploited to demonstrate the role of active oxygen species in interpreting the mechanism of *p*-aminothiophenol photo-oxidation in the absence of plasmon-derived hot electrons.[286]

Despite the development of numerous semiconductor-based SERS substrates, some of which have been applied to achieve self-monitoring of photocatalytic processes,[186,286,287] many efficient photocatalytic systems are based on composites of semiconductors and noble metals. This is because such composite systems, due to the presence of Mott−Shottky junctions, facilitate the separation of photogenerated charge carriers more effectively. Under illumination, both metals and semiconductors can be excited. Optimizing the separation efficiency, as well as rational control of the migration direction of photogenerated charge carriers, is crucial for improving efficiency and selectivity. However, most designs of metal−semiconductor systems are based on trial-and-error methods and often yield unsatisfactory performance. Currently, there is ample research indicating the significant advantages of SERS in understanding the migration behavior of charge carriers between metal−semiconductor interfaces. This advantage mainly stems from SERS allowing for monitoring of charge carrier migration behavior under actual reaction conditions, such as ambient temperature and pressure in aqueous environments. This is difficult to achieve with many conventional in situ tracking methods. For instance, synchronous illumination X-ray photoelectron spectroscopy requires a vacuum environment,[288] while fluorescence detection requires fluorescent molecules as probes.[289]

Monitoring under reaction conditions allows researchers to study the influence of different atmospheres, solvent conditions, and dielectric types on charge carrier migration, including the migration direction and distance. These studies are typically based on core−shell systems with noble metals as the core and dielectrics as the shell. For example, Tian et al. used the oxidation of PATP as a model reaction, tracking SERS signals of $Au@TiO_2$ and $Au@SiO_2$ under different atmospheres to understand the migration behavior of photogenerated carriers on Au, confirming that TiO_2 can achieve more effective carrier extraction.[198,290] They further demonstrated the extraction of hot electrons under aerobic conditions and hot holes under anaerobic conditions. Furthermore, Li et al. confirmed the migration distance of hot carriers in semiconductor shell layers by varying the shell thickness, revealing that electrons can migrate over 10 nm in TiO_2 and Cu_2O shell.

On the other hand, for semiconductor-noble metal systems combined through loading, since the noble metals are not encapsulated, they can directly contact reactants such as gases or liquids. Therefore, SERS can help understand the migration trends of photogenerated charge carriers to different dielectrics including semiconductors and reacting molecules. Camargo et al. investigated the impact of excitation wavelength on photogenerated carrier migration within an Au/TiO_2 system, using PATP oxidation as a model reaction.[291] Their findings revealed that UV light exposure significantly enhances PATP oxidation in the presence of TiO_2, as opposed to that of pure Au systems, resulting in PNTP formation. This enhancement is attributed to the efficient transfer of electrons from both Au and TiO_2 to O_2, leading to increased superoxide radical production and, thus, promoting PATP oxidation. Upon UV light cessation, DMAB regeneration occurs due to PNTP's lower molecular energy level, facilitating the acceptance of hot electrons from Au. Furthermore, Wang et al. studied the influence of Au size on electron transfer efficiency to TiO_2.[292] Size affects the Fermi level position of metal nanoparticles, impacting the electronic states of the Mott-Shottky heterojunction at the metal/semiconductor interface. Despite this knowledge, there remains a significant gap in understanding how size optimization can enhance the photocatalytic activity and selectivity of metal/semiconductor composites. They used PNTP reduction as a model reaction, exploring the influence of size on electron transfer kinetics and direction at the Au/TiO_2 interface using SERS. By tracking and analyzing SERS spectra of Au nanoparticles and TiO_2 with inverse opal photonic structures, they revealed size-dependent unidirectional/bidirectional transfer of light-induced electrons at the Au/TiO_2 interface. Based on the above findings, they designed a Au/TiO_2 system with two different sizes of Au nanoparticles. This design enables a directed flow of electrons from larger Au particles to TiO_2, and subsequently to smaller Au particles, thereby enhancing the separation efficiency of the charge carrier.

SERS has made significant progress in photocatalysis monitoring, but current monitoring of photocatalytic reactions generally relies on oxidation−reduction reactions involving model molecules with specific functional groups like -SH. There has not been a real breakthrough in detecting small molecule reactions such as CO_2 reduction, water splitting, H_2O_2 synthesis, nitrogen fixation, and VOC degradation, despite reports based on plasmonic systems like Ag for CO_2 reduction. Plasmonic catalysis occupies a small proportion in photocatalytic systems, requiring expanding monitoring to metal/semiconductor and pure semiconductor systems, necessitating improved sensitivity of semiconductors to match the activity of metal substrates during the evolution of small molecules, such as CO_2, H_2O, and O_2. Recently, Ye et al. developed ZnO@ZIF-8 based on core−shell structures,[293] achieving detection of toluene based on

https://doi.org/10.1021/acsnano.4c06192
ACS Nano XXXX, XXX, XXX−XXX

nonchemical adsorption. This strategy utilizes the MOF shell to extend the electromagnetic field enhancement region generated on the ZnO surface, simultaneously enriching and analyzing molecules, thus enhancing detection of volatile organic compounds through nonchemical adsorption. This strategy holds the promise of enabling the application of nonplasmonic resonance substrates in catalytic monitoring in a way similar to the SHINERs strategy.

PIERS—Monitoring Oxygen Vacancies in Semiconductors. Further exploration of the metal−semiconductor interface involves electrochemical and catalytic systems based on defected metal oxides, where charge diffusion, injection, and extraction are influenced by the presence of point defects, such as oxygen vacancies and interstitial ions. Establishing a correlation among oxygen vacancies and catalytic activity under practical working conditions is challenging, particularly in photocatalytic reactions where oxygen vacancies can act as dynamic active sites on the photocatalyst surface.[294] In 2016, Ben-Jaber et al. observed a transient signal boost for various Raman reporters, beyond that of typical SERS, induced upon high energy UV light irradiation of metal−semiconductor hybrid materials.[295] The effect was termed as photoinduced enhanced Raman spectroscopy, or PIERS, and it was originally correlated with the formation of surface oxygen vacancies. The PIERS boost would last up until surface healing in contact with air.[284,296,297]

The mechanism of Raman enhancement has been closely studied over recent years with a wide variety of scanning probe,[298] time-resolved optical and X-ray techniques.[299] Despite the popularity of band alignment arguments (MLCT/LMCT), Simpson and co-workers showed a change in polarizability of the surface bound analyte on irradiation, enabled by photoinduced electron transfer, as a key factor for PIERS enhancement.[299] Brognara et al. proposed an additional mechanism for systems containing metal nanoparticles embedded in the semiconductor, attributed to the narrowing of the depletion zone after UV irradiation, with creation of Ti^{3+} defects.[300] Dagdeviren et al. studied how the dynamics of hole migration are influenced by photoinduced oxygen vacancies.[298,301] These and other mechanistic studies have led to further work on how to optimize the geometry and construction of PIERS substrates to best couple the metal and semiconductor with oxygen vacancy creation for a long lasting defected (Raman enhancing) state.

While the utility of this method for measuring trace levels of analyte with high sensitivity is now widely recognized,[302] attention has turned to PIERS's utility in analyzing the semiconductor substrate itself.[303,304] The use of an analyte on metal nanoparticles deposited on a semiconductor and probed by PIERS enables the study of defect dynamics in a range of different metal oxides (TiO_2, WO_x, ZnO, SnO_2, and many others have been assessed).[296,297] Glass and co-workers used PIERS to correlate formation and lifetime of oxygen vacancy concentrations and photocatalytic behavior of standard ZnO thin films and TiO_2 nanoparticles. It was found that there was a "goldilocks zone" where oxygen vacancies were most long-lived and gave the highest substrate activity.[45]

Future studies may examine oxygen-vacancy induced material behavior beyond catalysis, such as ferroelectric properties.[305] Major technical developments in the use of Raman spectroscopy as an exploratory technique of catalytic systems under in situ/in operando conditions have been reviewed recently. Beyond metal oxides, organic semiconductors,[306] as well as MXenes[307] and metal−organic frameworks (MOFs) have also been shown to undergo a PIERS like effect,[308] and similar enhanced Raman approaches may well enable study of these exciting nonoxide catalytic materials in future.

11. EMERGING TOPICS IN SERS FOR ENERGY CONVERSION—PERSPECTIVES

In this final section, we intend to highlight emerging directions in energy conversion for which SERS could prove a relevant tool, from lithium-ion batteries to single atom catalysts and chiral catalysis. Therefore, this section not only reviews the existing literature but also addresses future perspectives for SERS in the field of energy conversion.

11a. Machine Learning-SERS for Catalysis. Machine learning (ML) has conquered most areas of science, offering powerful tools for data analysis, pattern recognition, and predictive modeling that are promising in addressing complex scientific challenges in multiple domains.[309−312] For instance, ML is utilized to predict chemical properties,[313,314] identify and characterize (nano)materials with desired properties,[312,315,316] and optimize chemical synthesis to accelerate organic and inorganic material discoveries for applications in energy, catalysis, and pharmaceutics.[290,312,317,318] In brief, supervised and unsupervised learning are two fundamental approaches in ML with different techniques, goals, and prospective applications. In supervised learning, the algorithm learns from labeled data, where each example in the training data set is associated with an input-output variable pair and then deduces a mapping function from the input (features) to the output (labels). Supervised classifiers or regressors predict either a discrete label or a continuous value. In unsupervised ML models, the algorithm learns from unlabeled data to elucidate hidden patterns, structures, or relationships in the data. They include clustering, which groups similar data points; dimensionality reduction, which reduces features while preserving important information; and association rule learning, which discovers relationships between variables. For catalysis, ML-driven SERS aids in understanding 1) reaction mechanism by extracting chemical information, 2) dynamics and kinetics by linking chemical and temporal information, and 3) catalyst structure−reactivity relationships using chemical and spatial information, significantly reducing the laboratory toil hours needed for trial and error (Figure 13). We discuss the synergistic role of ML in these three approaches below and the ultimate goal of realizing a predictive model to predict catalytic reactions.

Elucidating Reaction Mechanisms with SERS and Machine Learning. SERS can be employed to elucidate reaction mechanisms in catalysis by unraveling intricate chemical information; however, the SERS signal is often low and noisy due to the low abundance of chemical intermediates or products, especially at the detection limits.[290,319] ML's ability to efficiently denoise,[320] demix,[321] resolve spectral overlaps,[322] and extract molecule-specific information[323−325] from complex multiplex spectra, can help to automatically identify and quantify intermediates/products in catalytic reaction mixtures and push the limits of detection.[326−328] Critically, this fundamental capability to analyze complex, noisy, and multiplexed SERS spectra is central to ML's utility in addressing the challenges in catalytic reaction monitoring. By building a robust database from experimental data, density functional theory, or both, we can construct an ML model to identify rapidly and accurately "known" and "unknown" reaction intermediates or products. In this aspect, "known" chemical species are those whose spectra are trained in the ML model and can be automatically classified,

https://doi.org/10.1021/acsnano.4c06192
ACS Nano XXXX, XXX, XXX−XXX

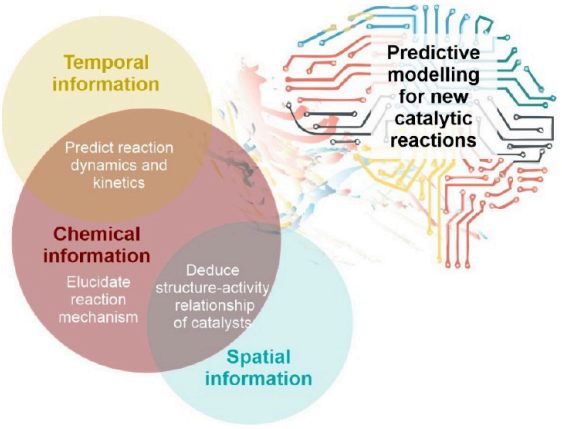

Figure 13. Machine-learning-enabled surface-enhanced Raman scattering for catalysis: using machine learning in SERS for predictive modeling of catalytic reactions through elucidating reaction mechanisms, understanding reaction dynamics and kinetics, and deducing structure−activity relationships of catalysts.

given their spectra. Such ML-driven SERS applications have been implemented in the trace detection of ions, small molecules, and structural analogs.[322,323,327,329,330] Besides identifying "known" species, a hierarchal SERS-based ML framework has been used to identify "unknown" species whose spectra are not trained in the model and elucidate their chemical structure.[331] Such forward predictive capability in SERS is critical for comprehensive interrogation and identification of the full panel of intermediates and products participating in the catalytic reactions, even those we do not anticipate to be present, to elucidate reaction mechanisms.

Understanding Reaction Dynamics and Kinetics with SERS and Machine Learning. ML can also be used to understand reaction dynamics and kinetics for reaction optimization by synergizing temporal and chemical information in time-resolved SERS spectra. SERS has been demonstrated to track the structural evolution of surface species in real-time in millisecond-time-resolved SERS studies of electrochemical redox processes[332] and carbon dioxide reduction reactions on copper electrodes.[43] Moreover, cross-correlation analysis made it possible to follow the evolution of groups of vibrational modes belonging to a particular chemical species and even observe their transient resonance forms.[333] Evidently, time-resolved SERS of interest to catalysis and since most of the time-resolved SERS data can be presented in the form of colormaps, convolutional neural networks (CNN) could be a good ML tool as they are generally successful at image processing.[334] Furthermore, ML-SERS has the potential to monitor the reaction progress and deduce the reaction kinetics. Recently, it was shown to simultaneously identify eight metabolite gradients from cell surfaces.[335] This can be translated to the identifying product mixture gradients near catalytic surfaces, and given that the rate of diffusion of the various analytes can be calculated, probabilistic ML models can be employed to elucidate the reaction rates.

Structure−Activity Relationships of Catalysts with SERS and Machine Learning. Besides spectral analysis, ML-driven SERS/TERS can provide invaluable spatial and chemical information about the catalytic surfaces and interfaces to unlock structure−activity relationships and build better catalysis materials.[336,337] Specifically, ML can correlate the spatial and chemical information in SERS/TERS spectra to identify the 1) electronic states of surface ligands, 2) physical phenomena that affect catalyst behavior, 3) dynamic changes to the catalyst structures and active sites, and 4) compounds that contribute to the catalyst poisoning effect. For instance, the molecular structure and the interface between the molecule and the conducting lead or catalyst are critical in molecular electronics and electrocatalysis. Fishing-mode TERS was demonstrated to successfully probe the molecule−metal−molecule junction during electron transport.[338] This is especially informative for chaotropic/cosmotropic surface agents in emerging water-splitting nanoelectrocatalysis.[339] We postulate that ML can accelerate the electron transfer rates vs. structure calculations using TERS data as input to simultaneously provide chemical and conductance information that can be related to the catalytic activity. This is because ML has been demonstrated to speed up the calculation of electron transfer,[314] hot electron lifetimes,[340] as well as the valence electron density and its relationship to the optical properties of plasmonic structures,[341] which are important in plasmonic catalysis. Recently, a ML framework was developed to predict compressive strain with site-specific precision, rationalizing how strain on Pt core−shell nanocatalysts can enhance oxygen reduction reactions.[313] Moreover, operando−TERS/SERS mapping can track the dynamic compositional,[342] topological,[343] and structural changes[43,342] to the nano/microstructure of catalytic surfaces as the reaction progresses, including identifying local defects and observing dynamic restructuring of surfaces. Similarly, shell-isolated nanoparticle-enhanced Raman spectroscopy revealed the surface-selectivity of hydroxide adsorbates to single crystal facets, where Au(100) < Au(110) < Au(111), which is inversely correlated to the oxygen reduction reaction (ORR) activity, leading to the postulation that hydroxide ions formed on the catalytic surface retards the ORRs.[344] Incorporating ML for rapid correlation and interpretation of TERS/SERS data in real-time can yield the relationship between the structure−reactivity and surface-selectivity to provide real-time feedback at every step of the way to better guide catalyst performance optimization.

Predictive Modeling on Catalytic Reaction Design. Currently, a vast majority of catalysts and their reaction performance are tested and discovered via trial-and-error methods, which lack predictability even for domain experts.[43,339,345] We envision that ML capable of multicorrelational analysis can be trained on a variety of data, including SERS/TERS, to build generalizable and comprehensive predictive models for catalysis in terms of catalyst design and reaction outcomes, including rates, yield, and selectivity. At present, ML has achieved some success in adjacent fields to discover catalysts or rediscover catalysts with certain compositions with optimal performance. For instance, ML trained on density functional theory data discovers that the Ni−Ni bond length is the main descriptor linked to hydrogen evolution reaction activity, highlighting that nonmetal dopants that induce a chemical-pressure-like effect on the Ni_3-hollow sites impact its reactivity.[346] Moreover, a promising ML-augmented chemisorption model trained on ab initio adsorption energies predicts [100]-terminated multimetallic alloys with improved efficiency and selectivity for CO_2 electrochemical reduction to C_2 species.[347] Similarly, an ML model can be trained to identify spectral features and/or anomalies using time-resolved and operando SERS data obtained in real-time during catalytic reactions and then rank the spectral feature in order of importance to deduce the most essential reaction parameter

https://doi.org/10.1021/acsnano.4c06192
ACS Nano XXXX, XXX, XXX−XXX

that experimentalists should focus on optimizing. This data-driven approach allows an objective and holistic understanding of reaction pathways, dynamics, kinetics, and catalyst performance to facilitate high-throughput catalyst and reaction screening. Once rigorously cross-validated with new and old experimental data from the literature, comprehensive predictive models can be used to predict catalytic reactions.

11b. SERS for Single Atom Catalysis. Single atom catalysts (SACs) are a class of catalytic materials that have gained recent interest, wherein the active catalytic site is atomically dispersed in or on a host.[106] While this definition could also describe Bronsted acid sites in zeolites, recent interest has primarily focused on atomically dispersed late transition metal active sites that have historically been studied in the form of active sites on nanoparticles and extended surfaces. The excitement surrounding SACs derives from the potential to maximize precious metal utilization efficiency and control reactivity by engineering the coordination environment of the active site.[348,349] Realizing this potential requires synthetic approaches to control active site structures and characterization tools that facilitate the development structure−function relationships.[350] SACs have been applied for range of chemical conversions as thermocatalysts, photocatalysts, and electrocatalysts, and thus the composition of SACs is variant in terms of the active site and support.[351] It is interesting to consider how and where SERS characterization of adsorbed molecules could contribute to the field of SACs.

For SACs consisting of precious metal active sites on oxide supports, focus has been given to the development of characterization tools that can detect small quantities of metallic clusters that could drastically influence reactivity.[352,353] SERS could be applied using probe molecules to identify the existence of metallic clusters and single atoms by differentiating the vibrational fingerprints of molecules bound at these different types of sites with different structures and oxidation states. The challenge is the lack of electromagnetic field enhancement for oxide-supported single metal atoms. This has been addressed by SHINERS that contain single atom active sites localized in the near fields of plasmonic antennas.[108,261,354] For example, the existence of Pd nanoparticles and/or single atoms on Pd/TiO_2 catalysts (deposited on Au nanoparticles) was characterized using phenyl isocyanide probe molecule SERS, Figure 14. Further, this SHINERS approach was used to assess differences in reactivity of Pd atoms and nanoparticles by in situ measurements of the conversion of p-NTP to p-ATP.[261] Interestingly, similar nanostructures have been adopted for plasmon photocatalysis and have been called "antenna-reactor" photocatalysts, suggesting that SERS may be inherently (requiring no additional material modifications) useful for studying the structure and reactivity of such systems that contain single atom active sites.[355]

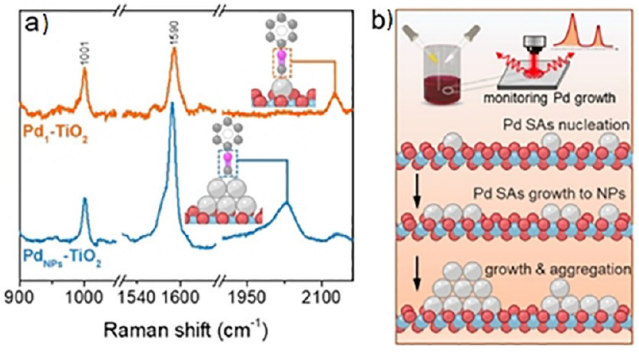

Figure 14. Surface-enhanced Raman scattering for monitoring single atom catalysis. a) SHINERS spectra of phenyl isocyanide (PIC) adsorbed on Pd SAs and NPs. b) Illustration of Raman studies of the growth of Pd species from SAs to NPs. Figure reprinted with permission from ref 261. Copyright 2021 Wiley.

There are classes of SACs that should be well suited for characterization via SERS. For example, it was reported that Au single atoms on amorphous C_3N_4 supports can exhibit 10^4 enhancements in SERS signals for adsorbed molecules, which was attributed to the local environment enhancing the polarizability of molecules.[356] Furthermore, single atom alloys (SAA) are a class of catalysts where late transition metal atoms (e.g., Pd, Ni) are alloyed into coinage metals (e.g., Ag, Au, and Cu) hosts at dilute quantities, such that the transition metals are atomically dispersed. SAAs offer interesting reactivity and selectivity for a wide range of reactions and inherent SERS activity as they are typically composed of coinage metal nanoparticles.[357]

Given the potential impact of SERS measurements for either characterizing the structure of SAC active sites (via probe molecule measurements) or reaction mechanisms on SACs (via in situ studies), it is interesting to consider why this tool has not been widely adopted. This is likely due to broad success of FTIR spectroscopy for similar studies as could be performed with SERS, the familiarity of the heterogeneous catalysis community with FTIR and the applicability of FTIR based characterization for most SACs materials (i.e., signal enhancement is not needed).[358] This suggests that SERS will most likely be used for characterizing SACs in circumstances in which FTIR fails. SAC applications requiring low concentration sensitivity (extremely low metal loading catalysis or low concentration adsorbed species),[359] operation in aqueous media as is common for electrocatalysis and environmental catalysis,[360−363] and for SACs with inherent signal enhancement seem most prime for characterization via SERS.

11c. SERS in Photocatalysis for Sustainability. It was recently demonstrated that plasmon-enhanced photocatalysis can provide technologically viable solutions for a range of important reactions, such as hydrogen production and release,[364,365] destruction of toxins,[366] and decomposition of environmentally undesirable chemicals.[345,367] The fundamental reason for the advantages of this strategy is that the plasmon excitation heats only the electrons in the system, which are mediators of bond dissociation and associative recombination in chemical transformations. While the highly nonequilibrium state of hot carriers only lasts for a few picoseconds before thermalization, resulting in heating, this time period is sufficient for initializing the bond-transformation process in chemical reactions.[347] The recent development of the antenna-reactor plasmonic photocatalyst provides a path for modular systematic optimization of photocatalytic processes.[368] In the antenna-reactor geometry, light harvesting is accomplished by a plasmonic nanoparticle: typically a noble or simple metal with good plasmonic properties but inert to most reactants. Through near-field coupling to an adjacent reactor particle made of a material with an affinity for the reaction of interest, the excited antenna channels energy into the reactor particle, enhancing its catalytic activity. This antenna-reactor geometry has recently been demonstrated in highly efficient chemical reactions of direct importance for society.[364,365,367]

https://doi.org/10.1021/acsnano.4c06192
ACS Nano XXXX, XXX, XXX−XXX

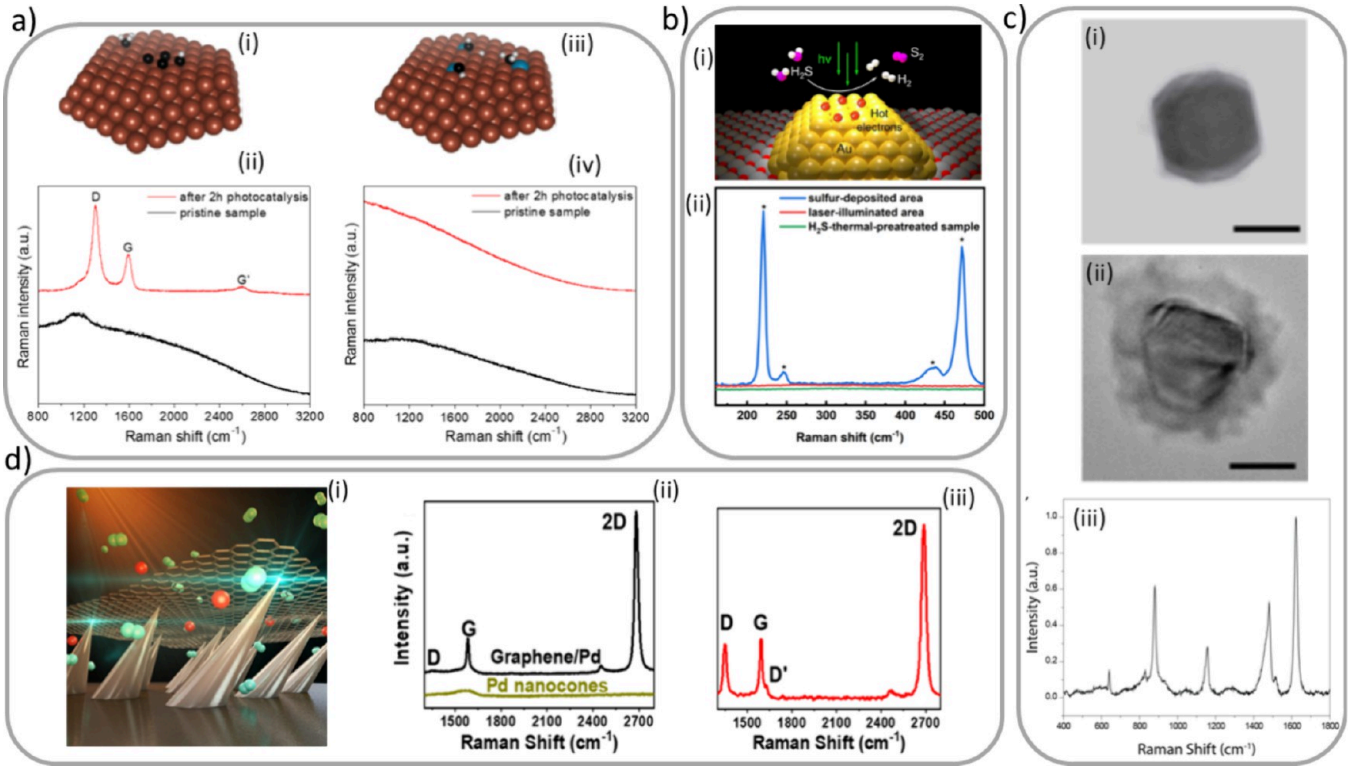

Figure 15. Surface-enhanced Raman scattering for monitoring a catalyst's composition. a) (i) Schematic of the compositional dependence of the Cu_xRu_y photocatalyst with respect to coke resistance: pure Cu. (ii) Raman spectra of pure Cu photocatalyst at the spot of light illumination before (black lines) and after (red lines) 2 h photocatalysis under 19.2 W·cm^{-2} white light illumination. (iii) Schematic of the compositional dependence of the Cu_xRu_y photocatalyst with respect to coke resistance: low Ru loading. (iv) Raman spectra of $Cu_{19.9}Ru_{0.01}$ photocatalyst at the spot of light illumination before (black lines) and after (red lines) 2h photocatalysis under 19.2 W·cm^{-2} white light illumination. b) (i) Schematic showing the Au plasmonic photocatalyst for the H_2S dissociation reaction. (ii) Raman spectra of the catalyst bed after photocatalysis in the sulfur-deposited area (blue) and laser-illuminated area (red). Peaks with * label is consistent with the in-plain movement of the S−S bonds in γ-S8. A control group of catalyst that was annealed in H_2S at 573 K for 60 min was also measured (green). c) (i)Transmission electron micrograph (TEM) image of single Al NC with the native oxide layer observable around the edge of the particle. (ii) TEM image of single Al NC@MIL-53(Al). (iii) Raman spectrum of Al@MIL-53(Al). d) (i) Schematic of graphene on a field of Pd nanocones. (ii) Raman spectra of pristine monolayer graphene on top of Pd nanocones (black line) and bare Pd nanocones (dark yellow line). Characteristic G and 2D peaks of graphene are observed, together with a very small D band. (iii) Raman spectra of the hydrogenated graphene on a representative spot where a significant increase of the D band is observed. Figure adapted with permission from refs 364, 372−374. Copyright 2020 Elsevier, 2019 and 2022 American Chemical Society, 2019 The American Association for the Advancement of Science.

Most chemical reactions proceed through a variety of intermediate steps. The optimization of a catalyst will involve selecting the ideal catalyst for each of these steps: a difficult task. Many of the intermediate states may be radicals or transient negative ion states or weakly bound species. The overall efficiency of the catalyst determines how the intermediates interact with the catalyst surface. Here SERS can play a crucial role in identifying the intermediate steps, aiding in the selection of the right catalyst for a given reaction. The catalyst does not have to be a single substrate. In a recent experiment, we demonstrated that a trimer, consisting of an "antenna" particle surrounded by two reactor particles consisting of two distinct materials, an iron and a Pd nanoparticle, provided a highly efficient substrate for hydrogen exchange in ammonia.[369] Here the Pd reactor provided the Hydrogen, while the Fe provided the binding site for ammonia. This simple reaction provides direct evidence of the importance of optimizing the catalyst for all relevant intermediate reaction steps. SERS can play a central role in determining these aspects of catalytic antenna-reactor design.

For chemical reactions that are highly relevant to the energy transition and to green, decarbonization chemistry, SERS can provide useful insight into the identification of reaction pathways, the development or suppression of side reactions, and the extent to which photothermal effects contribute to the overall reactivity of a plasmonic photocatalyst for a specific chemical reaction of interest. For example, SERS is particularly useful in identifying reaction products in plasmonic photocatalysis, particularly for species that remain bound to the photocatalyst following a chemical transformation.[367] Time-resolved SERS can be used to study chemical reactions in real time, to elucidate reaction mechanisms of photocatalytic transformations on surfaces.[370] Stokes and anti-Stokes analysis provides real-time thermometry, which, when applied to molecules on surfaces, enables the detection of energy transfer processes at time scales not yet achievable by other experimental methods.[371]

The most important reactions for the transition to the Hydrogen economy involve creating Hydrogen inexpensively from resource-abundant sources, such as methane, CO_2 and H_2S. These chemicals are also highly deleterious to the environment, as potent greenhouse gases. Plasmonic photocatalysts offer a path toward cheap Hydrogen, using high-efficiency light sources (such as light-emitting diodes, LEDs) as opposed to fossil fuels for thermal reactions at high temper-

https://doi.org/10.1021/acsnano.4c06192
ACS Nano XXXX, XXX, XXX−XXX

atures.[367,375] For these three molecules, the catalyst design involves some specific challenges. Both carbon and sulfur can bind to the reactive surfaces, polymerizing and poisoning (S) or coking (C) the catalyst surface, preventing the catalytic process from proceeding. In the development of an optimized catalyst for these reactions, it is crucial to monitor the presence of these types of impurities. SERS has been successfully used in several applications involving these reactions. In methane dry reforming, SERS was used to quantify the degree of coking on catalysts of various compositions, leading to the conclusion that the optimal stoichiometry of the catalyst involves single-atom reactive sites (Figure 15a).[364] SERS was also used to identify the reaction mechanism in a recent photocatalytic decomposition of H_2S for Hydrogen production (Figure 15b).[367] SERS can also be used to verify the composition and integrity of the catalyst. In a recent study of the catalysis promotion properties of a metal−organic framework (MOF) grown on a plasmonic Al nanocrystal antenna, SERS was used to accomplish this goal (Figure 15c).[373] Finally, we highlight the use of SERS in identifying the outcome of a plasmon-induced chemical reaction: the hydrogenation of graphene (Figure 15d).[372] This is an important step in the development of graphene as an electronic material. The hydrogenation of graphene introduces a bandgap, requisite for device functionalities. Changes in the Raman signature of graphene before and after hydrogenation provide a clear signature of this chemical transformation.

A less commonly used variant of SERS is surface-enhanced coherent antistokes Raman spectroscopy. With an intensity scaling as $|E|^8$ of the local field enhancement, a properly designed substrate can easily provide single-molecule sensitivity, even for nonresonant molecules.[376] This approach would be ideal for studying chemical reactions at the single-molecule level, allowing for intermediate steps and conformational changes as reactions progress, driven by incident light or temperature.

Finally, we note that SERS may not be a nonperturbative probe of adsorbate molecules in photocatalysis or as a general approach for chemical sensing. As is well-known, plasmon excitation results in hot carrier generation.[347] These hot carriers can chemically modify the analyte. For instance, hot carriers can incite vibrational pumping,[377] leading to an artificially enhanced effective temperature of the adsorbate. Hot carriers can transfer into the analyte/adsorbate and induce chemical transformations, which could drastically change the cross section of the various vibrational modes. The magnitude of these changes could be quite large and would be physically indistinguishable from the "chemical effect" discussed in previous studies. Hot carriers can also desorb the analyte, resulting in lower analyte concentrations at the surface and thus a reduced SERS signal compared with the results obtained under passive (non-plasmonic) illumination conditions.

11d. SERS in Batteries: Operando Monitoring and Reactions at Interfaces. The control/taming of interfaces and of electrode/electrolyte interfacial processes in electrochemical energy storage devices is key to the development of new-generation batteries (Li-ion (LIB) but also Na-ion (NIB), aqueous Zn-ion, Li-metal, Li−air, Li−S, All-solid-state, etc.). The operation and performance of LIB relies on the formation of stable semipassive layers on the surface of the electrodes upon contact/polarization with anhydrous organic electrolytes. The high voltage operation of LIB, ca. 4.5 V, beyond the stability window of the electrolyte, triggers oxidative and reductive decomposition reactions of the electrolyte components (organic carbonate solvent mixture and $LiPF_6$ salt) at the electrodes surface. This results in surface precipitation as a multilayer inorganic/organic film with components randomly distributed over the surface ("mosaic" model[378]), the so-called solid electrolyte interphase (SEI), which acts as an effective barrier to the electron transfer to the electrolyte. The characterization of the SEI (ex situ, in situ, operando) has been the focus of intense research efforts[379,380] because its structure, composition and formation/dissolution dynamics are strongly dependent on the electrode material, on the electrolyte, and on the operating voltage of the electrode. The Raman characterization of the thin battery interfaces under LIB cycling conditions has been achieved first on silver[381,382] and gold[383,384] electrodes, then using various SERS configurations.[385,386,18] Although various interfacial events have been captured with SERS (e.g., electric double layer (EDL) formation, Li accumulation, Li (de)-solvation[383,387] or formation and dissolution of species[385]), the demonstration of operando SHINERS in 2014[388,389] to assess compositional SEI dynamics was a game changer, both in terms of chemical inertia and tunable sensitivity under the experimental conditions specific to LIB operation. Since then, only a handful of studies have been conducted on both negative and positive electrodes,[390−395] the operando monitoring of thin and buried interfaces in LIB systems being particularly challenging.

As for any other operando experiment, the main concerns regarding the use of enhanced Raman (ER) for the characterization of interfacial processes are (i) the implementation under realistic conditions, i.e., as close to actual battery systems, (ii) the possible interference of the ER platform with the studied systems (photothermal damages, chemical interferences), and the translation of the Raman signature into chemical information especially at thick multilayer interfaces whose structure evolves with time.

Strategies for "unburying" interfaces in LIBs (i.e., to increase the ER sensitivity) while maintaining realistic operating conditions need to be pursued. The design of the spectro-electrochemical cell is of paramount importance in LIBs as the ratio of electrolyte volume to electrode area (i.e., flooding factor) is known to impact dramatically affect the very nature and extent of the interfacial processes.[393] Successful SHINERS studies have been reported in small volume cells both on the back (window) side[390,394−396] and on the front (separator) side of the electrode[388,389,392,393] on relatively flat electrodes (thin films or flattened composites). Interfaces can also be virtually unburied, by boosting the signal intensity originating from the interface while minimizing the Raman signal of the underlying electrode material (high Raman cross-section materials such as graphite, amorphous carbon, or TMOs) and most importantly the fluorescence background signal of the LIB baseline electrolyte (e.g., 1 M $LiPF_6$ salt in organic carbonate solvent mixtures). To this aim, near-infrared (NIR) excitations (785 nm)[392,393,396] should be combined with aggregates of SHINs on the electrode surface to create a large number of hot-spots.[397] Suitable NIR plasmonic resonators (large anisotropic SHINs with sharp tips, e.g., bipyramids[199]) and optimized SHIN deposition processes (wet[8,9,14,15] or dry[392]) may be desirable to achieve higher sensitivities. It has not yet been established whether mixing SHINs with the electrode slurry (carbon conducting agent, polymeric binder, and active material) would be beneficial on composites. Methods that can be applied to powders of active materials[385] without additives should also be pursued.

https://doi.org/10.1021/acsnano.4c06192
ACS Nano XXXX, XXX, XXX−XXX

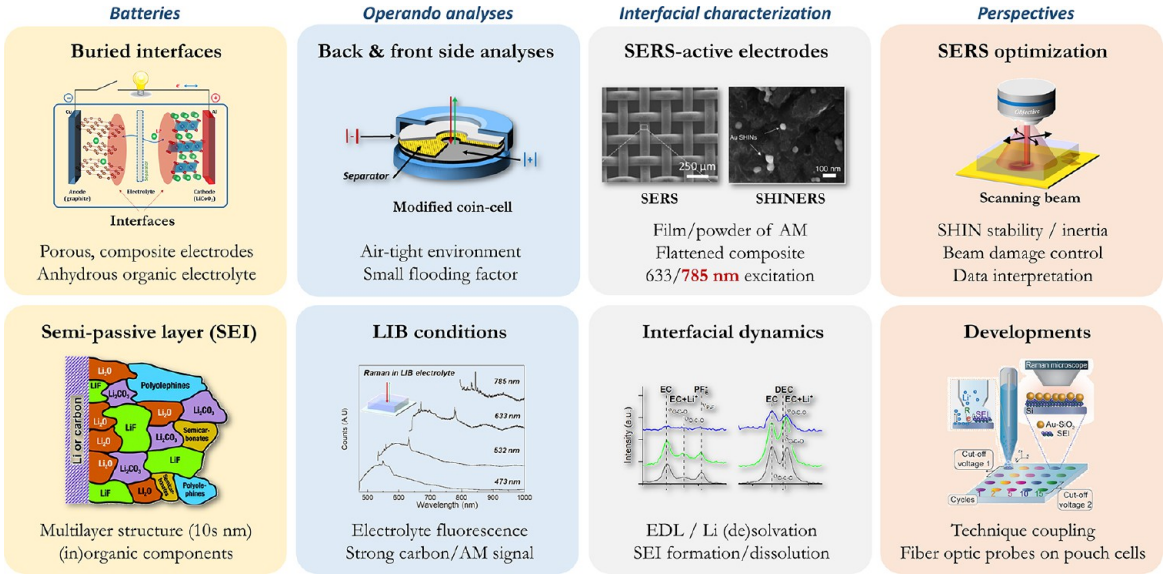

Figure 16. SERS in batteries. From left to right: A typical battery assembly (Li-ion),[406] the mosaic model of the solid electrolyte interphase (SEI) as proposed by E. Peled in 1997 as found on negative (but also positive) electrodes,[407] a typical spectro-electrochemical cell with small electrolyte volume for LIB characterization, the overlapping Raman and fluorescence signal (background) of baseline LIB electrolytes,[393] examples of SERS platforms proposed for LIB interfacial analysis, Li (de)solvation processes observed upon (dis)charging,[383] scanning Raman probes proposed to minimize beam damages at the electrode/electrolyte interface,[393] coupling of SHINERS and scanning electrochemical microscopy for fast screening of new battery material candidates and SEI formation cycling protocols.[405] Adapted or reproduced with permission from ref 406, Copyright 2013 The American Chemical Society; ref 408, Copyright 2018, Royal Society of Chemistry; ref 393, Copyright 2021 The American Chemical Society; ref 18, Copyright 2020, The American Chemical Society; ref 392, Copyright 2020 The American Chemical Society; ref 383, Copyright 2020 The American Chemical Society; ref 405, Copyright 2022 Wiley under a Creative Commons CC BY license.

Due to the multilayer structure of the SEI and its thickness, which is comparable to SHIN dimensions, SEI components cannot be resolved across the SEI, unless SHINERS is combined with SERS (see depth-sensitive plasmon-enhanced Raman spectroscopy DS-PERS[396]). Post mortem analyses of cycled electrodes have revealed SHINs either floating-like on the SEI or embedded within thick SEIs,[393] challenging the interpretation of real-time analyses of SEI composition and of its evolution upon cycling. Importantly, extinction of the SHINERS signature can be observed when thick SEI developed (e.g., Sn in contact with EC, EMC $LiPF_6$[393]) and may deserve further attention. Although a detailed composition of the SEI with SHINERS seems difficult to establish, its application for the detection of specifics events is still relevant (e.g., formation of soluble compounds,[393] reduction mechanism related to electrolyte additives[394,395]). For an unbiased interpretation of the interfacial signatures, the systematic use of chemometrics (e.g., principal component analysis (PCA)) on large data sets as well as spectral databases of synthetic analogues of (in)organic SEI components should be privileged to avoid the propagation of misconceptions in the field (see the SEI identity crisis related to LEMC and LEDC components[398,399]).

As mentioned above, the SEI chemistry is strongly material dependent (very distinct dynamics of SEI compositions[393] have been observed on gold and tin electrodes decorated with Au@SiO_2 SHIN), but the actual SHIN chemical inertia under LIB conditions especially during long-term cycling, is a recurring question that has not yet been fully addressed. Dissolution of silica can be expected in the LIB baseline electrolyte especially at elevated temperatures,[400,401] due to the generation of HF upon decomposition of the PF_6^- salt anion. The possible reactivity at very negative polarization of the SHIN in intimate contact with the electrode (despite the high contact resistance), is also a recurring question as SiO_x is known to be as an efficient alternative to the silicon electrode in LIB.[402]

Finally, the liquid electrolytes used in LIB are not only highly volatile but also air- and water-sensitive and prone to beam damage (photothermal degradation), causing artificial SEI on the electrode surface, especially at hot-spots. The combined effect of illumination and electrical polarization at large negative or positive potentials may further enhance this process. Methods to control of beam damage (e.g., scanning beam[393]) should be developed, and dose thresholds of LIB electrolytes established.

The development of SHINERS applied to the characterization of LIB interface is still at its infancy, and the possible interference of the SHINERS probe (SHIN stability in LIB conditions, beam damage at the electrolyte/electrode interface) remains to be addressed especially in long operando experiments. The second major challenge concerns the interpretation of the SHINER signatures given the complicated and evolving structure of the SEI (mosaic, multilayer structure) and the comparable dimensions of the SHIN (or SHIN aggregates) and the lack of spectral database for the (in)organic components of the SEI (Figure 16). There is no doubt that SHINERS will continue to grow in the coming years together with other operando tools, studies coupling optical fibers[403,404] with SHINERS to access operando characterization of real battery packs (pouch cells) or coupling SHINERS with complementary analytical techniques (electrogravimetry,[383] microscopy[405]) for accurate interfacial depiction or for rapid SEI composition screening[405] can be expected.

11e. Chiral Catalysis Monitored by SERS. Precise control and accurate monitoring of molecular stereochemistry during a chemical reaction are of paramount importance, particularly in

https://doi.org/10.1021/acsnano.4c06192
ACS Nano XXXX, XXX, XXX−XXX

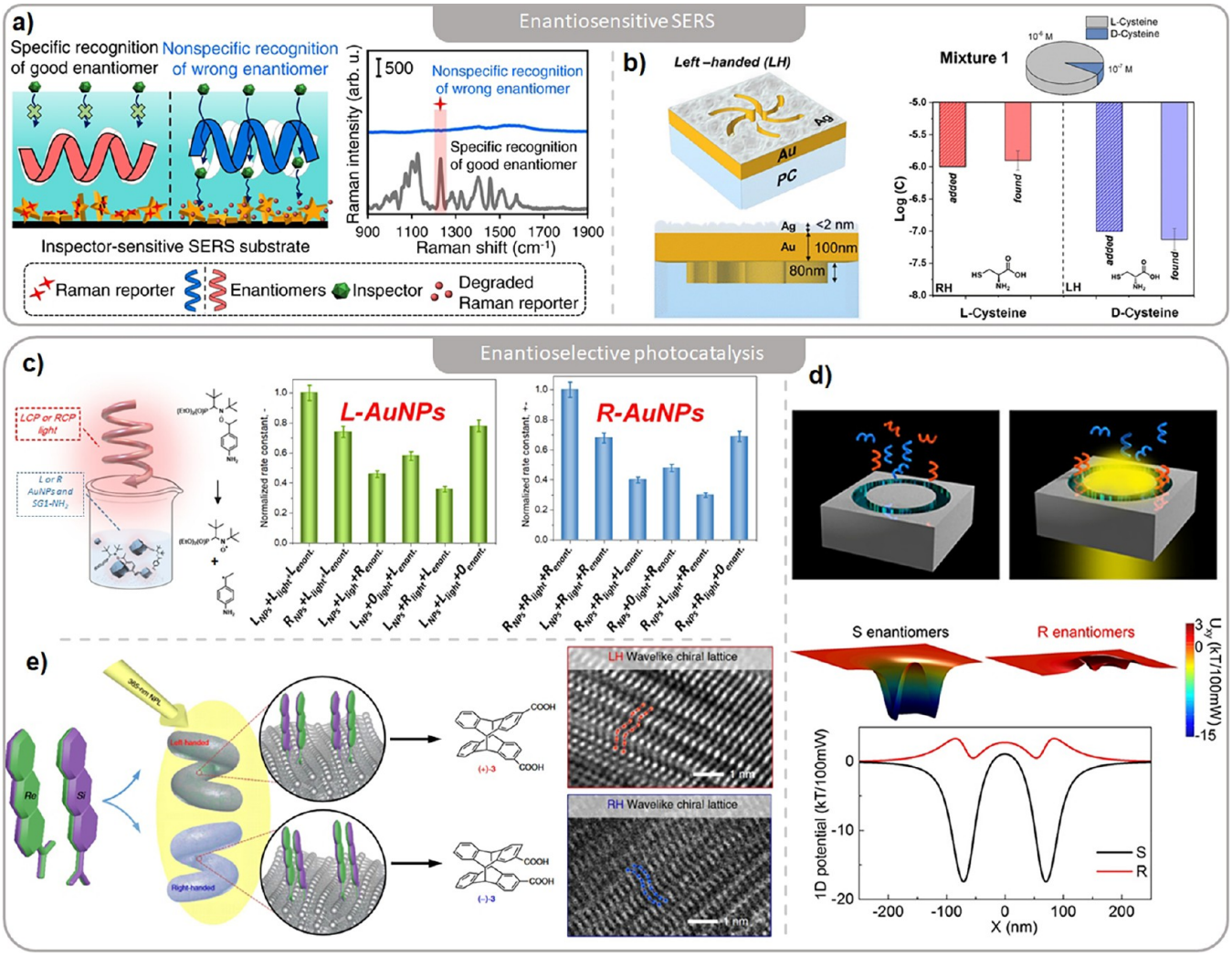

Figure 17. Examples of enantiosensitive SERS techniques and enantioselective photocatalytic strategies. a) Principle of an inspector recognition mechanism (IRM) implemented on a SERS chiral imprinted platform. Filled cavities block the inspector to access the Raman reporter on the substrate.[411] b) (Left) Schematic description of plasmon-active SERS substrates with coupled chiral active shuriken and cluster-like Ag layer, which exploits the interaction between near-chiral field and molecule for differentiating the enantiomers. (Right) Example of enantiomers content determination in L/D-cysteine mixtures using measurements on LH- and RH-S3/Ag SERS substrates, contrasted with the known concentrations in the sample.[412] c) (Left) Using CPL and chiral plasmonic nanoparticles to enantioselectively initiate the homolysis of a chiral organic probe (alkoxyamines) and the formation of radicals (Left, bottom). (Right) normalized reaction rate constants, obtained via utilization of L- or R-AuNPs, L- or R-light polarization (or nonpolarized light, labeled "0"), and different organic probes (with "0" labeling samples with negligible optical activity.[427] d) (Top) Schematic diagram of the enantiselective optical trapping combining coaxial plasmonic apertures and CPL. (Bottom) Trapping potentials for the enantiomers in a cavity under light-handed CPL.[429] e) (Left) Schematic illustration of the photocyclodimerization of 2-anthracenecarboxylic acid mediated by metal NHs. (Right) HRTEM images of the surface of LH-AgNHs and RH-AgNHs with a pitch of ∼5 nm, with colored dot overlay indicating the wavelike chiral lattices affecting the dimerization.[432] Adapted or reproduced with permissions from ref 411, Copyright 2022 Springer Nature under a Creative Commons CC BY license; ref 412, Copyright 2023 The Authors, Royal Society of Chemistry under a Creative Commons CC BY license; ref 427, Copyright 2023 American Chemical Society under a Creative Commons CC BY license; ref 429, Copyright 2016 American Chemical Society; and ref 432, Copyright 2020 Springer Nature.

organic chemistry and drug development. This becomes crucial when handling chiral compounds within a biological or medical framework because different enantiomers of the same compound may exhibit completely different effects within an organism, often with one enantiomer being curative and the other extremely toxic. These effects are directly connected to the homochiral properties inherent in most biomolecules that are crucial for life on our planet. In this context, enantioselective catalysis is required to synthesize compounds with the required handedness as well as having reliable and sensitive techniques to monitor the enantiomeric ratio of products in a reaction. For the latter purpose, SERS emerges as a promising avenue. Renowned for its exceptional sensitivity and selectivity, SERS offers a versatile platform that can be effectively utilized for enantiomeric discrimination. This is often achieved by using plasmonic substrates decorated with chiral molecules, which act as enantioselective sites.[409] However, ongoing research has demonstrated enantiomeric discrimination without chiral molecular linkers, e.g., using tailored substrates with enantioselective adsorption (Figure 17a),[410,411] or analyzing the distinct optical response of molecules under plasmonic near-fields with strong optical chirality (Figure 17b).[412,413] The former of the two requirements listed above, i.e., controlling the stereochemistry of products, simply invokes the study of asymmetric

https://doi.org/10.1021/acsnano.4c06192
ACS Nano XXXX, XXX, XXX−XXX

synthesis, a rich field of research using different types of catalysts to constrain the synthesis at the molecular scale to achieve enantioselectivity.[414] In search for more general techniques to drive enantioselectivity, researchers have appealed to using circularly polarized light to photocatalyze the reaction, in a way that preferentially excites one reaction path to—or from, in enantioselective photodegradation—one of the enantiomers.[415] Given that SERS requires the contribution from plasmonic nanomaterials, its application in photocatalysis naturally invites us to focus on the plasmonic material as a contributor to the photoreaction, a topic of great current interest.[416]

Whereas examples of chiral light-driven reactions have been reported for over a century,[417] research in asymmetric photocatalysis has seen significant progress during the past few decades, leading to large values of enantiomeric excess.[418,419] However, achieving such a high yield for a wide range of reactions is a pending challenge because of the relatively small circular dichroism (CD) of molecules. Molecular CD is fundamentally small because of the significant difference in spatial scales between the wavelength of absorbed light and the chiral stereochemistry of the molecules. In contrast, large CD values can be obtained with nanophotonic systems, including plasmonic nanostructures, because their geometry can be tailored to showcase strong chiral asymmetry at wavelengths in and above the UV range,[420] and especially strong when considering in-plane 2D chirality of metasurfaces.[421] Interestingly, an emerging path for creating chiral plasmonic nanostructures parallels enantioselective photocatalysis, in that it has been shown that circularly polarized light (CPL) can develop chiral features in originally achiral systems through photocatalytic growth.[422−424] One can in principle see plasmonic nanostructures as having three major features of interest for chiral photocatalysis: they work as photocatalysts and photosensitizers exploiting their strong coupling with light; the tunability of their plasmon resonances offers an extra degree of control over their chiral response, and they can enable operando monitoring of the reaction as SERS platforms. However, there is a critical gap between a plasmonic photocatalyst being chiral, thus sensitive to the polarization of incident CPL,[425] and offering reaction enantioselectivity, because the interaction between a plasmonic resonator and a nearby molecule is local and can therefore be "blind" to the overall chiral response of the nanostructure.

Extending bridges across this gap holds great scientific and technological interest, presenting an invitation that is being met by a variety of strategies to engineer intermediate-scale systems to connect incident CPL with chirality at the molecular scale in a causal cascade.[426] Recent explorations of this idea include an experimental study demonstrating asymmetric homolysis using CPL and chiral plasmonic NCs, uncovered by the systematic evaluation of the interplay between the handedness of molecular sample, plasmonic NCs, and CPL (see Figure 17c).[427] Another family of approaches use superchiral fields to manipulate molecules in an enantioselective manner, either to preferentially excite one enantiomer,[428] or to induce enantioselective optical trapping—using nonchiral cavities excited with CPL to create chiral cavity modes that preferentially trap one enantiomer—to then optically drive the evolution of the reaction inside the cavity (Figure 17d).[429−431] Other relevant works exploit plasmonic modes of colloidal nanoparticles, both chiral and nonchiral. In an example of the former, a study found that chiral gold helices induce enantioselective molecular dimerization, attributing this effect to the chiral arrangement of the metal surface atoms (Figure 17e).[432] Using nonchiral colloidal plasmonic systems, it has been shown that aggregated Ag NPs can induce chiral $NaClO_3$ crystal growth under CPL illumination.[433] Other perspectives include the possibility of leveraging the phenomenon of chirality induced spin selectivity (CISS) to affect injection rates of spin-polarized electrons into different molecular enantiomers or driving enantioselective polymerization of achiral monomers.[434,435] Overall, enantioselective photocatalysis using plasmonic nanostructures is a relatively young area of research that is explored with a combination of great expectation and cautious skepticism, in recognition of both its potential and the challenges it poses. Progress on techniques to monitor the enantiomeric composition of products obtained with a photocatalyst can clarify aspects of the mechanisms driving the reaction and identify avenues to improve upon them. It may be of special interest to develop real-time monitoring of enantiomer production/destruction with SERS substrates integrated with the photocatalysts, allowing to analyze the reaction dynamics and, e.g., discriminate between nonenantioselective processes and enantioselective processes that undergo subsequent racemization.

12. CONCLUSIONS

In catalytic processes, the journey toward operando spectroscopy began long before the advent of SERS, primarily driven by techniques like IR spectroscopy with its larger cross sections compared to Raman spectroscopy. However, the discovery of SERS marked a shift, enabling insights into chemical reactions through the analysis of SERS spectra, including even the observation of single-molecule reactivity. This breakthrough has contributed to our understanding of kinetics, reactivity, and active sites across photocatalysis, thermal catalysis, electrocatalysis and photoelectrocatalysis, fostering the design of materials to enhance chemical transformations and energy conversion. We have tried to summarize in this focus review article the impact of SERS in the fields of catalysis and energy conversion over the last 50 years.

Looking ahead, the future of SERS in catalysis holds significant promise. From harnessing machine learning to exploiting single-atom catalysts, advancing the development of batteries, and enabling chiral catalysis, SERS presents many opportunities. We have dedicated the last part of this Focus Review article to discussing these emerging applications in more detail. We stand at the threshold of an era for SERS, poised to unlock its full potential in the upcoming decades. SERS has firmly established itself as a sensitive and valuable analytical tool in materials science for scrutinizing chemical transformations and energy dynamics.

Nonetheless, for all of its potential, SERS also possesses some challenges that need to be addressed to make it part of standard industrial catalytic processes. Precisely because of the high sensitivity of SERS, it is prone to molecular contaminants, and one must be extremely careful in assigning the observed Raman peaks, including their exact intensities as well as their band positions and widths, to reaction intermediates or products. As possible solutions for the future, we highlight the use of more advanced theoretical tools for calculating the Raman tensor of adsorbed molecules and possible reaction intermediates or products. More recent approaches involve using machine learning tools for spectral deconvolution, denoising, and automatic identification or validation of molecules. Another hurdle that SERS needs to surpass is to move away from being a purely research tool toward becoming an industrially applied

https://doi.org/10.1021/acsnano.4c06192
ACS Nano XXXX, XXX, XXX−XXX

tool. For this, SERS must be applied in relevant catalytic or energy-conversion systems under true operando conditions thereby not only working on "test" systems with well-defined and known behavior and properties, such as the reduction reaction of 4-NTP. For example, gas-phase reactions or high temperature and/or pressure reactions represent big milestones for the field. These areas pose significant challenges, but overcoming them could elevate the role of SERS in catalysis and energy research. Addressing these challenges could substantially enhance the practical applications of SERS, driving advancements in both fundamental research and industrial processes.

AUTHOR INFORMATION

Corresponding Author

Emiliano Cortés − *Nanoinstitute Munich, Faculty of Physics, Ludwig-Maximilians-Universität München, 80539 Munich, Germany;* orcid.org/0000-0001-8248-4165; Email: Emiliano.Cortes@lmu.de

Authors

Andrei Stefancu − *Nanoinstitute Munich, Faculty of Physics, Ludwig-Maximilians-Universität München, 80539 Munich, Germany;* orcid.org/0000-0002-1455-2055

Javier Aizpurua − *IKERBASQUE, Basque Foundation for Science, 48011 Bilbao, Basque Country, Spain; Donostia International Physics Center (DIPC), 20018 San Sebastián-Donostia, Basque Country, Spain; Department of Electricity and Electronics, University of the Basque Country, 20018 San Sebastián-Donostia, Basque Country, Spain;* orcid.org/0000-0002-1444-7589

Ivano Alessandri − *INSTM, UdR Brescia, Brescia 25123, Italy; Department of Information Engineering (DII), University of Brescia, Brescia 25123, Italy; INO−CNR, Brescia 25123, Italy;* orcid.org/0000-0003-0332-0723

Ilko Bald − *Institute of Chemistry, University of Potsdam, D-14476 Potsdam, Germany*

Jeremy J. Baumberg − *Nanophotonics Centre, Department of Physics, Cavendish Laboratory, University of Cambridge, Cambridge CB3 0HE England, U.K.;* orcid.org/0000-0002-9606-9488

Lucas V. Besteiro − *CINBIO, Universidade de Vigo, Vigo 36310, Spain*

Phillip Christopher − *Department of Chemical Engineering, University of California Santa Barbara, Santa Barbara, California 93106, United States;* orcid.org/0000-0002-4898-5510

Miguel Correa-Duarte − *CINBIO, Universidade de Vigo, Vigo 36310, Spain; Biomedical Research Networking Center for Mental Health (CIBERSAM), Southern Galicia Institute of Health Research (IISGS), Vigo 36310, Spain*

Bart de Nijs − *Nanophotonics Centre, Department of Physics, Cavendish Laboratory, University of Cambridge, Cambridge CB3 0HE England, U.K.;* orcid.org/0000-0002-8234-723X

Angela Demetriadou − *School of Physics and Astronomy, University of Birmingham, Edgbaston, Birmingham B15 2TT, U.K.;* orcid.org/0000-0001-7240-597X

Renee R. Frontiera − *Department of Chemistry, University of Minnesota, Minneapolis, Minnesota 55455, United States;* orcid.org/0000-0001-8218-7574

Tomohiro Fukushima − *Department of Chemistry, Faculty of Science, Hokkaido University, Sapporo 060-0810, Japan; JST-PRESTO, Tokyo 332-0012, Japan;* orcid.org/0000-0002-0165-3818

Naomi J. Halas − *Department of Chemistry, Department of Electrical and Computer Engineering, and Department of Physics and Astronomy, Rice University, Houston, Texas 77005, United States; Technical University of Munich (TUM) and Institute for Advanced Study (IAS), D-85748 Garching, Germany;* orcid.org/0000-0002-8461-8494

Prashant K. Jain − *Department of Chemistry and Materials Research Laboratory, University of Illinois Urbana−Champaign, Urbana, Illinois 61801, United States;* orcid.org/0000-0002-7306-3972

Zee Hwan Kim − *Department of Chemistry, Seoul National University, Seoul 08826, Republic of Korea;* orcid.org/0000-0001-8870-4333

Dmitry Kurouski − *Department of Biochemistry and Biophysics and Department of Biomedical Engineering, Texas A&M University, College Station, Texas 77843, United States;* orcid.org/0000-0002-6040-4213

Holger Lange − *Institut für Physik und Astronomie, Universität Potsdam, 14476 Potsdam, Germany; The Hamburg Centre for Ultrafast Imaging, 22761 Hamburg, Germany;* orcid.org/0000-0002-4236-2806

Jian-Feng Li − *State Key Laboratory of Physical Chemistry of Solid Surfaces, iChEM, College of Chemistry and Chemical Engineering, College of Energy, College of Materials, Xiamen University, Xiamen 361005, China;* orcid.org/0000-0003-1598-6856

Luis M. Liz-Marzán − *IKERBASQUE, Basque Foundation for Science, 48011 Bilbao, Basque Country, Spain; CINBIO, Universidade de Vigo, Vigo 36310, Spain; CIC biomaGUNE, Basque Research and Technology Alliance (BRTA), Donostia-San Sebastián 20014, Spain; Centro de Investigación Biomédica en Red, Bioingeniería, Biomateriales y Nanomedicina (CIBER-BBN), Donostia-San Sebastián 20014, Spain;* orcid.org/0000-0002-6647-1353

Ivan T. Lucas − *Nantes Université, CNRS, IMN, F-44322 Nantes, France*

Alfred J. Meixner − *Institute of Physical and Theoretical Chemistry, University of Tubingen, 72076 Tubingen, Germany;* orcid.org/0000-0002-0187-2906

Kei Murakoshi − *Department of Chemistry, Faculty of Science, Hokkaido University, Sapporo 060-0810, Japan;* orcid.org/0000-0003-4786-0115

Peter Nordlander − *Department of Electrical and Computer Engineering and Department of Physics and Astronomy, Rice University, Houston, Texas 77005, United States; Technical University of Munich (TUM) and Institute for Advanced Study (IAS), D-85748 Garching, Germany;* orcid.org/0000-0002-1633-2937

William J. Peveler − *School of Chemistry, Joseph Black Building, University of Glasgow, Glasgow G12 8QQ, U.K.;* orcid.org/0000-0002-9829-2683

Raul Quesada-Cabrera − *Department of Chemistry, University College London, London WC1H 0AJ, U.K.; Department of Chemistry, Institute of Environmental Studies and Natural Resources (i-UNAT), Universidad de Las Palmas de Gran Canaria, Las Palmas de GC 35017, Spain*

Emilie Ringe − *Department of Materials Science and Metallurgy and Department of Earth Sciences, University of Cambridge, Cambridge CB3 0FS, United Kingdom;* orcid.org/0000-0003-3743-9204

https://doi.org/10.1021/acsnano.4c06192
ACS Nano XXXX, XXX, XXX−XXX

George C. Schatz − *Department of Chemistry, Northwestern University, Evanston, Illinois 60208, United States;* orcid.org/0000-0001-5837-4740

Sebastian Schlücker − *Physical Chemistry I and Center for Nanointegration Duisburg-Essen (CENIDE), Universität Duisburg-Essen, 45141 Essen, Germany;* orcid.org/0000-0003-4790-4616

Zachary D. Schultz − *Department of Chemistry and Biochemistry, The Ohio State University, Columbus, Ohio 43210, United States;* orcid.org/0000-0003-1741-8801

Emily Xi Tan − *School of Chemistry, Chemical Engineering and Biotechnology, Nanyang Technological University, Nanyang 637371, Singapore*

Zhong-Qun Tian − *State Key Laboratory of Physical Chemistry of Solid Surfaces, iChEM, College of Chemistry and Chemical Engineering, College of Energy, College of Materials, Xiamen University, Xiamen 361005, China;* orcid.org/0000-0002-9775-8189

Lingzhi Wang − *Shanghai Engineering Research Center for Multi-media Environmental Catalysis and Resource Utilization and Key Laboratory for Advanced Materials and Joint International Research Laboratory of Precision Chemistry and Molecular Engineering, Feringa Nobel Prize Scientist Joint Research Center, School of Chemistry and Molecular Engineering, East China University of Science and Technology, Shanghai 200237, P. R. China;* orcid.org/0000-0002-5792-041X

Bert M. Weckhuysen − *Debye Institute for Nanomaterials Science and Institute for Sustainable and Circular Chemistry, Department of Chemistry, Utrecht University, 3584 CG, Utrecht, The Netherlands;* orcid.org/0000-0001-5245-1426

Wei Xie − *Key Laboratory of Advanced Energy Materials Chemistry (Ministry of Education), Renewable Energy Conversion and Storage Center, College of Chemistry, Nankai University, Tianjin 300071, China;* orcid.org/0000-0002-8290-514X

Xing Yi Ling − *School of Chemistry, Chemical Engineering and Biotechnology, Nanyang Technological University, Nanyang 637371, Singapore; School of Chemical and Material Engineering, Jiangnan University, Wuxi 214122, People's Republic of China; Lee Kong Chian School of Medicine and Institute for Digital Molecular Analytics and Science (IDMxS), Nanyang Technological University, Singapore 636921, Singapore;* orcid.org/0000-0001-5495-6428

Jinlong Zhang − *Shanghai Engineering Research Center for Multi-media Environmental Catalysis and Resource Utilization and Key Laboratory for Advanced Materials and Joint International Research Laboratory of Precision Chemistry and Molecular Engineering, Feringa Nobel Prize Scientist Joint Research Center, School of Chemistry and Molecular Engineering, East China University of Science and Technology, Shanghai 200237, P. R. China;* orcid.org/0000-0002-1334-6436

Zhigang Zhao − *Key Lab of Nanodevices and Applications, Suzhou Institute of Nano-Tech and Nano-Bionics, Chinese Academy of Sciences, Suzhou 215123, China; Nano Science and Technology Institute, University of Science and Technology of China (USTC), Suzhou 215123, China;* orcid.org/0000-0002-9327-9893

Ru-Yu Zhou − *State Key Laboratory of Physical Chemistry of Solid Surfaces, iChEM, College of Chemistry and Chemical Engineering, College of Energy, College of Materials, Xiamen University, Xiamen 361005, China*

Complete contact information is available at: https://pubs.acs.org/10.1021/acsnano.4c06192

Notes

The authors declare no competing financial interest.

ACKNOWLEDGMENTS

A.S. and E.C. acknowledge funding and support from the Deutsche Forschungsgemeinschaft (DFG, German Research Foundation) under Germany's Excellence Strategy − EXC 2089/1-390776260, the Bavarian program Solar Technologies Go Hybrid (SolTech), the Center for NanoScience (CeNS), and the European Commission through the ERC SURFLIGHT. A.S. acknowledges support from the Alexander von Humboldt foundation. P.N. and N.J.H. acknowledge support from the Robert A. Welch Foundation under grants C-1222 and C-1220. N.H., P.N., and E.C. acknowledge the Institute for Advanced Study (IAS) from Technische Universität München (TUM) for financing the focus group on "Sustainable photocatalysis using plasmons and 2D materials (SusPhuP2M)" as part of the Hans Fisher Senior Fellowships program. I.B. acknowledges funding by the Deutsche Forschungsgemeinschaft (DFG) − CRC/SFB 1636 − Project ID 510943930. G.C.S. acknowledges grant DE-SC0004752 from the Department of Energy, Office of Basic Energy Sciences. I.T.L. acknowledges European Union's Horizon Europe research and innovation program (OPIN-CHARGE project, grant agreement ID: 101104032), Battery2030+, and French Agence Nationale de la Recherche ANR (ZORG project, grant ID: ANR-22-CE50-0005). This material is based upon work by P.K.J. supported by the National Science Foundation under Grant No. DMR-2323988. Z.H.K. acknowledges support from the National Research Foundation of Korea (NRF) funded by the Korean government, the Ministry of Science, and ICT (2021R1A2C3012659 and 2021R1A5A1030054). I.A. acknowledges funding and support of the Italian Ministry of University and Research (MUR) through the "HOT-META: HOT-carrier METAsurfaces for Advanced photonics" project (PRIN-2022). R.Q.C. acknowledges support from the Spanish Ministry of Education and Professional Training, Beatriz Galindo Senior Fellowship. Z.D.S. acknowledges support from the National Science Foundation award CHE-2107791. B.M.W. acknowledges financial support from The Netherlands Organization for Scientific Research (NWO) in the frame of a Gravitation Program MCEC (Netherlands Center for Multiscale Catalytic Energy Conversion, www.mcec-researchcenter.nl) as well as from the Advanced Research Center (ARC) Chemical Buildings Blocks Consortium (CBBC), a public-private research consortium in The Netherlands (www.arc-cbbc.nl). J.J.B. acknowledges funding from the EPSRC (EP/X037770/1, EP/L027151/1, and EP/R013012/1), and ERC (Project No. 883703 PICOFORCE). B.d.N. acknowledges funding and support from the Royal Society (URF/R1/211162) and the EPSRC (EP/Y008294/1). R.R.F. acknowledges support from the MRSEC Program of the National Science Foundation under award no. DMR-2011401. A.D. gratefully acknowledges support from the Royal Society University Research Fellowship URF/R1/180097 and URF/R/231024, Royal Society Research Fellows Enhancement Award RGF /EA/181038, and funding

from EPSRC EP/X012689/1, EP/Y008774/1, and CDT in Topological Design EP/S02297X/1.

VOCABULARY

Localized surface plasmon resonance:the collective oscillation of the free metal electrons when metal nanostructures of roughly 100 nm or less are irradiated with a specific light energy; Surface enhanced Raman spectroscopy:the enhancement of the Raman signal emitted by molecules adsorbed on metal surfaces due to the excitation of surface plasmon resonances and the subsequent enhancement of the local electromagnetic field; Catalysis:the increase in rate of a chemical reaction due to an added substance known as a catalyst; Dielectric medium:an electrical insulator that can be polarized by an applied electric field; Energy conversion and energy storage:Energy conversion represents the conversion of one form of energy into another (for example photons into electrons) while energy storage represents the storage of energy in different forms, such as chemical energy or thermal energy.

REFERENCES

(1) Liz-Marzán, L. M.; Willets, K. A.; Chen, X. Fifty Years of Surface-Enhanced Spectroscopy. *ACS Nano* **2024**, *18* (8), 5995−5997.
(2) Le Ru, E. C.; Etchegoin, P. G. *Principles of surface-enhanced Raman spectroscopy and related plasmonic effects*; Elsevier: Amsterdam, 2009.
(3) Fleischmann, M.; Hendra, P. J.; McQuillan, A. J. Raman spectra of pyridine adsorbed at a silver electrode. *Chem. Phys. Lett.* **1974**, *26* (2), 163−166.
(4) Jeanmaire, D. L.; Van Duyne, R. P. Surface raman spectroelectrochemistry: Part I. Heterocyclic, aromatic, and aliphatic amines adsorbed on the anodized silver electrode. *Journal of Electroanalytical Chemistry and Interfacial Electrochemistry* **1977**, *84* (1), 1−20.
(5) Albrecht, M. G.; Creighton, J. A. Anomalously intense Raman spectra of pyridine at a silver electrode. *J. Am. Chem. Soc.* **1977**, *99* (15), 5215−5217.
(6) Philpott, M. R. Effect of surface plasmons on transitions in molecules. *J. Chem. Phys.* **1975**, *62* (5), 1812−1817.
(7) Moskovits, M. Surface roughness and the enhanced intensity of Raman scattering by molecules adsorbed on metals. *J. Chem. Phys.* **1978**, *69* (9), 4159−4161.
(8) Stefancu, A.; Halas, N. J.; Nordlander, P.; Cortes, E. Electronic excitations at the plasmon−molecule interface. *Nat. Phys.* **2024**, *20* (7), 1065−1077.
(9) Bi, X.; Czajkowsky, D. M.; Shao, Z.; Ye, J. Digital colloid-enhanced Raman spectroscopy by single-molecule counting. *Nature* **2024**, *628* (8009), 771−775.
(10) Moisoiu, T.; Dragomir, M. P.; Iancu, S. D.; Schallenberg, S.; Birolo, G.; Ferrero, G.; Burghelea, D.; Stefancu, A.; Cozan, R. G.; Licarete, E.; Allione, A.; Matullo, G.; Iacob, G.; Bálint, Z.; Badea, R. I.; Naccarati, A.; Horst, D.; Pardini, B.; Leopold, N.; Elec, F. Combined miRNA and SERS urine liquid biopsy for the point-of-care diagnosis and molecular stratification of bladder cancer. *Mol. Med.* **2022**, *28* (1), 39.
(11) Moisoiu, V.; Iancu, S. D.; Stefancu, A.; Moisoiu, T.; Pardini, B.; Dragomir, M. P.; Crisan, N.; Avram, L.; Crisan, D.; Andras, I.; Fodor, D.; Leopold, L. F.; Socaciu, C.; Bálint, Z.; Tomuleasa, C.; Elec, F.; Leopold, N. SERS liquid biopsy: An emerging tool for medical diagnosis. *Colloids Surf., B* **2021**, *208*, 112064.
(12) Lombardi, J. R.; Birke, R. L. A Unified View of Surface-Enhanced Raman Scattering. *Acc. Chem. Res.* **2009**, *42* (6), 734−742.
(13) Ma, H.; Pan, S.-Q.; Wang, W.-L.; Yue, X.; Xi, X.-H.; Yan, S.; Wu, D.-Y.; Wang, X.; Liu, G.; Ren, B. Surface-Enhanced Raman Spectroscopy: Current Understanding, Challenges, and Opportunities. *ACS Nano* **2024**, *18* (22), 14000−14019.
(14) Le Ru, E. C.; Auguié, B. Enhancement Factors: A Central Concept during 50 Years of Surface-Enhanced Raman Spectroscopy. *ACS Nano* **2024**, *18* (14), 9773−9783.
(15) Schlücker, S. Surface-Enhanced Raman Spectroscopy: Concepts and Chemical Applications. *Angew. Chem., Int. Ed.* **2014**, *53* (19), 4756−4795.
(16) Moskovits, M. Surface-enhanced Raman spectroscopy: a brief retrospective. *J. Raman Spectrosc.* **2005**, *36* (6−7), 485−496.
(17) Willets, K. A.; Van Duyne, R. P. Localized Surface Plasmon Resonance Spectroscopy and Sensing. *Annu. Rev. Phys. Chem.* **2007**, *58* (1), 267−297.
(18) Langer, J.; Jimenez de Aberasturi, D.; Aizpurua, J.; Alvarez-Puebla, R. A.; Auguié, B.; Baumberg, J. J.; Bazan, G. C.; Bell, S. E. J.; Boisen, A.; Brolo, A. G.; Choo, J.; Cialla-May, D.; Deckert, V.; Fabris, L.; Faulds, K.; García de Abajo, F. J.; Goodacre, R.; Graham, D.; Haes, A. J.; Haynes, C. L.; Huck, C.; Itoh, T.; Käll, M.; Kneipp, J.; Kotov, N. A.; Kuang, H.; Le Ru, E. C.; Lee, H. K.; Li, J.-F.; Ling, X. Y.; Maier, S. A.; Mayerhöfer, T.; Moskovits, M.; Murakoshi, K.; Nam, J.-M.; Nie, S.; Ozaki, Y.; Pastoriza-Santos, I.; Perez-Juste, J.; Popp, J.; Pucci, A.; Reich, S.; Ren, B.; Schatz, G. C.; Shegai, T.; Schlücker, S.; Tay, L.-L.; Thomas, K. G.; Tian, Z.-Q.; Van Duyne, R. P.; Vo-Dinh, T.; Wang, Y.; Willets, K. A.; Xu, C.; Xu, H.; Xu, Y.; Yamamoto, Y. S.; Zhao, B.; Liz-Marzán, L. M. Present and Future of Surface-Enhanced Raman Scattering. *ACS Nano* **2020**, *14* (1), 28−117.
(19) Le Ru, E. C.; Etchegoin, P. G. Single-Molecule Surface-Enhanced Raman Spectroscopy. *Annu. Rev. Phys. Chem.* **2012**, *63* (1), 65−87.
(20) Bell, S. E. J.; Charron, G.; Cortés, E.; Kneipp, J.; de la Chapelle, M. L.; Langer, J.; Procházka, M.; Tran, V.; Schlücker, S. Towards Reliable and Quantitative Surface-Enhanced Raman Scattering (SERS): From Key Parameters to Good Analytical Practice. *Angew. Chem., Int. Ed.* **2020**, *59* (14), 5454−5462.
(21) Zybert, M. Applied Catalysis in Chemical Industry: Synthesis, Catalyst Design, and Evaluation Catalysts. *Catalysts* **2023**, *13* (3), 607.
(22) Poliakoff, M.; Licence, P. Green chemistry. *Nature* **2007**, *450* (7171), 810−812.
(23) Vogt, E. T. C.; Weckhuysen, B. M. The refinery of the future. *Nature* **2024**, *629* (8011), 295−306.
(24) Yuan, Y.; Zhou, L.; Robatjazi, H.; Bao, J. L.; Zhou, J.; Bayles, A.; Yuan, L.; Lou, M.; Lou, M.; Khatiwada, S.; Carter, E. A.; Nordlander, P.; Halas, N. J. Earth-abundant photocatalyst for H_2 generation from NH_3 with light-emitting diode illumination. *Science* **2022**, *378* (6622), 889−893.
(25) Cortes, E. Catalysts light a path to sustainable chemistry. *Nature* **2023**, *614*, 230−232.
(26) Martini, A.; Hursán, D.; Timoshenko, J.; Rüscher, M.; Haase, F.; Rettenmaier, C.; Ortega, E.; Etxebarria, A.; Roldan Cuenya, B. Tracking the Evolution of Single-Atom Catalysts for the CO_2 Electrocatalytic Reduction Using Operando X-ray Absorption Spectroscopy and Machine Learning. *J. Am. Chem. Soc.* **2023**, *145* (31), 17351−17366.
(27) Rettenmaier, C.; Herzog, A.; Casari, D.; Rüscher, M.; Jeon, H. S.; Kordus, D.; Luna, M. L.; Kühl, S.; Hejral, U.; Davis, E. M.; Chee, S. W.; Timoshenko, J.; Alexander, D. T. L.; Bergmann, A.; Cuenya, B. R. Operando insights into correlating CO coverage and Cu−Au alloying with the selectivity of Au NP-decorated Cu_2O nanocubes during the electrocatalytic CO_2 reduction. *EES Catalysis* **2024**, *2* (1), 311−323.
(28) Urakawa, A. Trends and advances in Operando methodology. *Current Opinion in Chemical Engineering* **2016**, *12*, 31−36.
(29) Vogt, C.; Weckhuysen, B. M. The concept of active site in heterogeneous catalysis. *Nature Reviews Chemistry* **2022**, *6* (2), 89−111.
(30) Devasia, D.; Wilson, A. J.; Heo, J.; Mohan, V.; Jain, P. K. A rich catalog of C−C bonded species formed in CO_2 reduction on a plasmonic photocatalyst. *Nat. Commun.* **2021**, *12* (1), 2612.
(31) Gunathunge, C. M.; Li, X.; Li, J.; Hicks, R. P.; Ovalle, V. J.; Waegele, M. M. Spectroscopic Observation of Reversible Surface Reconstruction of Copper Electrodes under CO_2 Reduction. *J. Phys. Chem. C* **2017**, *121* (22), 12337−12344.
(32) Auer, A.; Andersen, M.; Wernig, E.-M.; Hörmann, N. G.; Buller, N.; Reuter, K.; Kunze-Liebhäuser, J. Self-activation of copper electrodes during CO electro-oxidation in alkaline electrolyte. *Nature Catalysis* **2020**, *3* (10), 797−803.
(33) An, H.; de Ruiter, J.; Wu, L.; Yang, S.; Meirer, F.; van der Stam, W.; Weckhuysen, B. M. Spatiotemporal Mapping of Local Hetero-

https://doi.org/10.1021/acsnano.4c06192
ACS Nano XXXX, XXX, XXX−XXX

geneities during Electrochemical Carbon Dioxide Reduction. *JACS Au* **2023**, *3* (7), 1890−1901.
(34) Hartman, T.; Geitenbeek, R. G.; Wondergem, C. S.; van der Stam, W.; Weckhuysen, B. M. Operando Nanoscale Sensors in Catalysis: All Eyes on Catalyst Particles. *ACS Nano* **2020**, *14* (4), 3725−3735.
(35) Hartman, T.; Geitenbeek, R. G.; Whiting, G. T.; Weckhuysen, B. M. Operando monitoring of temperature and active species at the single catalyst particle level. *Nature Catalysis* **2019**, *2* (11), 986−996.
(36) Bentrup, U. Combining in situ characterization methods in one set-up: looking with more eyes into the intricate chemistry of the synthesis and working of heterogeneous catalysts. *Chem. Soc. Rev.* **2010**, *39* (12), 4718−4730.
(37) Meirer, F.; Weckhuysen, B. M. Spatial and temporal exploration of heterogeneous catalysts with synchrotron radiation. *Nature Reviews Materials* **2018**, *3* (9), 324−340.
(38) Chee, S. W.; Lunkenbein, T.; Schlögl, R.; Roldán Cuenya, B. Operando Electron Microscopy of Catalysts: The Missing Cornerstone in Heterogeneous Catalysis Research? *Chem. Rev.* **2023**, *123* (23), 13374−13418.
(39) Yuan, W.; Fang, K.; You, R.; Zhang, Z.; Wang, Y. Toward In Situ Atomistic Design of Catalytic Active Sites via Controlled Atmosphere Transmission Electron Microscopy. *Accounts of Materials Research* **2023**, *4* (3), 275−286.
(40) Barroo, C.; Wang, Z.-J.; Schlögl, R.; Willinger, M.-G. Imaging the dynamics of catalysed surface reactions by in situ scanning electron microscopy. *Nature Catalysis* **2020**, *3* (1), 30−39.
(41) Amirbeigiarab, R.; Tian, J.; Herzog, A.; Qiu, C.; Bergmann, A.; Roldan Cuenya, B.; Magnussen, O. M. Atomic-scale surface restructuring of copper electrodes under CO_2 electroreduction conditions. *Nature Catalysis* **2023**, *6* (9), 837−846.
(42) Stefancu, A.; Gargiulo, J.; Laufersky, G.; Auguié, B.; Chiş, V.; Le Ru, E. C.; Liu, M.; Leopold, N.; Cortés, E. Interface-Dependent Selectivity in Plasmon-Driven Chemical Reactions. *ACS Nano* **2023**, *17* (3), 3119−3127.
(43) de Ruiter, J.; An, H.; Wu, L.; Gijsberg, Z.; Yang, S.; Hartman, T.; Weckhuysen, B. M.; van der Stam, W. Probing the Dynamics of Low-Overpotential CO_2-to-CO Activation on Copper Electrodes with Time-Resolved Raman Spectroscopy. *J. Am. Chem. Soc.* **2022**, *144* (33), 15047−15058.
(44) Cortés, E.; Etchegoin, P. G.; Le Ru, E. C.; Fainstein, A.; Vela, M. E.; Salvarezza, R. C. Monitoring the Electrochemistry of Single Molecules by Surface-Enhanced Raman Spectroscopy. *J. Am. Chem. Soc.* **2010**, *132* (51), 18034−18037.
(45) Glass, D.; Quesada-Cabrera, R.; Bardey, S.; Promdet, P.; Sapienza, R.; Keller, V.; Maier, S. A.; Caps, V.; Parkin, I. P.; Cortés, E. Probing the Role of Atomic Defects in Photocatalytic Systems through Photoinduced Enhanced Raman Scattering. *ACS Energy Letters* **2021**, *6* (12), 4273−4281.
(46) Er, E.; Chow, T. H.; Liz-Marzán, L. M.; Kotov, N. A. Circular Polarization-Resolved Raman Optical Activity: A Perspective on Chiral Spectroscopies of Vibrational States. *ACS Nano* **2024**, *18*, 12589.
(47) Qiu, Y.; Kuang, C.; Liu, X.; Tang, L. Single-Molecule Surface-Enhanced Raman Spectroscopy. *Sensors* **2022**, *22* (13), 4889.
(48) Wang, Y.; Irudayaraj, J. Surface-enhanced Raman spectroscopy at single-molecule scale and its implications in biology. *Philosophical Transactions of the Royal Society B: Biological Sciences* **2013**, *368* (1611), 20120026.
(49) Benz, F.; Schmidt, M. K.; Dreismann, A.; Chikkaraddy, R.; Zhang, Y.; Demetriadou, A.; Carnegie, C.; Ohadi, H.; de Nijs, B.; Esteban, R.; Aizpurua, J.; Baumberg, J. J. Single-molecule optomechanics in "picocavities. *Science* **2016**, *354* (6313), 726−729.
(50) Zhu, W.; Esteban, R.; Borisov, A. G.; Baumberg, J. J.; Nordlander, P.; Lezec, H. J.; Aizpurua, J.; Crozier, K. B. Quantum mechanical effects in plasmonic structures with subnanometre gaps. *Nat. Commun.* **2016**, *7* (1), 11495.
(51) Varas, A.; García-González, P.; Feist, J.; García-Vidal, F. J.; Rubio, A. Quantum plasmonics: from jellium models to ab initio calculations. *Nanophotonics* **2016**, *5* (3), 409−426.
(52) Wiener, A.; Fernández-Domínguez, A. I.; Horsfield, A. P.; Pendry, J. B.; Maier, S. A. Nonlocal Effects in the Nanofocusing Performance of Plasmonic Tips. *Nano Lett.* **2012**, *12* (6), 3308−3314.
(53) Fernández-Domínguez, A. I.; Wiener, A.; García-Vidal, F. J.; Maier, S. A.; Pendry, J. B. Transformation-Optics Description of Nonlocal Effects in Plasmonic Nanostructures. *Phys. Rev. Lett.* **2012**, *108* (10), 106802.
(54) Mortensen, N. A.; Raza, S.; Wubs, M.; Søndergaard, T.; Bozhevolnyi, S. I. A generalized non-local optical response theory for plasmonic nanostructures. *Nat. Commun.* **2014**, *5* (1), 3809.
(55) Ciracì, C.; Della Sala, F. Quantum hydrodynamic theory for plasmonics: Impact of the electron density tail. *Phys. Rev. B* **2016**, *93* (20), 205405.
(56) Christensen, T.; Yan, W.; Jauho, A.-P.; Soljačić, M.; Mortensen, N. A. Quantum Corrections in Nanoplasmonics: Shape, Scale, and Material. *Phys. Rev. Lett.* **2017**, *118* (15), 157402.
(57) Esteban, R.; Borisov, A. G.; Nordlander, P.; Aizpurua, J. Bridging quantum and classical plasmonics with a quantum-corrected model. *Nat. Commun.* **2012**, *3* (1), 825.
(58) Tserkezis, C.; Stefanou, N.; Wubs, M.; Mortensen, N. A. Molecular fluorescence enhancement in plasmonic environments: exploring the role of nonlocal effects. *Nanoscale* **2016**, *8* (40), 17532−17541.
(59) Xu, H.; Aizpurua, J.; Käll, M.; Apell, P. Electromagnetic contributions to single-molecule sensitivity in surface-enhanced Raman scattering. *Phys. Rev. E* **2000**, *62* (3), 4318−4324.
(60) Jensen, L.; Zhao, L. L.; Schatz, G. C. Size-Dependence of the Enhanced Raman Scattering of Pyridine Adsorbed on Agn (n = 2−8, 20) Clusters. *J. Phys. Chem. C* **2007**, *111* (12), 4756−4764.
(61) Aikens, C. M.; Li, S.; Schatz, G. C. From Discrete Electronic States to Plasmons: TDDFT Optical Absorption Properties of Ag n (n = 10, 20, 35, 56, 84, 120) Tetrahedral Clusters. *J. Phys. Chem. C* **2008**, *112* (30), 11272−11279.
(62) Roelli, P.; Galland, C.; Piro, N.; Kippenberg, T. J. Molecular cavity optomechanics as a theory of plasmon-enhanced Raman scattering. *Nat. Nanotechnol.* **2016**, *11* (2), 164−169.
(63) Schmidt, M. K.; Esteban, R.; González-Tudela, A.; Giedke, G.; Aizpurua, J. Quantum Mechanical Description of Raman Scattering from Molecules in Plasmonic Cavities. *ACS Nano* **2016**, *10* (6), 6291−6298.
(64) Schmidt, M. K.; Esteban, R.; Benz, F.; Baumberg, J. J.; Aizpurua, J. Linking classical and molecular optomechanics descriptions of SERS. *Faraday Discuss.* **2017**, *205* (0), 31−65.
(65) Mukherjee, S.; Libisch, F.; Large, N.; Neumann, O.; Brown, L. V.; Cheng, J.; Lassiter, J. B.; Carter, E. A.; Nordlander, P.; Halas, N. J. Hot Electrons Do the Impossible: Plasmon-Induced Dissociation of H_2 on Au. *Nano Lett.* **2013**, *13* (1), 240−247.
(66) Giri, S. K.; Schatz, G. C. Photodissociation of H2 on Ag and Au Nanoparticles: Effect of Size and Plasmon versus Interband Transitions on Threshold Intensities for Dissociation. *J. Phys. Chem. C* **2023**, *127* (8), 4115−4123.
(67) Giri, S. K.; Schatz, G. C. Plasmon Enhanced Spectroscopy and Photocatalysis. *arXiv*, arXiv:2402.13478, Feb 21, 2024. .
(68) Frontiera, R. R.; Henry, A.-I.; Gruenke, N. L.; Van Duyne, R. P. Surface-Enhanced Femtosecond Stimulated Raman Spectroscopy. *J. Phys. Chem. Lett.* **2011**, *2* (10), 1199−1203.
(69) McAnally, M. O.; McMahon, J. M.; Van Duyne, R. P.; Schatz, G. C. Coupled wave equations theory of surface-enhanced femtosecond stimulated Raman scattering. *J. Chem. Phys.* **2016**, *145* (9), No. 094106.
(70) Le Ru, E. C.; Etchegoin, P. G. Rigorous justification of the |E|4 enhancement factor in Surface Enhanced Raman Spectroscopy. *Chem. Phys. Lett.* **2006**, *423* (1), 63−66.
(71) Zhang, P.; Feist, J.; Rubio, A.; García-González, P.; García-Vidal, F. J. Ab initio nanoplasmonics: The impact of atomic structure. *Phys. Rev. B* **2014**, *90* (16), 161407.
(72) Urbieta, M.; Barbry, M.; Zhang, Y.; Koval, P.; Sánchez-Portal, D.; Zabala, N.; Aizpurua, J. Atomic-Scale Lightning Rod Effect in Plasmonic Picocavities: A Classical View to a Quantum Effect. *ACS Nano* **2018**, *12* (1), 585−595.

https://doi.org/10.1021/acsnano.4c06192
ACS Nano XXXX, XXX, XXX−XXX

(73) Trautmann, S.; Aizpurua, J.; Götz, I.; Undisz, A.; Dellith, J.; Schneidewind, H.; Rettenmayr, M.; Deckert, V. A classical description of subnanometer resolution by atomic features in metallic structures. *Nanoscale* **2017**, *9* (1), 391−401.
(74) Baumberg, J. J. Picocavities: a Primer. *Nano Lett.* **2022**, *22* (14), 5859−5865.
(75) Griffiths, J.; de Nijs, B.; Chikkaraddy, R.; Baumberg, J. J. Locating Single-Atom Optical Picocavities Using Wavelength-Multiplexed Raman Scattering. *ACS Photonics* **2021**, *8* (10), 2868−2875.
(76) Barbry, M.; Koval, P.; Marchesin, F.; Esteban, R.; Borisov, A. G.; Aizpurua, J.; Sánchez-Portal, D. Atomistic Near-Field Nanoplasmonics: Reaching Atomic-Scale Resolution in Nanooptics. *Nano Lett.* **2015**, *15* (5), 3410−3419.
(77) Wu, T.; Yan, W.; Lalanne, P. Bright Plasmons with Cubic Nanometer Mode Volumes through Mode Hybridization. *ACS Photonics* **2021**, *8* (1), 307−314.
(78) Zhang, R.; Zhang, Y.; Dong, Z. C.; Jiang, S.; Zhang, C.; Chen, L. G.; Zhang, L.; Liao, Y.; Aizpurua, J.; Luo, Y.; Yang, J. L.; Hou, J. G. Chemical mapping of a single molecule by plasmon-enhanced Raman scattering. *Nature* **2013**, *498* (7452), 82−86.
(79) Yang, B.; Chen, G.; Ghafoor, A.; Zhang, Y.; Zhang, Y.; Zhang, Y.; Luo, Y.; Yang, J.; Sandoghdar, V.; Aizpurua, J.; Dong, Z.; Hou, J. G. Sub-nanometre resolution in single-molecule photoluminescence imaging. *Nat. Photonics* **2020**, *14* (11), 693−699.
(80) Lyu, S.; Zhang, Y.; Zhang, Y.; Chang, K.; Zheng, G.; Wang, L. Picocavity-Controlled Subnanometer-Resolved Single-Molecule Fluorescence Imaging and Mollow Triplets. *J. Phys. Chem. C* **2022**, *126* (27), 11129−11137.
(81) Liu, P.; Chulhai, D. V.; Jensen, L. Single-Molecule Imaging Using Atomistic Near-Field Tip-Enhanced Raman Spectroscopy. *ACS Nano* **2017**, *11* (5), 5094−5102.
(82) Lee, J.; Crampton, K. T.; Tallarida, N.; Apkarian, V. A. Visualizing vibrational normal modes of a single molecule with atomically confined light. *Nature* **2019**, *568* (7750), 78−82.
(83) Zhang, Y.; Yang, B.; Ghafoor, A.; Zhang, Y.; Zhang, Y.-F.; Wang, R.-P.; Yang, J.-L.; Luo, Y.; Dong, Z.-C.; Hou, J. G. Visually constructing the chemical structure of a single molecule by scanning Raman picoscopy. *National Science Review* **2019**, *6* (6), 1169−1175.
(84) Latorre, F.; Kupfer, S.; Bocklitz, T.; Kinzel, D.; Trautmann, S.; Gräfe, S.; Deckert, V. Spatial resolution of tip-enhanced Raman spectroscopy − DFT assessment of the chemical effect. *Nanoscale* **2016**, *8* (19), 10229−10239.
(85) Zhang, Y.; Dong, Z.-C.; Aizpurua, J. Theoretical treatment of single-molecule scanning Raman picoscopy in strongly inhomogeneous near fields. *J. Raman Spectrosc.* **2021**, *52* (2), 296−309.
(86) Shin, H.-H.; Yeon, G. J.; Choi, H.-K.; Park, S.-M.; Lee, K. S.; Kim, Z. H. Frequency-Domain Proof of the Existence of Atomic-Scale SERS Hot-Spots. *Nano Lett.* **2018**, *18* (1), 262−271.
(87) Lin, Q.; Hu, S.; Földes, T.; Huang, J.; Wright, D.; Griffiths, J.; Elliott, E.; de Nijs, B.; Rosta, E.; Baumberg, J. J. Optical suppression of energy barriers in single molecule-metal binding. *Science Advances* **2022**, *8* (25), eabp9285.
(88) Lee, S. Nanoparticle-on-mirror cavity: a historical view across nanophotonics and nanochemistry. *Journal of the Korean Physical Society* **2022**, *81* (6), 502−509.
(89) Griffiths, J.; Földes, T.; de Nijs, B.; Chikkaraddy, R.; Wright, D.; Deacon, W. M.; Berta, D.; Readman, C.; Grys, D.-B.; Rosta, E.; Baumberg, J. J. Resolving sub-angstrom ambient motion through reconstruction from vibrational spectra. *Nat. Commun.* **2021**, *12* (1), 6759.
(90) Carnegie, C.; Griffiths, J.; de Nijs, B.; Readman, C.; Chikkaraddy, R.; Deacon, W. M.; Zhang, Y.; Szabó, I.; Rosta, E.; Aizpurua, J.; Baumberg, J. J. Room-Temperature Optical Picocavities below 1 nm3 Accessing Single-Atom Geometries. *J. Phys. Chem. Lett.* **2018**, *9* (24), 7146−7151.
(91) Poppe, A.; Griffiths, J.; Hu, S.; Baumberg, J. J.; Osadchy, M.; Gibson, S.; de Nijs, B. Mapping Atomic-Scale Metal−Molecule Interactions: Salient Feature Extraction through Autoencoding of Vibrational Spectroscopy Data. *J. Phys. Chem. Lett.* **2023**, *14* (34), 7603−7610.
(92) Koy, M.; Bellotti, P.; Das, M.; Glorius, F. N-Heterocyclic carbenes as tunable ligands for catalytic metal surfaces. *Nature Catalysis* **2021**, *4* (5), 352−363.
(93) Jensen, I. M.; Chowdhury, S.; Hu, G.; Jensen, L.; Camden, J. P.; Jenkins, D. M. Seeking a Au−C stretch on gold nanoparticles with 13C-labeled N-heterocyclic carbenes. *Chem. Commun.* **2023**, *59* (98), 14524−14527.
(94) Thimes, R. L.; Santos, A. V. B.; Chen, R.; Kaur, G.; Jensen, L.; Jenkins, D. M.; Camden, J. P. Using Surface-Enhanced Raman Spectroscopy to Unravel the Wingtip-Dependent Orientation of N-Heterocyclic Carbenes on Gold Nanoparticles. *J. Phys. Chem. Lett.* **2023**, *14* (18), 4219−4224.
(95) Yuan, L.; Jiang, L.; Nijhuis, C. A. The Drive Force of Electrical Breakdown of Large-Area Molecular Tunnel Junctions. *Adv. Funct. Mater.* **2018**, *28* (28), 1801710.
(96) Kim, Y.; Ji, S.; Nam, J.-M. A Chemist's View on Electronic and Steric Effects of Surface Ligands on Plasmonic Metal Nanostructures. *Acc. Chem. Res.* **2023**, *56* (16), 2139−2150.
(97) Lindquist, N. C.; Bido, A. T.; Brolo, A. G. Single-Molecule SERS Hotspot Dynamics in Both Dry and Aqueous Environments. *J. Phys. Chem. C* **2022**, *126* (16), 7117−7126.
(98) Lindquist, N. C.; de Albuquerque, C. D. L.; Sobral-Filho, R. G.; Paci, I.; Brolo, A. G. High-speed imaging of surface-enhanced Raman scattering fluctuations from individual nanoparticles. *Nat. Nanotechnol.* **2019**, *14* (10), 981−987.
(99) Kamp, M.; de Nijs, B.; Kongsuwan, N.; Saba, M.; Chikkaraddy, R.; Readman, C. A.; Deacon, W. M.; Griffiths, J.; Barrow, S. J.; Ojambati, O. S.; Wright, D.; Huang, J.; Hess, O.; Scherman, O. A.; Baumberg, J. J. Cascaded nanooptics to probe microsecond atomic-scale phenomena. *Proc. Natl. Acad. Sci. U. S. A.* **2020**, *117* (26), 14819−14826.
(100) Schmidt, M. M.; Farley, E. A.; Engevik, M. A.; Adelsman, T. N.; Tuckmantel Bido, A.; Lemke, N. D.; Brolo, A. G.; Lindquist, N. C. High-Speed Spectral Characterization of Single-Molecule SERS Fluctuations. *ACS Nano* **2023**, *17* (7), 6675−6686.
(101) Zhou, J.; Guo, J.; Mebel, A. M.; Ghimire, G.; Liang, F.; Chang, S.; He, J. Probing the Intermediates of Catalyzed Dehydration Reactions of Primary Amide to Nitrile in Plasmonic Junctions. *ACS Catal.* **2022**, *12* (13), 7737−7747.
(102) Zhou, J.; Guo, J.; Ghimire, G.; Mebel, A. M.; Chang, S.; He, J. Plasmon-mediated dehydrogenation of the aromatic methyl group and benzyl radical formation. *Chemical Science* **2023**, *14* (47), 13951−13961.
(103) Huang, J.; Grys, D.-B.; Griffiths, J.; de Nijs, B.; Kamp, M.; Lin, Q.; Baumberg, J. J. Tracking interfacial single-molecule pH and binding dynamics via vibrational spectroscopy. *Science Advances* **2021**, *7* (23), eabg1790.
(104) Jakob, L. A.; Deacon, W. M.; Zhang, Y.; de Nijs, B.; Pavlenko, E.; Hu, S.; Carnegie, C.; Neuman, T.; Esteban, R.; Aizpurua, J.; Baumberg, J. J. Giant optomechanical spring effect in plasmonic nano- and picocavities probed by surface-enhanced Raman scattering. *Nat. Commun.* **2023**, *14* (1), 3291.
(105) Björk, J.; Sánchez-Sánchez, C.; Chen, Q.; Pignedoli, C. A.; Rosen, J.; Ruffieux, P.; Feng, X.; Narita, A.; Müllen, K.; Fasel, R. The Role of Metal Adatoms in a Surface-Assisted Cyclodehydrogenation Reaction on a Gold Surface. *Angew. Chem., Int. Ed.* **2022**, *61* (49), e202212354.
(106) Yang, X.-F.; Wang, A.; Qiao, B.; Li, J.; Liu, J.; Zhang, T. Single-Atom Catalysts: A New Frontier in Heterogeneous Catalysis. *Acc. Chem. Res.* **2013**, *46* (8), 1740−1748.
(107) Si, S.; Shou, H.; Mao, Y.; Bao, X.; Zhai, G.; Song, K.; Wang, Z.; Wang, P.; Liu, Y.; Zheng, Z.; Dai, Y.; Song, L.; Huang, B.; Cheng, H. Low-Coordination Single Au Atoms on Ultrathin ZnIn2S4 Nanosheets for Selective Photocatalytic CO_2 Reduction towards CH_4. *Angew. Chem., Int. Ed.* **2022**, *61* (41), e202209446.
(108) Wright, D.; Lin, Q.; Berta, D.; Földes, T.; Wagner, A.; Griffiths, J.; Readman, C.; Rosta, E.; Reisner, E.; Baumberg, J. J. Mechanistic

https://doi.org/10.1021/acsnano.4c06192
ACS Nano XXXX, XXX, XXX−XXX

study of an immobilized molecular electrocatalyst by in situ gap-plasmon-assisted spectro-electrochemistry. *Nature Catalysis* **2021**, *4* (2), 157−163.
(109) Doppagne, B.; Neuman, T.; Soria-Martinez, R.; López, L. E. P.; Bulou, H.; Romeo, M.; Berciaud, S.; Scheurer, F.; Aizpurua, J.; Schull, G. Single-molecule tautomerization tracking through space- and time-resolved fluorescence spectroscopy. *Nat. Nanotechnol.* **2020**, *15* (3), 207−211.
(110) Esteban, R.; Baumberg, J. J.; Aizpurua, J. Molecular Optomechanics Approach to Surface-Enhanced Raman Scattering. *Acc. Chem. Res.* **2022**, *55* (14), 1889−1899.
(111) Choi, H.-K.; Lee, K. S.; Shin, H.-H.; Koo, J.-J.; Yeon, G. J.; Kim, Z. H. Single-Molecule Surface-Enhanced Raman Scattering as a Probe of Single-Molecule Surface Reactions: Promises and Current Challenges. *Acc. Chem. Res.* **2019**, *52* (11), 3008−3017.
(112) Zrimsek, A. B.; Chiang, N.; Mattei, M.; Zaleski, S.; McAnally, M. O.; Chapman, C. T.; Henry, A.-I.; Schatz, G. C.; Van Duyne, R. P. Single-Molecule Chemistry with Surface- and Tip-Enhanced Raman Spectroscopy. *Chem. Rev.* **2017**, *117* (11), 7583−7613.
(113) Kumari, G.; Zhang, X.; Devasia, D.; Heo, J.; Jain, P. K. Watching Visible Light-Driven CO_2 Reduction on a Plasmonic Nanoparticle Catalyst. *ACS Nano* **2018**, *12* (8), 8330−8340.
(114) Devasia, D.; Jain, P. K. Stochastic Noise in Single-Nanoparticle Catalysis. *J. Phys. Chem. C* **2021**, *125* (32), 17734−17741.
(115) Wilson, A. J.; Jain, P. K. Structural Dynamics of the Oxygen-Evolving Complex of Photosystem II in Water-Splitting Action. *J. Am. Chem. Soc.* **2018**, *140* (17), 5853−5859.
(116) Zhang, X.; Kumari, G.; Heo, J.; Jain, P. K. In situ formation of catalytically active graphene in ethylene photo-epoxidation. *Nat. Commun.* **2018**, *9* (1), 3056.
(117) Dieringer, J. A.; Lettan, R. B.; Scheidt, K. A.; Van Duyne, R. P. A Frequency Domain Existence Proof of Single-Molecule Surface-Enhanced Raman Spectroscopy. *J. Am. Chem. Soc.* **2007**, *129* (51), 16249−16256.
(118) Le Ru, E. C.; Meyer, M.; Etchegoin, P. G. Proof of Single-Molecule Sensitivity in Surface Enhanced Raman Scattering (SERS) by Means of a Two-Analyte Technique. *J. Phys. Chem. B* **2006**, *110* (4), 1944−1948.
(119) Le Ru, E. C.; Blackie, E.; Meyer, M.; Etchegoin, P. G. Surface Enhanced Raman Scattering Enhancement Factors: A Comprehensive Study. *J. Phys. Chem. C* **2007**, *111* (37), 13794−13803.
(120) Choi, H.-K.; Park, W.-H.; Park, C.-G.; Shin, H.-H.; Lee, K. S.; Kim, Z. H. Metal-Catalyzed Chemical Reaction of Single Molecules Directly Probed by Vibrational Spectroscopy. *J. Am. Chem. Soc.* **2016**, *138* (13), 4673−4684.
(121) Blackie, E. J.; Le Ru, E. C.; Etchegoin, P. G. Single-Molecule Surface-Enhanced Raman Spectroscopy of Nonresonant Molecules. *J. Am. Chem. Soc.* **2009**, *131* (40), 14466−14472.
(122) Shin, H.-H.; Jeong, J.; Nam, Y.; Lee, K. S.; Yeon, G. J.; Lee, H.; Lee, S. Y.; Park, S.; Park, H.; Lee, J. Y.; Kim, Z. H. Vibrationally Hot Reactants in a Plasmon-Assisted Chemical Reaction. *J. Am. Chem. Soc.* **2023**, *145* (22), 12264−12274.
(123) Maher, R. C.; Hou, J.; Cohen, L. F.; Le Ru, E. C.; Hadfield, J. M.; Harvey, J. E.; Etchegoin, P. G.; Liu, F. M.; Green, M.; Brown, R. J. C.; Milton, M. J. T. Resonance contributions to anti-Stokes/Stokes ratios under surface enhanced Raman scattering conditions. *J. Chem. Phys.* **2005**, *123* (8), No. 084702.
(124) Boerigter, C.; Campana, R.; Morabito, M.; Linic, S. Evidence and implications of direct charge excitation as the dominant mechanism in plasmon-mediated photocatalysis. *Nat. Commun.* **2016**, *7* (1), 10545.
(125) Keller, E. L.; Frontiera, R. R. Ultrafast Nanoscale Raman Thermometry Proves Heating Is Not a Primary Mechanism for Plasmon-Driven Photocatalysis. *ACS Nano* **2018**, *12* (6), 5848−5855.
(126) dos Santos, D. P.; Temperini, M. L. A.; Brolo, A. G. Mapping the Energy Distribution of SERRS Hot Spots from Anti-Stokes to Stokes Intensity Ratios. *J. Am. Chem. Soc.* **2012**, *134* (32), 13492−13500.
(127) Park, S.; Yeon, G. J.; Lee, H.; Shin, H.-H.; Kim, Z. H. Self-Referenced SERS Thermometry of Molecules on a Metallic Nanostructure. *J. Phys. Chem. C* **2022**, *126* (1), 451−458.
(128) Pozzi, E. A.; Zrimsek, A. B.; Lethiec, C. M.; Schatz, G. C.; Hersam, M. C.; Van Duyne, R. P. Evaluating Single-Molecule Stokes and Anti-Stokes SERS for Nanoscale Thermometry. *J. Phys. Chem. C* **2015**, *119* (36), 21116−21124.
(129) Barella, M.; Violi, I. L.; Gargiulo, J.; Martinez, L. P.; Goschin, F.; Guglielmotti, V.; Pallarola, D.; Schlücker, S.; Pilo-Pais, M.; Acuna, G. P.; Maier, S. A.; Cortés, E.; Stefani, F. D. In Situ Photothermal Response of Single Gold Nanoparticles through Hyperspectral Imaging Anti-Stokes Thermometry. *ACS Nano* **2021**, *15* (2), 2458−2467.
(130) Kumar, N.; Wondergem, C. S.; Wain, A. J.; Weckhuysen, B. M. In Situ Nanoscale Investigation of Catalytic Reactions in the Liquid Phase Using Zirconia-Protected Tip-Enhanced Raman Spectroscopy Probes. *J. Phys. Chem. Lett.* **2019**, *10* (8), 1669−1675.
(131) Kumar, N.; Su, W.; Veselý, M.; Weckhuysen, B. M.; Pollard, A. J.; Wain, A. J. Nanoscale chemical imaging of solid−liquid interfaces using tip-enhanced Raman spectroscopy. *Nanoscale* **2018**, *10* (4), 1815−1824.
(132) Kumar, N.; Weckhuysen, B. M.; Wain, A. J.; Pollard, A. J. Nanoscale chemical imaging using tip-enhanced Raman spectroscopy. *Nat. Protoc.* **2019**, *14* (4), 1169−1193.
(133) Dong, B.; Fang, Y.; Chen, X.; Xu, H.; Sun, M. Substrate-, Wavelength-, and Time-Dependent Plasmon-Assisted Surface Catalysis Reaction of 4-Nitrobenzenethiol Dimerizing to p,p-Dimercaptoazobenzene on Au, Ag, and Cu Films. *Langmuir* **2011**, *27*, 10677−10682.
(134) Van Der Spoel, D.; Lindahl, E.; Hess, B.; Groenhof, G.; Mark, A. E.; Berendsen, H. J. GROMACS: fast, flexible, and free. *J. Comput. Chem.* **2005**, *26* (16), 1701−18.
(135) Sun, M.; Zhang, Z.; Zheng, H.; Xu, H. In-situ plasmon-driven chemical reactions revealed by high vacuum tip-enhanced Raman spectroscopy. *Sci. Rep.* **2012**, *2*, 647.
(136) Joseph, V.; Engelbrekt, C.; Zhang, J.; Gernert, U.; Ulstrup, J.; Kneipp, J. Characterizing the kinetics of nanoparticle-catalyzed reactions by surface-enhanced Raman scattering. *Angew. Chem., Int. Ed. Engl.* **2012**, *51* (30), 7592−6.
(137) Sun, M.; Xu, H. A Novel Application of Plasmonics: Plasmon-Driven Surface-Catalyzed Reactions. *Small* **2012**, *8* (18), 2777−2786.
(138) Zhang, Z.; Deckert-Gaudig, T.; Singh, P.; Deckert, V. Single molecule level plasmonic catalysis - a dilution study of p-nitrothiophenol on gold dimers. *Chem. Commun. (Camb)* **2015**, *51* (15), 3069−72.
(139) Gieseking, R. L. M.; Lee, J.; Tallarida, N.; Apkarian, V. A.; Schatz, G. C. Bias-Dependent Chemical Enhancement and Nonclassical Stark Effect in Tip-Enhanced Raman Spectromicroscopy of CO-Terminated Ag Tips. *J. Phys. Chem. Lett.* **2018**, *9* (11), 3074−3080.
(140) Braun, K.; Hauler, O.; Zhang, D.; Wang, X.; Chasse, T.; Meixner, A. J. Probing Bias-Induced Electron Density Shifts in Metal-Molecule Interfaces via Tip-Enhanced Raman Scattering. *J. Am. Chem. Soc.* **2021**, *143* (4), 1816−1821.
(141) Li, Z.; Kurouski, D. Probing the Redox Selectivity on Au@Pd and Au@Pt Bimetallic Nanoplates by Tip-Enhanced Raman Spectroscopy. *Acs Photonics* **2021**, *8* (7), 2112−2119.
(142) Sarycheva, A.; Shanmugasundaram, M.; Krayev, A.; Gogotsi, Y. Tip-Enhanced Raman Scattering Imaging of Single- to Few-Layer Ti3C2Tx MXene. *ACS Nano* **2022**, *16*, 6858.
(143) Mahapatra, S.; Ning, Y.; Schultz, J. F.; Li, L.; Zhang, J. L.; Jiang, N. Angstrom Scale Chemical Analysis of Metal Supported Trans- and Cis-Regioisomers by Ultrahigh Vacuum Tip-Enhanced Raman Mapping. *Nano Lett.* **2019**, *19* (5), 3267−3272.
(144) Mahapatra, S.; Schultz, J. F.; Li, L.; Zhang, X.; Jiang, N. Controlling Localized Plasmons via an Atomistic Approach: Attainment of Site-Selective Activation inside a Single Molecule. *J. Am. Chem. Soc.* **2022**, *144* (5), 2051−2055.
(145) Mahapatra, S.; Schultz, J. F.; Ning, Y.; Zhang, J. L.; Jiang, N. Probing surface mediated configurations of nonplanar regioisomeric adsorbates using ultrahigh vacuum tip-enhanced Raman spectroscopy. *Nanoscale* **2019**, *11* (42), 19877−19883.
(146) Xu, J.; Zhu, X.; Tan, S.; Zhang, Y.; Li, B.; Tian, Y.; Shan, H.; Cui, X.; Zhao, A.; Dong, Z.; Yang, J.; Luo, Y.; Wang, B.; Hou, J. G.

https://doi.org/10.1021/acsnano.4c06192
ACS Nano XXXX, XXX, XXX−XXX

Determining structural and chemical heterogeneities of surface species at the single-bond limit. *Science* **2021**, *371* (6531), 818−822.
(147) Zhang, Y.; Yang, B.; Ghafoor, A.; Zhang, Y.; Zhang, Y. F.; Wang, R. P.; Yang, J. L.; Luo, Y.; Dong, Z. C.; Hou, J. G. Visually constructing the chemical structure of a single molecule by scanning Raman picoscopy. *Natl. Sci. Rev.* **2019**, *6* (6), 1169−1175.
(148) Lee, C.; Jeong, B. G.; Kim, S. H.; Kim, D.-H.; Yun, S. J.; Choi, W.; An, S.-J.; Lee, D.; Kim, Y.-M.; KIm, K. K.; Lee, S. M.; Jeong, M. S. Investigating heterogeneous defects in single-crystalline WS2 via tip-enhanced Raman spectroscopy. *npj 2D Materials and Applications* **2022**, *6*, 67.
(149) Lee, C.; Jeong, B. G.; Yun, S. J.; Lee, Y. H.; Lee, S. M.; Jeong, M. S. Unveiling Defect-Related Raman Mode of Monolayer WS(2) via Tip-Enhanced Resonance Raman Scattering. *ACS Nano* **2018**, *12* (10), 9982−9990.
(150) Patil, S. J.; Kurouski, D. Tip-enhanced Raman imaging of plasmon-driven dimerization of 4-bromothiophenol on nickel-decorated gold nanoplate bimetallic nanostructures. *Chem. Commun. (Camb)* **2023**, *59* (73), 10976−10979.
(151) Kurouski, D.; Mattei, M.; Van Duyne, R. P. Probing Redox Reactions at the Nanoscale with Electrochemical Tip-Enhanced Raman Spectroscopy. *Nano Lett.* **2015**, *15* (12), 7956−62.
(152) Huang, S. C.; Zhao, Q. Q.; Feng, H. S.; Ma, H.; Zhao, L. B.; Wang, X.; Ren, B. Probing the Intermediate in the Electrochemical Reduction of Nitrobenzene Derivative by EC-TERS. *J. Phys. Chem. C* **2023**, *127*, 12568−12575.
(153) Shao, F.; Wang, W.; Yang, W.; Yang, Z.; Zhang, Y.; Lan, J.; Dieter Schluter, A.; Zenobi, R. In-situ nanospectroscopic imaging of plasmon-induced two-dimensional [4 + 4]-cycloaddition polymerization on Au(111). *Nat. Commun.* **2021**, *12* (1), 4557.
(154) Chiang, N.; Chen, X.; Goubert, G.; Chulhai, D. V.; Chen, X.; Pozzi, E. A.; Jiang, N.; Hersam, M. C.; Seideman, T.; Jensen, L.; Van Duyne, R. P. Conformational Contrast of Surface-Mediated Molecular Switches Yields Angstrom-Scale Spatial Resolution in Ultrahigh Vacuum Tip-Enhanced Raman Spectroscopy. *Nano Lett.* **2016**, *16* (12), 7774−7778.
(155) Zhong, J.-H.; Jin, X.; Meng, L.; Wang, X.; Su, H.-S.; Yang, Z.-L.; Williams, C. T.; Ren, B. Probing the electronic and catalytic properties of a bimetallic surface with 3 nm resolution. *Nat. Nanotechnol.* **2017**, *12* (2), 132−136.
(156) Nelson, D. A.; Schultz, Z. D. Influence of Optically Rectified Electric Fields on the Plasmonic Photocatalysis of 4-Nitrothiophenol and 4-Aminothiophenol to 4,4-Dimercaptoazobenzene. *J. Phys. Chem. C* **2018**, *122* (15), 8581−8588.
(157) Landaeta, E.; Kadosh, N. I.; Schultz, Z. D. Mechanistic Study of Plasmon-Assisted In Situ Photoelectrochemical CO_2 Reduction to Acetate with a Ag/Cu_2O Nanodendrite Electrode. *ACS Catal.* **2023**, *13*, 1638−1648.
(158) Li, C. S.; Xiong, H. C.; He, M.; Xu, B. J.; Lu, Q. Oxyhydroxide Species Enhances CO_2 Electroreduction to CO on Ag via Coelectrolysis with O_2. *ACS Catal.* **2021**, *11* (19), 12029−12037.
(159) He, M.; Chang, X. X.; Chao, T. H.; Li, C. S.; Goddard, W. A.; Cheng, M. J.; Xu, B. J.; Lu, Q. Selective Enhancement of Methane Formation in Electrochemical CO $_2$ Reduction Enabled by a Raman-Inactive Oxygen-Containing Species on Cu. *ACS Catal.* **2022**, *12* (10), 6036−6046.
(160) Paliwal, A.; Bandas, C. D.; Thornburg, E. S.; Haasch, R. T.; Gewirth, A. A. Enhanced Nitrate Reduction Activity from Cu-Alloy Electrodes in an Alkaline Electrolyte. *ACS Catal.* **2023**, *13* (10), 6754−6762.
(161) Tolia, A. A.; Williams, C. T.; Takoudis, C. G.; Weaver, M. J. Surface-Enhanced Raman-Spectroscopy as an in-situ Real-Time Probe of Catalytic Mechanisms at High Gas-Pressures - The CO-NO Reaction on Rhodium. *J. Phys. Chem.* **1995**, *99* (13), 4599−4608.
(162) Williams, C. T.; Tolia, A. A.; Chan, H. Y. H.; Takoudis, C. G.; Weaver, M. J. Surface-enhanced Raman spectroscopy as an in situ real-time probe of catalytic mechanisms at high gas pressures: The CO-NO reaction on platinum and palladium. *J. Catal.* **1996**, *163* (1), 63−76.
(163) Wang, Y.-H.; Wang, X.-T.; Ze, H.; Zhang, X.-G.; Radjenovic, P. M.; Zhang, Y.-J.; Dong, J.-C.; Tian, Z.-Q.; Li, J.-F. Spectroscopic Verification of Adsorbed Hydroxy Intermediates in the Bifunctional Mechanism of the Hydrogen Oxidation Reaction. *Angew. Chem., Int. Ed.* **2021**, *60* (11), 5708−5711.
(164) Nazemi, M.; Ou, P. F.; Alabbady, A.; Soule, L.; Liu, A.; Song, J.; Sulchek, T. A.; Liu, M. L.; El-Sayed, M. A. Electrosynthesis of Ammonia Using Porous Bimetallic Pd-Ag Nanocatalysts in Liquid- and Gas-Phase Systems. *ACS Catal.* **2020**, *10* (17), 10197−10206.
(165) Salmistraro, M.; Schwartzberg, A.; Bao, W.; Depero, L. E.; Weber-Bargioni, A.; Cabrini, S.; Alessandri, I. Triggering and Monitoring Plasmon-Enhanced Reactions by Optical Nanoantennas Coupled to Photocatalytic Beads. *Small* **2013**, *9* (19), 3301−3307.
(166) Zhan, C.; Chen, X.-J.; Huang, Y.-F.; Wu, D.-Y.; Tian, Z.-Q. Plasmon-Mediated Chemical Reactions on Nanostructures Unveiled by Surface-Enhanced Raman Spectroscopy. *Acc. Chem. Res.* **2019**, *52* (10), 2784−2792.
(167) Huh, H.; Trinh, H. D.; Lee, D.; Yoon, S. How Does a Plasmon-Induced Hot Charge Carrier Break a C−C Bond? *ACS Appl. Mater. Interfaces* **2019**, *11* (27), 24715−24724.
(168) Jiang, P.; Dong, Y.; Yang, L.; Zhao, Y.; Xie, W. Hot Electron-Induced Carbon−Halogen Bond Cleavage Monitored by in Situ Surface-Enhanced Raman Spectroscopy. *J. Phys. Chem. C* **2019**, *123* (27), 16741−16746.
(169) Huynh, L. T. M.; Kim, S.; Yoon, S. Effect of Material and Shape of Nanoparticles on Hot Carrier Generation. *ACS Photonics* **2022**, *9* (10), 3260−3267.
(170) Schürmann, R.; Dutta, A.; Ebel, K.; Tapio, K.; Milosavljević, A. R.; Bald, I. Plasmonic reactivity of halogen thiophenols on gold nanoparticles studied by SERS and XPS. *J. Chem. Phys.* **2022**, *157* (8), 084708.
(171) Dutta, A.; Schürmann, R.; Kogikoski, S., Jr.; Mueller, N. S.; Reich, S.; Bald, I. Kinetics and Mechanism of Plasmon-Driven Dehalogenation Reaction of Brominated Purine Nucleobases on Ag and Au. *ACS Catal.* **2021**, *11* (13), 8370−8381.
(172) Swaminathan, S.; Rao, V. G.; Bera, J. K.; Chandra, M. The Pivotal Role of Hot Carriers in Plasmonic Catalysis of C−N Bond Forming Reaction of Amines. *Angew. Chem., Int. Ed.* **2021**, *60* (22), 12532−12538.
(173) van Schrojenstein Lantman, E. M.; Gijzeman, O. L. J.; Mank, A. J. G.; Weckhuysen, B. M. Investigation of the Kinetics of a Surface Photocatalytic Reaction in Two Dimensions with Surface-enhanced Raman Scattering. *ChemCatChem.* **2014**, *6* (12), 3342−3346.
(174) Schürmann, R.; Nagel, A.; Juergensen, S.; Pathak, A.; Reich, S.; Pacholski, C.; Bald, I. Microscopic Understanding of Reaction Rates Observed in Plasmon Chemistry of Nanoparticle−Ligand Systems. *J. Phys. Chem. C* **2022**, *126* (11), 5333−5342.
(175) Schürmann, R.; Ebel, K.; Nicolas, C.; Milosavljević, A. R.; Bald, I. Role of Valence Band States and Plasmonic Enhancement in Electron-Transfer-Induced Transformation of Nitrothiophenol. *J. Phys. Chem. Lett.* **2019**, *10* (11), 3153−3158.
(176) Jain, P. K. Taking the Heat Off of Plasmonic Chemistry. *J. Phys. Chem. C* **2019**, *123* (40), 24347−24351.
(177) Baffou, G.; Bordacchini, I.; Baldi, A.; Quidant, R. Simple experimental procedures to distinguish photothermal from hot-carrier processes in plasmonics. *Light: Science & Applications* **2020**, *9* (1), 108.
(178) Koopman, W.; Sarhan, R. M.; Stete, F.; Schmitt, C. N. Z.; Bargheer, M. Decoding the kinetic limitations of plasmon catalysis: the case of 4-nitrothiophenol dimerization. *Nanoscale* **2020**, *12* (48), 24411−24418.
(179) Kim, Y.; Dumett Torres, D.; Jain, P. K. Activation Energies of Plasmonic Catalysts. *Nano Lett.* **2016**, *16* (5), 3399−3407.
(180) Zoltowski, C. M.; Shoup, D. N.; Schultz, Z. D. Investigation of SERS Frequency Fluctuations Relevant to Sensing and Catalysis. *J. Phys. Chem. C* **2022**, *126* (34), 14547−14557.
(181) de Albuquerque, C. D. L.; Zoltowski, C. M.; Scarpitti, B. T.; Shoup, D. N.; Schultz, Z. D. Spectrally Resolved Surface-Enhanced Raman Scattering Imaging Reveals Plasmon-Mediated Chemical Transformations. *ACS Nanosci Au* **2021**, *1* (1), 38−46.

https://doi.org/10.1021/acsnano.4c06192
ACS Nano XXXX, XXX, XXX−XXX

(182) Hartland, G. V. Optical Studies of Dynamics in Noble Metal Nanostructures. *Chem. Rev.* **2011**, *111* (6), 3858−3887.
(183) Liu, J. G.; Zhang, H.; Link, S.; Nordlander, P. Relaxation of Plasmon-Induced Hot Carriers. *ACS Photonics* **2018**, *5* (7), 2584−2595.
(184) Wu, K.; Chen, J.; McBride, J. R.; Lian, T. Efficient hot-electron transfer by a plasmon-induced interfacial charge-transfer transition. *Science* **2015**, *349* (6248), 632−635.
(185) Keller, E. L.; Brandt, N. C.; Cassabaum, A. A.; Frontiera, R. R. Ultrafast surface-enhanced Raman spectroscopy. *Analyst* **2015**, *140* (15), 4922−4931.
(186) Zheng, X.; Ye, Z.; Akmal, Z.; He, C.; Zhang, J.; Wang, L. Recent progress in SERS monitoring of photocatalytic reactions. *Chem. Soc. Rev.* **2024**, *53* (2), 656−683.
(187) Gruenke, N. L.; Cardinal, M. F.; McAnally, M. O.; Frontiera, R. R.; Schatz, G. C.; Van Duyne, R. P. Ultrafast and nonlinear surface-enhanced Raman spectroscopy. *Chem. Soc. Rev.* **2016**, *45* (8), 2263−2290.
(188) Warkentin, C. L.; Frontiera, R. R. Quantifying the ultrafast and steady-state molecular reduction potential of a plasmonic photocatalyst. *Proc. Natl. Acad. Sci. U. S. A.* **2023**, *120* (44), e2305932120.
(189) Boerigter, C.; Aslam, U.; Linic, S. Mechanism of Charge Transfer from Plasmonic Nanostructures to Chemically Attached Materials. *ACS Nano* **2016**, *10* (6), 6108−6115.
(190) Wu, S.; Sheldon, M. Mechanisms of Photothermalization in Plasmonic Nanostructures: Insights into the Steady State. *Annu. Rev. Phys. Chem.* **2023**, *74* (1), 521−545.
(191) Yu, Z.; Frontiera, R. R. Intermolecular Forces Dictate Vibrational Energy Transfer in Plasmonic−Molecule Systems. *ACS Nano* **2022**, *16* (1), 847−854.
(192) Prince, R. C.; Frontiera, R. R.; Potma, E. O. Stimulated Raman Scattering: From Bulk to Nano. *Chem. Rev.* **2017**, *117* (7), 5070−5094.
(193) Buchanan, L. E.; Gruenke, N. L.; McAnally, M. O.; Negru, B.; Mayhew, H. E.; Apkarian, V. A.; Schatz, G. C.; Van Duyne, R. P. Surface-Enhanced Femtosecond Stimulated Raman Spectroscopy at 1 MHz Repetition Rates. *J. Phys. Chem. Lett.* **2016**, *7* (22), 4629−4634.
(194) Zong, C.; Premasiri, R.; Lin, H.; Huang, Y.; Zhang, C.; Yang, C.; Ren, B.; Ziegler, L. D.; Cheng, J.-X. Plasmon-enhanced stimulated Raman scattering microscopy with single-molecule detection sensitivity. *Nat. Commun.* **2019**, *10* (1), 5318.
(195) Yampolsky, S.; Fishman, D. A.; Dey, S.; Hulkko, E.; Banik, M.; Potma, E. O.; Apkarian, V. A. Seeing a single molecule vibrate through time-resolved coherent anti-Stokes Raman scattering. *Nat. Photonics* **2014**, *8* (8), 650−656.
(196) Kumar, P.; Kuramochi, H.; Takeuchi, S.; Tahara, T. Photoexcited Plasmon-Driven Ultrafast Dynamics of the Adsorbate Probed by Femtosecond Time-Resolved Surface-Enhanced Time-Domain Raman Spectroscopy. *J. Phys. Chem. Lett.* **2023**, *14* (11), 2845−2853.
(197) Brosseau, C. L.; Colina, A.; Perales-Rondon, J. V.; Wilson, A. J.; Joshi, P. B.; Ren, B.; Wang, X. Electrochemical surface-enhanced Raman spectroscopy. *Nature Reviews Methods Primers* **2023**, *3* (1), 79.
(198) Zhang, H.; Wei, J.; Zhang, X.-G.; Zhang, Y.-J.; Radjenovica, P. M.; Wu, D.-Y.; Pan, F.; Tian, Z.-Q.; Li, J.-F. Plasmon-Induced Interfacial Hot-Electron Transfer Directly Probed by Raman Spectroscopy. *Chem.* **2020**, *6* (3), 689−702.
(199) Li, J. F.; Huang, Y. F.; Ding, Y.; Yang, Z. L.; Li, S. B.; Zhou, X. S.; Fan, F. R.; Zhang, W.; Zhou, Z. Y.; Wu, D. Y.; Ren, B.; Wang, Z. L.; Tian, Z. Q. Shell-isolated nanoparticle-enhanced Raman spectroscopy. *Nature* **2010**, *464* (7287), 392−395.
(200) Zhang, H.; Zhang, X.-G.; Wei, J.; Wang, C.; Chen, S.; Sun, H.-L.; Wang, Y.-H.; Chen, B.-H.; Yang, Z.-L.; Wu, D.-Y.; Li, J.-F.; Tian, Z.-Q. Revealing the Role of Interfacial Properties on Catalytic Behaviors by in Situ Surface-Enhanced Raman Spectroscopy. *J. Am. Chem. Soc.* **2017**, *139* (30), 10339−10346.
(201) Li, C.-Y.; Le, J.-B.; Wang, Y.-H.; Chen, S.; Yang, Z.-L.; Li, J.-F.; Cheng, J.; Tian, Z.-Q. In situ probing electrified interfacial water structures at atomically flat surfaces. *Nat. Mater.* **2019**, *18* (7), 697−701.
(202) Hartman, T.; Wondergem, C. S.; Weckhuysen, B. M. Practical Guidelines for Shell-Isolated Nanoparticle-Enhanced Raman Spectroscopy of Heterogeneous Catalysts. *ChemPhysChem* **2018**, *19* (19), 2461−2467.
(203) Hartman, T.; Weckhuysen, B. M. Thermally Stable TiO_2- and SiO_2-Shell-Isolated Au Nanoparticles for In Situ Plasmon-Enhanced Raman Spectroscopy of Hydrogenation Catalysts. *Chemistry − A European Journal* **2018**, *24* (15), 3733−3741.
(204) Wondergem, C. S.; van Swieten, T. P.; Geitenbeek, R. G.; Erné, B. H.; Weckhuysen, B. M. Extending Surface-Enhanced Raman Spectroscopy to Liquids Using Shell-Isolated Plasmonic Superstructures. *Chemistry − A European Journal* **2019**, *25* (69), 15772−15778.
(205) Wondergem, C. S.; Hartman, T.; Weckhuysen, B. M. In Situ Shell-Isolated Nanoparticle-Enhanced Raman Spectroscopy to Unravel Sequential Hydrogenation of Phenylacetylene over Platinum Nanoparticles. *ACS Catal.* **2019**, *9* (12), 10794−10802.
(206) Ze, H.; Chen, X.; Wang, X.-T.; Wang, Y.-H.; Chen, Q.-Q.; Lin, J.-S.; Zhang, Y.-J.; Zhang, X.-G.; Tian, Z.-Q.; Li, J.-F. Molecular Insight of the Critical Role of Ni in Pt-Based Nanocatalysts for Improving the Oxygen Reduction Reaction Probed Using an In Situ SERS Borrowing Strategy. *J. Am. Chem. Soc.* **2021**, *143* (3), 1318−1322.
(207) Sun, Y.-L.; A, Y.-L.; Yue, M.-F.; Chen, H.-Q.; Ze, H.; Wang, Y.-H.; Dong, J.-C.; Tian, Z.-Q.; Fang, P.-P.; Li, J.-F. Exploring the Effect of Pd on the Oxygen Reduction Performance of Pt by In Situ Raman Spectroscopy. *Anal. Chem.* **2022**, *94* (11), 4779−4786.
(208) Lin, X.-M.; Wang, X.-T.; Deng, Y.-L.; Chen, X.; Chen, H.-N.; Radjenovic, P. M.; Zhang, X.-G.; Wang, Y.-H.; Dong, J.-C.; Tian, Z.-Q.; Li, J.-F. In Situ Probe of the Hydrogen Oxidation Reaction Intermediates on PtRu a Bimetallic Catalyst Surface by Core−Shell Nanoparticle-Enhanced Raman Spectroscopy. *Nano Lett.* **2022**, *22* (13), 5544−5552.
(209) Chen, X.; Wang, X.-T.; Le, J.-B.; Li, S.-M.; Wang, X.; Zhang, Y.-J.; Radjenovic, P.; Zhao, Y.; Wang, Y.-H.; Lin, X.-M.; Dong, J.-C.; Li, J.-F. Revealing the role of interfacial water and key intermediates at ruthenium surfaces in the alkaline hydrogen evolution reaction. *Nat. Commun.* **2023**, *14* (1), 5289.
(210) Chen, J.; Liu, G.; Zhu, Y.-z.; Su, M.; Yin, P.; Wu, X.-j.; Lu, Q.; Tan, C.; Zhao, M.; Liu, Z.; Yang, W.; Li, H.; Nam, G.-H.; Zhang, L.; Chen, Z.; Huang, X.; Radjenovic, P. M.; Huang, W.; Tian, Z.-q.; Li, J.-f.; Zhang, H. Ag@MoS_2 Core−Shell Heterostructure as SERS Platform to Reveal the Hydrogen Evolution Active Sites of Single-Layer MoS_2. *J. Am. Chem. Soc.* **2020**, *142* (15), 7161−7167.
(211) Hu, Y.; Hu, C.; Du, A.; Xiao, T.; Yu, L.; Yang, C.; Xie, W. Interfacial Evolution on Co-based Oxygen Evolution Reaction Electrocatalysts Probed by Using In Situ Surface-Enhanced Raman Spectroscopy. *Anal. Chem.* **2022**, *95* (2), 1703−1709.
(212) Xu, C.; Ge, A.; Kannari, K.; Peng, B.; Xue, M.; Ding, B.; Inoue, K.-i.; Zhang, X.; Ye, S. The Decisive Role of Li_2O_2 Desorption for Oxygen Reduction Reaction in Li−O2 Batteries. *ACS Energy Letters* **2023**, *8* (3), 1289−1299.
(213) Dong, J.-C.; Zhang, X.-G.; Briega-Martos, V.; Jin, X.; Yang, J.; Chen, S.; Yang, Z.-L.; Wu, D.-Y.; Feliu, J. M.; Williams, C. T.; Tian, Z.-Q.; Li, J.-F. In situ Raman spectroscopic evidence for oxygen reduction reaction intermediates at platinum single-crystal surfaces. *Nature Energy* **2019**, *4* (1), 60−67.
(214) Dong, J.-C.; Su, M.; Briega-Martos, V.; Li, L.; Le, J.-B.; Radjenovic, P.; Zhou, X.-S.; Feliu, J. M.; Tian, Z.-Q.; Li, J.-F. Direct In Situ Raman Spectroscopic Evidence of Oxygen Reduction Reaction Intermediates at High-Index Pt(hkl) Surfaces. *J. Am. Chem. Soc.* **2020**, *142* (2), 715−719.
(215) Zhao, Y.; Zhang, X.-G.; Bodappa, N.; Yang, W.-M.; Liang, Q.; Radjenovica, P. M.; Wang, Y.-H.; Zhang, Y.-J.; Dong, J.-C.; Tian, Z.-Q.; Li, J.-F. Elucidating electrochemical CO_2 reduction reaction processes on Cu(hkl) single-crystal surfaces by in situ Raman spectroscopy. *Energy Environ. Sci.* **2022**, *15* (9), 3968−3977.
(216) Zheng, M.; Wang, P.; Zhi, X.; Yang, K.; Jiao, Y.; Duan, J.; Zheng, Y.; Qiao, S.-Z. Electrocatalytic CO_2-to-C_{2+} with Ampere-Level Current

https://doi.org/10.1021/acsnano.4c06192
ACS Nano XXXX, XXX, XXX−XXX

on Heteroatom-Engineered Copper via Tuning *CO Intermediate Coverage. *J. Am. Chem. Soc.* **2022**, *144* (32), 14936−14944.
(217) Shan, W.; Liu, R.; Zhao, H.; He, Z.; Lai, Y.; Li, S.; He, G.; Liu, J. In Situ Surface-Enhanced Raman Spectroscopic Evidence on the Origin of Selectivity in CO_2 Electrocatalytic Reduction. *ACS Nano* **2020**, *14* (9), 11363−11372.
(218) Wang, Y.-H.; Zheng, S.; Yang, W.-M.; Zhou, R.-Y.; He, Q.-F.; Radjenovic, P.; Dong, J.-C.; Li, S.; Zheng, J.; Yang, Z.-L.; Attard, G.; Pan, F.; Tian, Z.-Q.; Li, J.-F. In situ Raman spectroscopy reveals the structure and dissociation of interfacial water. *Nature* **2021**, *600* (7887), 81−85.
(219) Rowe, J. E.; Shank, C. V.; Zwemer, D. A.; Murray, C. A. Ultrahigh-Vacuum Studies of Enhanced Raman Scattering from Pyridine on Ag Surfaces. *Phys. Rev. Lett.* **1980**, *44* (26), 1770−1773.
(220) King, F. W.; Van Duyne, R. P.; Schatz, G. C. Theory of Raman scattering by molecules adsorbed on electrode surfaces. *J. Chem. Phys.* **1978**, *69* (10), 4472−4481.
(221) Ayars, E. J.; Hallen, H. D.; Jahncke, C. L. Electric Field Gradient Effects in Raman Spectroscopy. *Phys. Rev. Lett.* **2000**, *85* (19), 4180−4183.
(222) Gersten, J. I.; Birke, R. L.; Lombardi, J. R. Theory of Enhance I Light Scattering from Molecules Adsorbed at the Metal-Solution Interface. *Phys. Rev. Lett.* **1979**, *43* (2), 147−150.
(223) Lombardi, J. R.; Birke, R. L.; Lu, T.; Xu, J. Charge-transfer theory of surface enhanced Raman spectroscopy: Herzberg−Teller contributions. *J. Chem. Phys.* **1986**, *84* (8), 4174−4180.
(224) Ueba, H. Theory of charge transfer excitation in surface enhanced Raman scattering. *Surf. Sci.* **1983**, *131* (2), 347−366.
(225) Furtak, T. E.; Macomber, S. H. Voltage-induced shifting of charge-transfer excitations and their role in surface-enhanced Raman scattering. *Chem. Phys. Lett.* **1983**, *95* (4), 328−332.
(226) Osawa, M.; Matsuda, N.; Yoshii, K.; Uchida, I. Charge transfer resonance Raman process in surface-enhanced Raman scattering from p-aminothiophenol adsorbed on silver: Herzberg-Teller contribution. *J. Phys. Chem.* **1994**, *98* (48), 12702−12707.
(227) Cai, W.-B.; Amano, T.; Osawa, M. A comparison of surface-enhanced infrared and surface-enhanced Raman spectra of pyrazine adsorbed on polycrystalline gold electrodes. *J. Electroanal. Chem.* **2001**, *500* (1), 147−155.
(228) Sawai, Y.; Takimoto, B.; Nabika, H.; Ajito, K.; Murakoshi, K. Observation of a Small Number of Molecules at a Metal Nanogap Arrayed on a Solid Surface Using Surface-Enhanced Raman Scattering. *J. Am. Chem. Soc.* **2007**, *129* (6), 1658−1662.
(229) Nagasawa, F.; Takase, M.; Nabika, H.; Murakoshi, K. Polarization characteristics of surface-enhanced Raman scattering from a small number of molecules at the gap of a metal nano-dimer. *Chem. Commun.* **2011**, *47* (15), 4514−4516.
(230) Oyamada, N.; Minamimoto, H.; Wakisaka, Y.; Murakoshi, K. Determination of Molecular Orientation in Bi-analyte Mono-molecule Layer through Electrochemical Surface-enhanced Raman Scattering Measurements. *Chem. Lett.* **2019**, *48* (8), 820−823.
(231) Oyamada, N.; Minamimoto, H.; Murakoshi, K. In Situ Observation of Unique Bianalyte Molecular Behaviors at the Gap of a Single Metal Nanodimer Structure via Electrochemical Surface-Enhanced Raman Scattering Measurements. *J. Phys. Chem. C* **2019**, *123* (40), 24740−24745.
(232) Oyamada, N.; Minamimoto, H.; Murakoshi, K. Room-Temperature Molecular Manipulation via Plasmonic Trapping at Electrified Interfaces. *J. Am. Chem. Soc.* **2022**, *144* (6), 2755−2764.
(233) Konishi, T.; Kiguchi, M.; Takase, M.; Nagasawa, F.; Nabika, H.; Ikeda, K.; Uosaki, K.; Ueno, K.; Misawa, H.; Murakoshi, K. Single Molecule Dynamics at a Mechanically Controllable Break Junction in Solution at Room Temperature. *J. Am. Chem. Soc.* **2013**, *135* (3), 1009−1014.
(234) Takase, M.; Ajiki, H.; Mizumoto, Y.; Komeda, K.; Nara, M.; Nabika, H.; Yasuda, S.; Ishihara, H.; Murakoshi, K. Selection-rule breakdown in plasmon-induced electronic excitation of an isolated single-walled carbon nanotube. *Nat. Photonics* **2013**, *7* (7), 550−554.
(235) Zhang, J.; Zhou, R.; Minamimoto, H.; Yasuda, S.; Murakoshi, K. Nonzero Wavevector Excitation of Graphene by Localized Surface Plasmons. *Nano Lett.* **2019**, *19* (11), 7887−7894.
(236) Nagarajan, K.; Thomas, A.; Ebbesen, T. W. Chemistry under Vibrational Strong Coupling. *J. Am. Chem. Soc.* **2021**, *143* (41), 16877−16889.
(237) Hutchison, J. A.; Schwartz, T.; Genet, C.; Devaux, E.; Ebbesen, T. W. Modifying Chemical Landscapes by Coupling to Vacuum Fields. *Angew. Chem., Int. Ed.* **2012**, *51* (7), 1592−1596.
(238) Thomas, A.; Lethuillier-Karl, L.; Nagarajan, K.; Vergauwe, R. M. A.; George, J.; Chervy, T.; Shalabney, A.; Devaux, E.; Genet, C.; Moran, J.; Ebbesen, T. W. Tilting a ground-state reactivity landscape by vibrational strong coupling. *Science* **2019**, *363* (6427), 615−619.
(239) Fukushima, T.; Yoshimitsu, S.; Murakoshi, K. Inherent Promotion of Ionic Conductivity via Collective Vibrational Strong Coupling of Water with the Vacuum Electromagnetic Field. *J. Am. Chem. Soc.* **2022**, *144* (27), 12177−12183.
(240) Fukushima, T.; Yoshimitsu, S.; Murakoshi, K. Unlimiting ionic conduction: manipulating hydration dynamics through vibrational strong coupling of water. *Chemical Science* **2023**, *14* (41), 11441−11446.
(241) Orgiu, E.; George, J.; Hutchison, J. A.; Devaux, E.; Dayen, J. F.; Doudin, B.; Stellacci, F.; Genet, C.; Schachenmayer, J.; Genes, C.; Pupillo, G.; Samorì, P.; Ebbesen, T. W. Conductivity in organic semiconductors hybridized with the vacuum field. *Nat. Mater.* **2015**, *14* (11), 1123−1129.
(242) Nagasawa, F.; Takase, M.; Murakoshi, K. Raman Enhancement via Polariton States Produced by Strong Coupling between a Localized Surface Plasmon and Dye Excitons at Metal Nanogaps. *J. Phys. Chem. Lett.* **2014**, *5* (1), 14−19.
(243) Fainstein, A.; Jusserand, B. Raman Scattering in Resonant Cavities. In *Light Scattering in Solid IX*, Cardona, M.; Merlin, R., Eds.; Springer Berlin Heidelberg: Berlin, Heidelberg, 2007; pp 17−110.
(244) Zou, S.; Weaver, M. J. Surface-Enhanced Raman Scattering on Uniform Transition-Metal Films: Toward a Versatile Adsorbate Vibrational Strategy for Solid-Nonvacuum Interfaces? *Anal. Chem.* **1998**, *70* (11), 2387−2395.
(245) Zou, S.; Williams, C. T.; Chen, E. K. Y.; Weaver, M. J. Probing Molecular Vibrations at Catalytically Significant Interfaces: A New Ubiquity of Surface-Enhanced Raman Scattering. *J. Am. Chem. Soc.* **1998**, *120* (15), 3811−3812.
(246) Weaver, M. J.; Zou, S.; Chan, H. Y. H. Peer Reviewed: The New Interfacial Ubiquity of Surface-Enhanced Raman Spectroscopy. *Anal. Chem.* **2000**, *72* (1), 38A−47A.
(247) Tian, Z.-Q.; Ren, B.; Wu, D.-Y. Surface-Enhanced Raman Scattering: From Noble to Transition Metals and from Rough Surfaces to Ordered Nanostructures. *J. Phys. Chem. B* **2002**, *106* (37), 9463−9483.
(248) Tian, Z.-Q.; Ren, B.; Li, J.-F.; Yang, Z.-L. Expanding generality of surface-enhanced Raman spectroscopy with borrowing SERS activity strategy. *Chem. Commun.* **2007**, *34*, 3514−3534.
(249) Cortés, E.; Grzeschik, R.; Maier, S. A.; Schlücker, S. Experimental characterization techniques for plasmon-assisted chemistry. *Nature Reviews Chemistry* **2022**, *6* (4), 259−274.
(250) Pradhan, N.; Pal, A.; Pal, T. Silver nanoparticle catalyzed reduction of aromatic nitro compounds. *Colloids Surf., A* **2002**, *196* (2), 247−257.
(251) Xie, W.; Herrmann, C.; Kömpe, K.; Haase, M.; Schlücker, S. Synthesis of Bifunctional Au/Pt/Au Core/Shell Nanoraspberries for in Situ SERS Monitoring of Platinum-Catalyzed Reactions. *J. Am. Chem. Soc.* **2011**, *133* (48), 19302−19305.
(252) Xie, W.; Walkenfort, B.; Schlücker, S. Label-Free SERS Monitoring of Chemical Reactions Catalyzed by Small Gold Nanoparticles Using 3D Plasmonic Superstructures. *J. Am. Chem. Soc.* **2013**, *135* (5), 1657−1660.
(253) Xie, W.; Grzeschik, R.; Schlücker, S. Metal Nanoparticle-Catalyzed Reduction Using Borohydride in Aqueous Media: A Kinetic Analysis of the Surface Reaction by Microfluidic SERS. *Angew. Chem., Int. Ed.* **2016**, *55* (44), 13729−13733.

https://doi.org/10.1021/acsnano.4c06192
ACS Nano XXXX, XXX, XXX−XXX

(254) Zhao, Y.; Du, L.; Li, H.; Xie, W.; Chen, J. Is the Suzuki−Miyaura Cross-Coupling Reaction in the Presence of Pd Nanoparticles Heterogeneously or Homogeneously Catalyzed? An Interfacial Surface-Enhanced Raman Spectroscopy Study. *J. Phys. Chem. Lett.* **2019**, *10* (6), 1286−1291.
(255) Ling, X. Y.; Yan, R.; Lo, S.; Hoang, D. T.; Liu, C.; Fardy, M. A.; Khan, S. B.; Asiri, A. M.; Bawaked, S. M.; Yang, P. Alumina-coated Ag nanocrystal monolayers as surfaceenhanced Raman spectroscopy platforms for the direct spectroscopic detection of water splitting reaction intermediates. *Nano Research* **2014**, *7* (1), 132−143.
(256) Wang, Y.-H.; Le, J.-B.; Li, W.-Q.; Wei, J.; Radjenovic, P. M.; Zhang, H.; Zhou, X.-S.; Cheng, J.; Tian, Z.-Q.; Li, J.-F. In situ Spectroscopic Insight into the Origin of the Enhanced Performance of Bimetallic Nanocatalysts towards the Oxygen Reduction Reaction (ORR). *Angew. Chem., Int. Ed.* **2019**, *58* (45), 16062−16066.
(257) Zhang, H.; Wang, C.; Sun, H.-L.; Fu, G.; Chen, S.; Zhang, Y.-J.; Chen, B.-H.; Anema, J. R.; Yang, Z.-L.; Li, J.-F.; Tian, Z.-Q. In situ dynamic tracking of heterogeneous nanocatalytic processes by shell-isolated nanoparticle-enhanced Raman spectroscopy. *Nat. Commun.* **2017**, *8* (1), 15447.
(258) Li, Y.; Hu, Y.; Shi, F.; Li, H.; Xie, W.; Chen, J. C−H Arylation on Nickel Nanoparticles Monitored by In Situ Surface-Enhanced Raman Spectroscopy. *Angew. Chem., Int. Ed.* **2019**, *58* (27), 9049−9053.
(259) Hu, C.; Hu, Y.; Fan, C.; Yang, L.; Zhang, Y.; Li, H.; Xie, W. Surface-Enhanced Raman Spectroscopic Evidence of Key Intermediate Species and Role of NiFe Dual-Catalytic Center in Water Oxidation. *Angew. Chem., Int. Ed.* **2021**, *60* (36), 19774−19778.
(260) Chen, H.-Q.; Ze, H.; Yue, M.-F.; Wei, D.-Y.; A, Y.-L.; Wu, Y.-F.; Dong, J.-C.; Zhang, Y.-J.; Zhang, H.; Tian, Z.-Q.; Li, J.-F. Unmasking the Critical Role of the Ordering Degree of Bimetallic Nanocatalysts on Oxygen Reduction Reaction by In Situ Raman Spectroscopy. *Angew. Chem., Int. Ed.* **2022**, *61* (16), e202117834.
(261) Wei, J.; Qin, S.-N.; Yang, J.; Ya, H.-L.; Huang, W.-H.; Zhang, H.; Hwang, B. J.; Tian, Z.-Q.; Li, J.-F. Probing Single-Atom Catalysts and Catalytic Reaction Processes by Shell-Isolated Nanoparticle-Enhanced Raman Spectroscopy. *Angew. Chem., Int. Ed.* **2021**, *60* (17), 9306−9310.
(262) Yang, L.; Grzeschik, R.; Jiang, P.; Yu, L.; Hu, C.; Du, A.; Schlücker, S.; Xie, W. Tuning the Electronic Properties of Platinum in Hybrid-Nanoparticle Assemblies for use in Hydrogen Evolution Reaction. *Angew. Chem., Int. Ed.* **2023**, *62* (25), e202301065.
(263) Hess, C. New advances in using Raman spectroscopy for the characterization of catalysts and catalytic reactions. *Chem. Soc. Rev.* **2021**, *50* (5), 3519−3564.
(264) Hartman, T.; Wondergem, C. S.; Kumar, N.; van den Berg, A.; Weckhuysen, B. M. Surface- and Tip-Enhanced Raman Spectroscopy in Catalysis. *J. Phys. Chem. Lett.* **2016**, *7* (8), 1570−1584.
(265) Alessandri, I.; Depero, L. E. All-Oxide Raman-Active Traps for Light and Matter: Probing Redox Homeostasis Model Reactions in Aqueous Environment. *Small* **2014**, *10* (7), 1294−1298.
(266) Alessandri, I.; Lombardi, J. R. Enhanced Raman Scattering with Dielectrics. *Chem. Rev.* **2016**, *116* (24), 14921−14981.
(267) Bontempi, N.; Vassalini, I.; Alessandri, I. All-dielectric core/shell resonators: From plasmon-free SERS to multimodal analysis. *J. Raman Spectrosc.* **2018**, *49* (6), 943−953.
(268) Alessandri, I.; Carletti, L.; Ferroni, M.; De Angelis, C.; Vassalini, I. Bioinspired self-similar all-dielectric antennas: probing the effect of secondary scattering centres by Raman spectroscopy. *Materials Advances* **2020**, *1* (7), 2443−2449.
(269) Vassalini, I.; Sisman, O.; Comini, E.; Alessandri, I. The role of morphology in all-dielectric SERS: A comparison between conformal (T-rex) and non conformal TiO_2 shells. *Vib. Spectrosc.* **2020**, *109*, 103085.
(270) Alessandri, I. Enhancing Raman Scattering without Plasmons: Unprecedented Sensitivity Achieved by TiO_2 Shell-Based Resonators. *J. Am. Chem. Soc.* **2013**, *135* (15), 5541−5544.
(271) Bontempi, N.; Carletti, L.; De Angelis, C.; Alessandri, I. Plasmon-free SERS detection of environmental CO_2 on TiO_2 surfaces. *Nanoscale* **2016**, *8* (6), 3226−3231.
(272) Alessandri, I.; Vassalini, I.; Bertuzzi, M.; Bontempi, N.; Memo, M.; Gianoncelli, A. RaMassays": Synergistic Enhancement of Plasmon-Free Raman Scattering and Mass Spectrometry for Multimodal Analysis of Small Molecules. *Sci. Rep.* **2016**, *6* (1), 34521.
(273) Bontempi, N.; Vassalini, I.; Danesi, S.; Alessandri, I. ZORRO: zirconium oxide resonators for all-in-one Raman and whispering-gallery-mode optical sensing. *Chem. Commun.* **2017**, *53* (75), 10382−10385.
(274) Qi, D.; Lu, L.; Wang, L.; Zhang, J. Improved SERS Sensitivity on Plasmon-Free TiO_2 Photonic Microarray by Enhancing Light-Matter Coupling. *J. Am. Chem. Soc.* **2014**, *136* (28), 9886−9889.
(275) Alessandri, I.; Zucca, M.; Ferroni, M.; Bontempi, E.; Depero, L. E. Tailoring the Pore Size and Architecture of CeO_2/TiO_2 Core/Shell Inverse Opals by Atomic Layer Deposition. *Small* **2009**, *5* (3), 336−340.
(276) Zheng, X.; Zhang, W.; Zhang, J.; Wang, L. Synthesis of yolk-shell Fe_3O_4@void@CeO_2 nanoparticles and their application in SERS. *Appl. Surf. Sci.* **2021**, *541*, 148422.
(277) Ji, W.; Li, L.; Song, W.; Wang, X.; Zhao, B.; Ozaki, Y. Enhanced Raman Scattering by ZnO Superstructures: Synergistic Effect of Charge Transfer and Mie Resonances. *Angew. Chem., Int. Ed.* **2019**, *58* (41), 14452−14456.
(278) Bontempi, N.; Salmistraro, M.; Ferroni, M.; Depero, L. E.; Alessandri, I. Probing the spatial extension of light trapping-induced enhanced Raman scattering in high-density Si nanowire arrays. *Nanotechnology* **2014**, *25* (46), 465705.
(279) Qiu, B.; Xing, M.; Yi, Q.; Zhang, J. Chiral Carbonaceous Nanotubes Modified with Titania Nanocrystals: Plasmon-Free and Recyclable SERS Sensitivity. *Angew. Chem., Int. Ed.* **2015**, *54* (36), 10643−10647.
(280) Hu, H.; Pal, A. K.; Berestennikov, A.; Weber, T.; Stefancu, A.; Cortés, E.; Maier, S. A.; Tittl, A. Surface-Enhanced Raman Scattering in BIC-Driven Semiconductor Metasurfaces. *Advanced Optical Materials* **2024**, *12* (14), 2302812.
(281) Barros, E. B.; Dresselhaus, M. S. Theory of Raman enhancement by two-dimensional materials: Applications for graphene-enhanced Raman spectroscopy. *Phys. Rev. B* **2014**, *90* (3), No. 035443.
(282) He, Z.; Rong, T.; Li, Y.; Ma, J.; Li, Q.; Wu, F.; Wang, Y.; Wang, F. Two-Dimensional TiVC Solid-Solution MXene as Surface-Enhanced Raman Scattering Substrate. *ACS Nano* **2022**, *16* (3), 4072−4083.
(283) Lai, H.; Li, G.; Xu, F.; Zhang, Z. Metal−organic frameworks: opportunities and challenges for surface-enhanced Raman scattering − a review. *Journal of Materials Chemistry C* **2020**, *8* (9), 2952−2963.
(284) Cong, S.; Yuan, Y.; Chen, Z.; Hou, J.; Yang, M.; Su, Y.; Zhang, Y.; Li, L.; Li, Q.; Geng, F.; Zhao, Z. Noble metal-comparable SERS enhancement from semiconducting metal oxides by making oxygen vacancies. *Nat. Commun.* **2015**, *6* (1), 7800.
(285) Alessandri, I.; Vassalini, I. Oxygen-Mediated Surface Photoreactions: Exploring New Pathways for Sustainable Chemistry. *ChemPhotoChem.* **2023**, *7* (12), e202300069.
(286) Alessandri, I. 4-Aminothiophenol Photodimerization Without Plasmons**. *Angew. Chem., Int. Ed.* **2022**, *61* (28), e202205013.
(287) Yan, X.; Xu, Y.; Tian, B.; Lei, J.; Zhang, J.; Wang, L. Operando SERS self-monitoring photocatalytic oxidation of aminophenol on TiO_2 semiconductor. *Applied Catalysis B: Environmental* **2018**, *224*, 305−309.
(288) Liu, X.; Dong, G.; Li, S.; Lu, G.; Bi, Y. Direct Observation of Charge Separation on Anatase TiO_2 Crystals with Selectively Etched {001} Facets. *J. Am. Chem. Soc.* **2016**, *138* (9), 2917−2920.
(289) Tachikawa, T.; Yamashita, S.; Majima, T. Evidence for Crystal-Face-Dependent TiO_2 Photocatalysis from Single-Molecule Imaging and Kinetic Analysis. *J. Am. Chem. Soc.* **2011**, *133* (18), 7197−7204.
(290) Zhan, C.; Wang, Z.-Y.; Zhang, X.-G.; Chen, X.-J.; Huang, Y.-F.; Hu, S.; Li, J.-F.; Wu, D.-Y.; Moskovits, M.; Tian, Z.-Q. Interfacial Construction of Plasmonic Nanostructures for the Utilization of the Plasmon-Excited Electrons and Holes. *J. Am. Chem. Soc.* **2019**, *141* (20), 8053−8057.
(291) Wang, J.; Ando, R. A.; Camargo, P. H. C. Controlling the Selectivity of the Surface Plasmon Resonance Mediated Oxidation of p-

https://doi.org/10.1021/acsnano.4c06192
ACS Nano XXXX, XXX, XXX−XXX

Aminothiophenol on Au Nanoparticles by Charge Transfer from UV-excited TiO_2. *Angew. Chem., Int. Ed.* **2015**, *54* (23), 6909−6912.
(292) Zheng, X.; Yan, X.; Ma, J.; Yao, X.; Zhang, J.; Wang, L. Unidirectional/Bidirectional Electron Transfer at the Au/TiO_2 Interface Operando Tracked by SERS Spectra from Au and TiO2. *ACS Appl. Mater. Interfaces* **2021**, *13* (14), 16498−16506.
(293) Liu, X.; Ye, Z.; Xiang, Q.; Xu, Z.; Yue, W.; Li, C.; Xu, Y.; Wang, L.; Cao, X.; Zhang, J. Boosting electromagnetic enhancement for detection of non-adsorbing analytes on semiconductor SERS substrates. *Chem.* **2023**, *9* (6), 1464−1476.
(294) Liu, Y.-C.; Yu, C.-C.; Wang, C.-C.; Juang, L.-C. New application of photocatalytic TiO_2 nanoparticles on the improved surface-enhanced Raman scattering. *Chem. Phys. Lett.* **2006**, *420* (1), 245−249.
(295) Ben-Jaber, S.; Peveler, W. J.; Quesada-Cabrera, R.; Cortés, E.; Sotelo-Vazquez, C.; Abdul-Karim, N.; Maier, S. A.; Parkin, I. P. Photo-induced enhanced Raman spectroscopy for universal ultra-trace detection of explosives, pollutants and biomolecules. *Nat. Commun.* **2016**, *7* (1), 12189.
(296) Glass, D.; Cortés, E.; Ben-Jaber, S.; Brick, T.; Peveler, W. J.; Blackman, C. S.; Howle, C. R.; Quesada-Cabrera, R.; Parkin, I. P.; Maier, S. A. Dynamics of Photo-Induced Surface Oxygen Vacancies in Metal-Oxide Semiconductors Studied Under Ambient Conditions. *Advanced Science* **2019**, *6* (22), 1901841.
(297) Zheng, Z.; Cong, S.; Gong, W.; Xuan, J.; Li, G.; Lu, W.; Geng, F.; Zhao, Z. Semiconductor SERS enhancement enabled by oxygen incorporation. *Nat. Commun.* **2017**, *8* (1), 1993.
(298) Dagdeviren, O. E.; Glass, D.; Sapienza, R.; Cortés, E.; Maier, S. A.; Parkin, I. P.; Grütter, P.; Quesada-Cabrera, R. The Effect of Photoinduced Surface Oxygen Vacancies on the Charge Carrier Dynamics in TiO2 Films. *Nano Lett.* **2021**, *21* (19), 8348−8354.
(299) Ye, J.; Arul, R.; Nieuwoudt, M. K.; Dong, J.; Zhang, T.; Dai, L.; Greenham, N. C.; Rao, A.; Hoye, R. L. Z.; Gao, W.; Simpson, M. C. Understanding the Chemical Mechanism behind Photoinduced Enhanced Raman Spectroscopy. *J. Phys. Chem. Lett.* **2023**, *14* (19), 4607−4616.
(300) Brognara, A.; Bricchi, B. R.; William, L.; Brinza, O.; Konstantakopoulou, M.; Bassi, A. L.; Ghidelli, M.; Lidgi-Guigui, N. New Mechanism for Long Photo-Induced Enhanced Raman Spectroscopy in Au Nanoparticles Embedded in TiO_2. *Small* **2022**, *18* (25), 2201088.
(301) Guner, B.; Dincer, O.; Dagdeviren, O. E. Fast and Slow Time-Scale Effects of Photoinduced Surface Oxygen Vacancies on the Charge Carrier Dynamics of TiO2. *ACS Applied Energy Materials* **2024**, *7* (6), 2292−2298.
(302) Davison, G.; Yin, Y.; Jones, T.; Parkin, I. P.; Peveler, W. J.; Lee, T.-C. Multi-mode enhanced Raman scattering spectroscopy using aggregation-free hybrid metal/metal-oxide nanoparticles with intrinsic oxygen vacancies. *Journal of Materials Chemistry C* **2023**, *11* (9), 3334−3341.
(303) Song, G.; Cong, S.; Zhao, Z. Defect engineering in semiconductor-based SERS. *Chemical Science* **2022**, *13* (5), 1210−1224.
(304) Ben-Jaber, S.; Glass, D.; Brick, T.; Maier, S. A.; Parkin, I. P.; Cortés, E.; Peveler, W. J.; Quesada-Cabrera, R. Photo-induced enhanced Raman spectroscopy as a probe for photocatalytic surfaces. *Philosophical Transactions of the Royal Society A: Mathematical, Physical and Engineering Sciences* **2023**, *381* (2259), 20220343.
(305) Shimizu, T.; Yokouchi, T.; Oikawa, T.; Shiraishi, T.; Kiguchi, T.; Akama, A.; Konno, T. J.; Gruverman, A.; Funakubo, H. Contribution of oxygen vacancies to the ferroelectric behavior of $Hf_{0.5}Zr_{0.5}O_2$ thin films. *Appl. Phys. Lett.* **2015**, *106* (11), 112904.
(306) Yilmaz, M.; Babur, E.; Ozdemir, M.; Gieseking, R. L.; Dede, Y.; Tamer, U.; Schatz, G. C.; Facchetti, A.; Usta, H.; Demirel, G. Nanostructured organic semiconductor films for molecular detection with surface-enhanced Raman spectroscopy. *Nat. Mater.* **2017**, *16* (9), 918−924.
(307) Abid, K.; Belkhir, N. H.; Jaber, S. B.; Zribi, R.; Donato, M. G.; Di Marco, G.; Gucciardi, P. G.; Neri, G.; Maâlej, R. Photoinduced Enhanced Raman Spectroscopy with Hybrid Au@WS2 Nanosheets. *J. Phys. Chem. C* **2020**, *124* (37), 20350−20358.
(308) Sun, H.; Song, G.; Gong, W.; Lu, W.; Cong, S.; Zhao, Z. Stabilizing photo-induced vacancy defects in MOF matrix for high-performance SERS detection. *Nano Research* **2022**, *15* (6), 5347−5354.
(309) Alloghani, M.; Al-Jumeily, D.; Mustafina, J.; Hussain, A.; Aljaaf, A. J. A Systematic Review on Supervised and Unsupervised Machine Learning Algorithms for Data Science. In *Supervised and Unsupervised Learning for Data Science*, Berry, M. W.; Mohamed, A.; Yap, B. W., Eds.; Springer International Publishing: Cham, 2020; pp 3−21.
(310) Hu, W.; Ye, S.; Zhang, Y.; Li, T.; Zhang, G.; Luo, Y.; Mukamel, S.; Jiang, J. Machine Learning Protocol for Surface-Enhanced Raman Spectroscopy. *J. Phys. Chem. Lett.* **2019**, *10* (20), 6026−6031.
(311) Leong, Y. X.; Tan, E. X.; Leong, S. X.; Lin Koh, C. S.; Thanh Nguyen, L. B.; Ting Chen, J. R.; Xia, K.; Ling, X. Y. Where Nanosensors Meet Machine Learning: Prospects and Challenges in Detecting Disease X. *ACS Nano* **2022**, *16* (9), 13279−13293.
(312) Masson, J.-F.; Biggins, J. S.; Ringe, E. Machine learning for nanoplasmonics. *Nat. Nanotechnol.* **2023**, *18* (2), 111−123.
(313) Rück, M.; Garlyyev, B.; Mayr, F.; Bandarenka, A. S.; Gagliardi, A. Oxygen Reduction Activities of Strained Platinum Core−Shell Electrocatalysts Predicted by Machine Learning. *J. Phys. Chem. Lett.* **2020**, *11* (5), 1773−1780.
(314) Sun, B.; Fernandez, M.; Barnard, A. S. Machine Learning for Silver Nanoparticle Electron Transfer Property Prediction. *J. Chem. Inf. Model.* **2017**, *57* (10), 2413−2423.
(315) Tan, E. X.; Chen, Y.; Lee, Y. H.; Leong, Y. X.; Leong, S. X.; Stanley, C. V.; Pun, C. S.; Ling, X. Y. Incorporating plasmonic featurization with machine learning to achieve accurate and bidirectional prediction of nanoparticle size and size distribution. *Nanoscale Horizons* **2022**, *7* (6), 626−633.
(316) Tan, E. X.; Tang, J.; Leong, Y. X.; Phang, I. Y.; Lee, Y. H.; Pun, C. S.; Ling, X. Y. Creating 3D Nanoparticle Structural Space via Data Augmentation to Bidirectionally Predict Nanoparticle Mixture's Purity, Size, and Shape from Extinction Spectra. *Angew. Chem., Int. Ed.* **2024**, *63* (14), e202317978.
(317) Masood, H.; Toe, C. Y.; Teoh, W. Y.; Sethu, V.; Amal, R. Machine Learning for Accelerated Discovery of Solar Photocatalysts. *ACS Catal.* **2019**, *9* (12), 11774−11787.
(318) Zhong, X.; Gallagher, B.; Liu, S.; Kailkhura, B.; Hiszpanski, A.; Han, T. Y.-J. Explainable machine learning in materials science. *npj Computational Materials* **2022**, *8* (1), 204.
(319) Son, J.; Kim, G.-H.; Lee, Y.; Lee, C.; Cha, S.; Nam, J.-M. Toward Quantitative Surface-Enhanced Raman Scattering with Plasmonic Nanoparticles: Multiscale View on Heterogeneities in Particle Morphology, Surface Modification, Interface, and Analytical Protocols. *J. Am. Chem. Soc.* **2022**, *144* (49), 22337−22351.
(320) Bi, X.; Lin, L.; Chen, Z.; Ye, J. Artificial Intelligence for Surface-Enhanced Raman Spectroscopy. *Small Methods* **2024**, *8* (1), 2301243.
(321) Bajomo, M. M.; Ju, Y.; Zhou, J.; Elefterescu, S.; Farr, C.; Zhao, Y.; Neumann, O.; Nordlander, P.; Patel, A.; Halas, N. J. Computational chromatography: A machine learning strategy for demixing individual chemical components in complex mixtures. *Proc. Natl. Acad. Sci. U. S. A.* **2022**, *119* (52), e2211406119.
(322) de Albuquerque, C. D. L.; Sobral-Filho, R. G.; Poppi, R. J.; Brolo, A. G. Digital Protocol for Chemical Analysis at Ultralow Concentrations by Surface-Enhanced Raman Scattering. *Anal. Chem.* **2018**, *90* (2), 1248−1254.
(323) Cai, J.; Wu, Y.; Bai, H.; He, Y.; Qin, Y. SERS and machine learning based effective feature extraction for detection and identification of amphetamine analogs. *Heliyon* **2023**, *9* (12), e23109.
(324) Xie, Y.; You, Q.; Dai, P.; Wang, S.; Hong, P.; Liu, G.; Yu, J.; Sun, X.; Zeng, Y. How to achieve auto-identification in Raman analysis by spectral feature extraction & Adaptive Hypergraph. *Spectrochimica Acta Part A: Molecular and Biomolecular Spectroscopy* **2019**, *222*, 117086.
(325) Zhang, J.; Xin, P.-L.; Wang, X.-Y.; Chen, H.-Y.; Li, D.-W. Deep Learning-Based Spectral Extraction for Improving the Performance of Surface-Enhanced Raman Spectroscopy Analysis on Multiplexed

https://doi.org/10.1021/acsnano.4c06192
ACS Nano XXXX, XXX, XXX−XXX

Identification and Quantitation. *J. Phys. Chem. A* **2022**, *126* (14), 2278−2285.
(326) Luo, S.-h.; Wang, W.-l.; Zhou, Z.-f.; Xie, Y.; Ren, B.; Liu, G.-k.; Tian, Z.-q. Visualization of a Machine Learning Framework toward Highly Sensitive Qualitative Analysis by SERS. *Anal. Chem.* **2022**, *94* (28), 10151−10158.
(327) Beeram, R.; Banerjee, D.; Narlagiri, L. M.; Soma, V. R. Machine learning for rapid quantification of trace analyte molecules using SERS and flexible plasmonic paper substrates. *Analytical Methods* **2022**, *14* (18), 1788−1796.
(328) Thrift, W. J.; Ragan, R. Quantification of Analyte Concentration in the Single Molecule Regime Using Convolutional Neural Networks. *Anal. Chem.* **2019**, *91* (21), 13337−13342.
(329) Fang, S.; Wu, S.; Chen, Z.; He, C.; Lin, L. L.; Ye, J. Recent progress and applications of Raman spectrum denoising algorithms in chemical and biological analyses: A review. *TrAC Trends in Analytical Chemistry* **2024**, *172*, 117578.
(330) Leong, S. X.; Tan, E. X.; Han, X.; Luhung, I.; Aung, N. W.; Nguyen, L. B. T.; Tan, S. Y.; Li, H.; Phang, I. Y.; Schuster, S.; Ling, X. Y. Surface-Enhanced Raman Scattering-Based Surface Chemotaxonomy: Combining Bacteria Extracellular Matrices and Machine Learning for Rapid and Universal Species Identification. *ACS Nano* **2023**, *17* (22), 23132−23143.
(331) Tan, E. X.; Leong, S. X.; Liew, W. A.; Phang, I. Y.; Ng, J. Y.; Tan, N. S.; Lee, Y. H.; Ling, X. Y. Forward-predictive SERS-based chemical taxonomy for untargeted structural elucidation of epimeric cerebrosides. *Nat. Commun.* **2024**, *15* (1), 2582.
(332) Zong, C.; Chen, C.-J.; Zhang, M.; Wu, D.-Y.; Ren, B. Transient Electrochemical Surface-Enhanced Raman Spectroscopy: A Millisecond Time-Resolved Study of an Electrochemical Redox Process. *J. Am. Chem. Soc.* **2015**, *137* (36), 11768−11774.
(333) Smith, G.; Girardon, J.-S.; Paul, J.-F.; Berrier, E. Dynamics of a plasmon-activated p-mercaptobenzoic acid layer deposited over Au nanoparticles using time-resolved SERS. *Phys. Chem. Chem. Phys.* **2016**, *18* (29), 19567−19573.
(334) Zhang, K.; Zuo, W.; Chen, Y.; Meng, D.; Zhang, L. Beyond a Gaussian Denoiser: Residual Learning of Deep CNN for Image Denoising. *IEEE Transactions on Image Processing* **2017**, *26* (7), 3142−3155.
(335) Lussier, F.; Missirlis, D.; Spatz, J. P.; Masson, J.-F. Machine-Learning-Driven Surface-Enhanced Raman Scattering Optophysiology Reveals Multiplexed Metabolite Gradients Near Cells. *ACS Nano* **2019**, *13* (2), 1403−1411.
(336) Martirez, J. M. P.; Bao, J. L.; Carter, E. A. First-Principles Insights into Plasmon-Induced Catalysis. *Annu. Rev. Phys. Chem.* **2021**, *72* (1), 99−119.
(337) Ding, S.-Y.; Yi, J.; Li, J.-F.; Ren, B.; Wu, D.-Y.; Panneerselvam, R.; Tian, Z.-Q. Nanostructure-based plasmon-enhanced Raman spectroscopy for surface analysis of materials. *Nature Reviews Materials* **2016**, *1* (6), 16021.
(338) Liu, Z.; Ding, S.-Y.; Chen, Z.-B.; Wang, X.; Tian, J.-H.; Anema, J. R.; Zhou, X.-S.; Wu, D.-Y.; Mao, B.-W.; Xu, X.; Ren, B.; Tian, Z.-Q. Revealing the molecular structure of single-molecule junctions in different conductance states by fishing-mode tip-enhanced Raman spectroscopy. *Nat. Commun.* **2011**, *2* (1), 305.
(339) Ng, L. S.; Chah, E. L. C.; Ngieng, M. H.; Boong, S. K.; Chong, C.; Raja Mogan, T.; Lee, J.-K.; Li, H.; Lee, C.-L. K.; Lee, H. K. Chaotropic Nanoelectrocatalysis: Chemically Disrupting Water Intermolecular Network at the Point-of-Catalysis to Boost Green Hydrogen Electrosynthesis. *Angew. Chem., Int. Ed.* **2024**, *63* (8), e202317751.
(340) Chu, W.; Saidi, W. A.; Prezhdo, O. V. Long-Lived Hot Electron in a Metallic Particle for Plasmonics and Catalysis: Ab Initio Nonadiabatic Molecular Dynamics with Machine Learning. *ACS Nano* **2020**, *14* (8), 10608−10615.
(341) Chen, C.; Li, S. Valence Electron Density-Dependent Pseudopermittivity for Nonlocal Effects in Optical Properties of Metallic Nanoparticles. *ACS Photonics* **2018**, *5* (6), 2295−2304.
(342) Rüscher, M.; Herzog, A.; Timoshenko, J.; Jeon, H. S.; Frandsen, W.; Kühl, S.; Roldan Cuenya, B. Tracking heterogeneous structural motifs and the redox behaviour of copper−zinc nanocatalysts for the electrocatalytic CO2 reduction using operando time resolved spectroscopy and machine learning. *Catalysis Science & Technology* **2022**, *12* (9), 3028−3043.
(343) Chen, C.; Hayazawa, N.; Kawata, S. A 1.7 nm resolution chemical analysis of carbon nanotubes by tip-enhanced Raman imaging in the ambient. *Nat. Commun.* **2014**, *5* (1), 3312.
(344) Li, C.-Y.; Dong, J.-C.; Jin, X.; Chen, S.; Panneerselvam, R.; Rudnev, A. V.; Yang, Z.-L.; Li, J.-F.; Wandlowski, T.; Tian, Z.-Q. In Situ Monitoring of Electrooxidation Processes at Gold Single Crystal Surfaces Using Shell-Isolated Nanoparticle-Enhanced Raman Spectroscopy. *J. Am. Chem. Soc.* **2015**, *137* (24), 7648−7651.
(345) Robatjazi, H.; Bao, J. L.; Zhang, M.; Zhou, L. N.; Christopher, P.; Carter, E. A.; Nordlander, P.; Halas, N. J. Plasmon-driven carbon-fluorine (C(sp^3)-F) bond activation with mechanistic insights into hot-carrier-mediated pathways. *Nature Catalysis* **2020**, *3* (7), 564−573.
(346) Wexler, R. B.; Martirez, J. M. P.; Rappe, A. M. Chemical Pressure-Driven Enhancement of the Hydrogen Evolving Activity of Ni2P from Nonmetal Surface Doping Interpreted via Machine Learning. *J. Am. Chem. Soc.* **2018**, *140* (13), 4678−4683.
(347) Brongersma, M. L.; Halas, N. J.; Nordlander, P. Plasmon-induced hot carrier science and technology. *Nat. Nanotechnol.* **2015**, *10* (1), 25−34.
(348) Babucci, M.; Guntida, A.; Gates, B. C. Atomically Dispersed Metals on Well-Defined Supports including Zeolites and Metal−Organic Frameworks: Structure, Bonding, Reactivity, and Catalysis. *Chem. Rev.* **2020**, *120* (21), 11956−11985.
(349) Giannakakis, G.; Mitchell, S.; Pérez-Ramírez, J. Single-atom heterogeneous catalysts for sustainable organic synthesis. *Trends in Chemistry* **2022**, *4* (4), 264−276.
(350) Resasco, J.; Christopher, P. Atomically Dispersed Pt-group Catalysts: Reactivity, Uniformity, Structural Evolution, and Paths to Increased Functionality. *J. Phys. Chem. Lett.* **2020**, *11* (23), 10114−10123.
(351) Kaiser, S. K.; Chen, Z.; Faust Akl, D.; Mitchell, S.; Pérez-Ramírez, J. Single-Atom Catalysts across the Periodic Table. *Chem. Rev.* **2020**, *120* (21), 11703−11809.
(352) Finzel, J.; Sanroman Gutierrez, K. M.; Hoffman, A. S.; Resasco, J.; Christopher, P.; Bare, S. R. Limits of Detection for EXAFS Characterization of Heterogeneous Single-Atom Catalysts. *ACS Catal.* **2023**, *13* (9), 6462−6473.
(353) Li, X.; Yang, X.; Zhang, J.; Huang, Y.; Liu, B. In Situ/Operando Techniques for Characterization of Single-Atom Catalysts. *ACS Catal.* **2019**, *9* (3), 2521−2531.
(354) Tang, Y.; Haruta, N.; Kuzume, A.; Yamamoto, K. Development of Highly Sensitive Raman Spectroscopy for Subnano and Single-Atom Detection. *Molecules* **2021**, *26* (16), 5099.
(355) Robatjazi, H.; Battsengel, T.; Finzel, J.; Tieu, P.; Xu, M.; Hoffman, A. S.; Qi, J.; Bare, S. R.; Pan, X.; Chmelka, B. F.; Halas, N. J.; Christopher, P. Dynamic Behavior of Platinum Atoms and Clusters in the Native Oxide Layer of Aluminum Nanocrystals. *ACS Nano* **2024**, *18* (8), 6638−6649.
(356) Yu, J.; Chen, C.; Zhang, Q.; Lin, J.; Yang, X.; Gu, L.; Zhang, H.; Liu, Z.; Wang, Y.; Zhang, S.; Wang, X.; Guo, L. Au Atoms Anchored on Amorphous C3N4 for Single-Site Raman Enhancement. *J. Am. Chem. Soc.* **2022**, *144* (48), 21908−21915.
(357) Hannagan, R. T.; Giannakakis, G.; Flytzani-Stephanopoulos, M.; Sykes, E. C. H. Single-Atom Alloy Catalysis. *Chem. Rev.* **2020**, *120* (21), 12044−12088.
(358) Asokan, C.; DeRita, L.; Christopher, P. Using probe molecule FTIR spectroscopy to identify and characterize Pt-group metal based single atom catalysts. *Chinese Journal of Catalysis* **2017**, *38* (9), 1473−1480.
(359) Feng, R.; Miao, Q.; Zhang, X.; Cui, P.; Wang, C.; Feng, Y.; Gan, L.; Fu, J.; Wang, S.; Dai, Z.; Hu, L.; Luo, Y.; Sun, W.; Zhang, X.; Xiao, J.; Wu, J.; Zhou, B.; Zou, M.; He, D.; Zhou, X.; Han, X. Single-atom sites on perovskite chips for record-high sensitivity and quantification in SERS. *Science China Materials* **2022**, *65* (6), 1601−1614.

https://doi.org/10.1021/acsnano.4c06192
ACS Nano XXXX, XXX, XXX−XXX

(360) Joshi, P. B.; Wilson, A. J. Understanding electrocatalysis at nanoscale electrodes and single atoms with operando vibrational spectroscopy. *Current Opinion in Green and Sustainable Chemistry* **2022**, *38*, 100682.
(361) Zou, H.; Zhao, G.; Dai, H.; Dong, H.; Luo, W.; Wang, L.; Lu, Z.; Luo, Y.; Zhang, G.; Duan, L. Electronic Perturbation of Copper Single-Atom CO2 Reduction Catalysts in a Molecular Way. *Angew. Chem., Int. Ed.* **2023**, *62* (6), e202217220.
(362) Su, H.-S.; Chang, X.; Xu, B. Surface-enhanced vibrational spectroscopies in electrocatalysis: Fundamentals, challenges, and perspectives. *Chinese Journal of Catalysis* **2022**, *43* (11), 2757−2771.
(363) Nutt, M. O.; Hughes, J. B.; Wong, M. S. Designing Pd-on-Au Bimetallic Nanoparticle Catalysts for Trichloroethene Hydrodechlorination. *Environ. Sci. Technol.* **2005**, *39* (5), 1346−1353.
(364) Zhou, L. A.; Martirez, J. M. P.; Finzel, J.; Zhang, C.; Swearer, D. F.; Tian, S.; Robatjazi, H.; Lou, M. H.; Dong, L. L.; Henderson, L.; Christopher, P.; Carter, E. A.; Nordlander, P.; Halas, N. J. Light-driven methane dry reforming with single atomic site antenna-reactor plasmonic photocatalysts. *Nature Energy* **2020**, *5* (1), 61−70.
(365) Zhou, L. A.; Swearer, D. F.; Zhang, C.; Robatjazi, H.; Zhao, H. Q.; Henderson, L.; Dong, L. L.; Christopher, P.; Carter, E. A.; Nordlander, P.; Halas, N. J. Quantifying hot carrier and thermal contributions in plasmonic photocatalysis. *Science* **2018**, *362* (6410), 69.
(366) Lou, M. H.; Bayles, A.; Everitt, H. O.; Halas, N. J. Selective Photodetoxification of a Sulfur Mustard Simulant Using Plasmonic Aluminum Nanoparticles. *Nano Lett.* **2022**, *22* (18), 7699−7705.
(367) Yuan, Y. G.; Zhou, L. N.; Robatjazi, H.; Bao, J. L.; Zhou, J. Y.; Bayles, A.; Yuan, L.; Lou, M. H.; Lou, M. H.; Khatiwada, S.; Carter, E. A.; Nordlander, P.; Halas, N. J. Earth-abundant photocatalyst for H_2 generation from NH_3 with light-emitting diode illumination. *Science* **2022**, *378* (6622), 889−893.
(368) Swearer, D. F.; Zhao, H. Q.; Zhou, L. N.; Zhang, C.; Robatjazi, H.; Martirez, J. M. P.; Krauter, C. M.; Yazdi, S.; McClain, M. J.; Ringe, E.; Carter, E. A.; Nordlander, P.; Halas, N. J. Heterometallic antenna-reactor complexes for photocatalysis. *Proc. Natl. Acad. Sci. U.S.A.* **2016**, *113* (32), 8916−8920.
(369) Yuan, L.; Zhou, J. Y.; Zhang, M.; Wen, X. L.; Martirez, J. M. P.; Robatjazi, H.; Zhou, L. A.; Carter, E. A.; Nordlander, P.; Halas, N. J. Plasmonic Photocatalysis with Chemically and Spatially Specific Antenna-Dual Reactor Complexes. *ACS Nano* **2022**, *16* (10), 17365−17375.
(370) Lynch, P. G.; Das, A.; Alam, S.; Rich, C. C.; Frontiera, R. R. Mastering Femtosecond Stimulated Raman Spectroscopy: A Practical Guide. *Acs Physical Chemistry Au* **2024**, *4* (1), 1−18.
(371) Frontiera, R. R.; Yu, Z. W. Ostensible Steady-State Molecular Cooling with Plasmonic Gold Nanoparticles. *ACS Nano* **2023**, *17* (5), 4306−4314.
(372) Yuan, L.; Zhang, C.; Zhang, X.; Lou, M. H.; Ye, F.; Jacobson, C. R.; Dong, L. L.; Zhou, L. N.; Lou, M. H.; Cheng, Z. H.; Ajayan, P. M.; Nordlander, P.; Halas, N. J. Photocatalytic Hydrogenation of Graphene Using Pd Nanocones. *Nano Lett.* **2019**, *19* (7), 4413−4419.
(373) Robatjazi, H.; Weinberg, D.; Swearer, D. F.; Jacobson, C.; Zhang, M.; Tian, S.; Zhou, L. N.; Nordlander, P.; Halas, N. J. Metal-organic frameworks tailor the properties of aluminum nanocrystals. *Science Advances* **2019**, *5* (2), aav5340.
(374) Lou, M.; Bao, J. L.; Zhou, L.; Naidu, G. N.; Robatjazi, H.; Bayles, A. I.; Everitt, H. O.; Nordlander, P.; Carter, E. A.; Halas, N. J. Direct H2S Decomposition by Plasmonic Photocatalysis: Efficient Remediation plus Sustainable Hydrogen Production. *ACS Energy Letters* **2022**, *7* (10), 3666−3674.
(375) Schroeder, E.; Christopher, P. Chemical Production Using Light: Are Sustainable Photons Cheap Enough? *Acs Energy Letters* **2022**, *7* (2), 880−884.
(376) Zhang, Y.; Zhen, Y. R.; Neumann, O.; Day, J. K.; Nordlander, P.; Halas, N. J. Coherent anti-Stokes Raman scattering with single-molecule sensitivity using a plasmonic Fano resonance. *Nat. Commun.* **2014**, *5*, 4424.
(377) Zhou, L. N.; Lou, M. H.; Bao, J. L.; Zhang, C.; Liu, J. G.; Martirez, J. M. P.; Tian, S.; Yuan, L.; Swearer, D. F.; Robatjazi, H.; Carter, E. A.; Nordlander, P.; Halas, N. J. Hot carrier multiplication in plasmonic photocatalysis. *Proc. Natl. Acad. Sci. U.S.A.* **2021**, *118* (20), e2022109118.
(378) Peled, E.; Golodnitsky, D.; Ardel, G. Advanced Model for Solid Electrolyte Interphase Electrodes in Liquid and Polymer Electrolytes. *J. Electrochem. Soc.* **1997**, *144* (8), L208−L210.
(379) Villevieille, C. Interfaces and Interphases in Batteries: How to Identify and Monitor Them Properly Using Surface Sensitive Characterization Techniques. *Adv. Mater. Interfaces* **2022**, *9* (8), 2101865.
(380) Weiling, M.; Pfeiffer, F.; Baghernejad, M. Vibrational Spectroscopy Insight into the Electrodelelectrolyte Interface/Interphase in Lithium Batteries. *Adv. Energy Mater.* **2022**, *12*, 2202504.
(381) Li, H.; Mo, Y.; Pei, N.; Xu, X.; Huang, X.; Chen, L. Surface-Enhanced Raman Scattering Study on Passivating Films of Ag Electrodes in Lithium Batteries. *J. Phys. Chem. B* **2000**, *104* (35), 8477−8480.
(382) Li, G.; Li, H.; Mo, Y.; Chen, L.; Huang, X. Further identification to the SEI film on Ag electrode in lithium batteries by surface enhanced Raman scattering (SERS). *J. Power Sources* **2002**, *104* (2), 190−194.
(383) Mozhzhukhina, N.; Flores, E.; Lundstrom, R.; Nystrom, V.; Kitz, P. G.; Edstrom, K.; Berg, E. J. Direct Operando Observation of Double Layer Charging and Early Solid Electrolyte Interphase Formation in Li-Ion Battery Electrolytes. *J. Phys. Chem. Lett.* **2020**, *11* (10), 4119−4123.
(384) Gogoi, N.; Melin, T.; Berg, E. J. Elucidating the Step-Wise Solid Electrolyte Interphase Formation in Lithium-Ion Batteries with Operando Raman Spectroscopy. *Adv. Mater. Interfaces* **2022**, *9* (22), 2200945.
(385) Chen, D.; Mahmoud, M. A.; Wang, J.-H.; Waller, G. H.; Zhao, B.; Qu, C.; El-Sayed, M. A.; Liu, M. Operando Investigation into Dynamic Evolution of Cathode−Electrolyte Interfaces in a Li-Ion Battery. *Nano Lett.* **2019**, *19* (3), 2037−2043.
(386) Piernas-Muñoz, M. J.; Tornheim, A.; Trask, S.; Zhang, Z.; Bloom, I. Surface-enhanced Raman spectroscopy (SERS): a powerful technique to study the SEI layer in batteries. *Chem. Commun.* **2021**, *57* (18), 2253−2256.
(387) Yang, G.; Ivanov, I. N.; Ruther, R. E.; Sacci, R. L.; Subjakova, V.; Hallinan, D. T.; Nanda, J. Electrolyte Solvation Structure at Solid-Liquid Interface Probed by Nanogap Surface-Enhanced Raman Spectroscopy. *ACS Nano* **2018**, *12* (10), 10159−10170.
(388) Hy, S.; Felix; Chen, Y.-H.; Liu, J.-y.; Rick, J.; Hwang, B.-J. In situ surface enhanced Raman spectroscopic studies of solid electrolyte interphase formation in lithium ion battery electrodes. *J. Power Sources* **2014**, *256*, 324−328.
(389) Hy, S.; Felix, F.; Rick, J.; Su, W.-N.; Hwang, B. J. Direct In situ Observation of Li_2O Evolution on Li-Rich High-Capacity Cathode Material, $Li[Ni_xLi_{(1-2x)/3}Mn_{(2-x)/3}]O_2$ $(0 \le x \le 0.5)$. *J. Am. Chem. Soc.* **2014**, *136* (3), 999−1007.
(390) Cabo-Fernandez, L.; Bresser, D.; Braga, F.; Passerini, S.; Hardwick, L. J. In-Situ Electrochemical SHINERS Investigation of SEI Composition on Carbon-Coated $Zn_{0.9}Fe_{0.1}O$ Anode for Lithium-Ion Batteries. *Batteries & Supercaps* **2019**, *2* (2), 168−177.
(391) Galloway, T. A.; Cabo-Fernandez, L.; Aldous, I. M.; Braga, F.; Hardwick, L. J. Shell isolated nanoparticles for enhanced Raman spectroscopy studies in lithium−oxygen cells. *Farad. Discuss.* **2017**, *205* (0), 469−490.
(392) Li, C.-Y.; Yu, Y.; Wang, C.; Zhang, Y.; Zheng, S.-Y.; Li, J.-F.; Maglia, F.; Jung, R.; Tian, Z.-Q.; Shao-Horn, Y. Surface Changes of $LiNi_xMn_yCo_{1-x-y}O_2$ in Li-Ion Batteries Using in Situ Surface-Enhanced Raman Spectroscopy. *J. Phys. Chem. C* **2020**, *124* (7), 4024−4031.
(393) Gajan, A.; Lecourt, C.; Torres Bautista, B. E.; Fillaud, L.; Demeaux, J.; Lucas, I. T. Solid Electrolyte Interphase Instability in Operating Lithium-Ion Batteries Unraveled by Enhanced-Raman Spectroscopy. *ACS Energy Letters* **2021**, *6* (5), 1757−1763.
(394) Pfeiffer, F.; Diddens, D.; Weiling, M.; Baghernejad, M. Study of a High-Voltage NMC Interphase in the Presence of a Thiophene

https://doi.org/10.1021/acsnano.4c06192
ACS Nano XXXX, XXX, XXX−XXX

Additive Realized by Operando SHINERS. *ACS Appl. Mater. Interfaces* **2023**, *15* (5), 6676−6686.
(395) Pfeiffer, F.; Diddens, D.; Weiling, M.; Frankenstein, L.; Kühn, S.; Cekic-Laskovic, I.; Baghernejad, M. Quadrupled Cycle Life of High-Voltage Nickel-Rich Cathodes: Understanding the Effective Thiophene-Boronic Acid-Based CEI via Operando SHINERS. *Adv. Energy Mater.* **2023**, *13* (25), 2300827.
(396) Gu, Y.; You, E. M.; Lin, J. D.; Wang, J. H.; Luo, S. H.; Zhou, R. Y.; Zhang, C. J.; Yao, J. L.; Li, H. Y.; Li, G.; Wang, W. W.; Qiao, Y.; Yan, J. W.; Wu, D. Y.; Liu, G. K.; Zhang, L.; Li, J. F.; Xu, R.; Tian, Z. Q.; Cui, Y.; Mao, B. W. Resolving nanostructure and chemistry of solid-electrolyte interphase on lithium anodes by depth-sensitive plasmon-enhanced Raman spectroscopy. *Nat. Commun.* **2023**, *14* (1), 3536.
(397) Kleinman, S. L.; Sharma, B.; Blaber, M. G.; Henry, A.-I.; Valley, N.; Freeman, R. G.; Natan, M. J.; Schatz, G. C.; Van Duyne, R. P. Structure Enhancement Factor Relationships in Single Gold Nanoantennas by Surface-Enhanced Raman Excitation Spectroscopy. *J. Am. Chem. Soc.* **2013**, *135* (1), 301−308.
(398) Wang, L.; Menakath, A.; Han, F.; Wang, Y.; Zavalij, P. Y.; Gaskell, K. J.; Borodin, O.; Iuga, D.; Brown, S. P.; Wang, C.; Xu, K.; Eichhorn, B. W. Identifying the components of the solid-electrolyte interphase in Li-ion batteries. *Nature Chem.* **2019**, *11* (9), 789−796.
(399) Freunberger, S. A.; Chen, Y.; Peng, Z.; Griffin, J. M.; Hardwick, L. J.; Bardé, F.; Novák, P.; Bruce, P. G. *J. Am. Chem. Soc.* **2011**, *133*, 8040−7.
(400) Lux, S. F.; Lucas, I. T.; Pollak, E.; Passerini, S.; Winter, M.; Kostecki, R. The mechanism of HF formation in LiPF6 based organic carbonate electrolytes. *Electrochem. Commun.* **2012**, *14* (1), 47−50.
(401) Lux, S. F.; Lucas, I. T.; Chevalier, J. S.; Richardson, T. J.; Kostecki, R. M. Time-Dependent Determination of HF Formation in $LiPF_6$ -Containing Electrolytes in Different Cell Types by Spectroscopic Ellipsometry. *ECS Trans.* **2013**, *50* (1), 27−30.
(402) Chen, T.; Wu, J.; Zhang, Q.; Su, X. Recent advancement of SiO_x based anodes for lithium-ion batteries. *J. Power Sources* **2017**, *363*, 126−144.
(403) Yamanaka, T.; Nakagawa, H.; Tsubouchi, S.; Domi, Y.; Doi, T.; Abe, T.; Ogumi, Z. In situ diagnosis of the electrolyte solution in a laminate lithium ion battery by using ultrafine multi-probe Raman spectroscopy. *J. Power Sources* **2017**, *359*, 435−440.
(404) Miele, E.; Dose, W. M.; Manyakin, I.; Frosz, M. H.; Ruff, Z.; De Volder, M. F. L.; Grey, C. P.; Baumberg, J. J.; Euser, T. G. Hollow-core optical fibre sensors for operando Raman spectroscopy investigation of Li-ion battery liquid electrolytes. *Nat. Commun.* **2022**, *13* (1), 1651.
(405) Martin-Yerga, D.; Milan, D. C.; Xu, X.; Fernandez-Vidal, J.; Whalley, L.; Cowan, A. J.; Hardwick, L. J.; Unwin, P. R. Dynamics of Solid-Electrolyte Interphase Formation on Silicon Electrodes Revealed by Combinatorial Electrochemical Screening. *Angew. Chem.* **2022**, *61* (34), e202207184.
(406) Goodenough, J. B.; Park, K. S. The Li-ion rechargeable battery: a perspective. *J. Am. Chem. Soc.* **2013**, *135* (4), 1167−76.
(407) Peled, E.; Golodnitsky, D.; Ardel, G. Advanced Model for Solid Electrolyte Interphase Electrodes in Liquid and Polymer Electrolytes. *J. Electrochem. Soc.* **1997**, *144*, L208.
(408) Yu, X.; Manthiram, A. *Energy Environ. Sci.* **2018**, *11*, 527.
(409) Wang, N.; Zhao, L.; Liu, C.; Zhang, J.; He, Y.; Yang, H.; Liu, X. Chiral Detection of Glucose: An Amino Acid-Assisted Surface-Enhanced Raman Scattering Strategy Showing Opposite Enantiomeric Effects on SERS Signals. *Anal. Chem.* **2022**, *94* (42), 14565−14572.
(410) Liu, Z.; Ai, J.; Kumar, P.; You, E.; Zhou, X.; Liu, X.; Tian, Z.; Bouř, P.; Duan, Y.; Han, L.; Kotov, N. A.; Ding, S.; Che, S. Enantiomeric Discrimination by Surface-Enhanced Raman Scattering−Chiral Anisotropy of Chiral Nanostructured Gold Films. *Angew. Chem., Int. Ed.* **2020**, *59* (35), 15226−15231.
(411) Arabi, M.; Ostovan, A.; Wang, Y.; Mei, R.; Fu, L.; Li, J.; Wang, X.; Chen, L. Chiral molecular imprinting-based SERS detection strategy for absolute enantiomeric discrimination. *Nat. Commun.* **2022**, *13* (1), 5757.
(412) Guselnikova, O.; Elashnikov, R.; Svorcik, V.; Kartau, M.; Gilroy, C.; Gadegaard, N.; Kadodwala, M.; Karimullah, A. S.; Lyutakov, O. Coupling of plasmonic hot spots with shurikens for superchiral SERS-based enantiomer recognition. *Nanoscale Horizons* **2023**, *8* (4), 499−508.
(413) Wu, F.; Li, F.; Tian, Y.; Lv, X.; Luan, X.; Xu, G.; Niu, W. Surface Topographical Engineering of Chiral Au Nanocrystals with Chiral Hot Spots for Plasmon-Enhanced Chiral Discrimination. *Nano Lett.* **2023**, *23* (17), 8233−8240.
(414) Han, B.; He, X.-H.; Liu, Y.-Q.; He, G.; Peng, C.; Li, J.-L. Asymmetric organocatalysis: an enabling technology for medicinal chemistry. *Chem. Soc. Rev.* **2021**, *50* (3), 1522−1586.
(415) Inoue, Y. Asymmetric photochemical reactions in solution. *Chem. Rev.* **1992**, *92* (5), 741−770.
(416) Jain, V.; Kashyap, R. K.; Pillai, P. P. Plasmonic Photocatalysis: Activating Chemical Bonds through Light and Plasmon. *Advanced Optical Materials* **2022**, *10* (15), 2200463.
(417) Kuhn, W.; Braun, E. Photochemische Erzeugung optisch aktiver Stoffe. *Naturwissenschaften* **1929**, *17* (14), 227−228.
(418) Yao, W.; Bazan-Bergamino, E. A.; Ngai, M. Y. Asymmetric Photocatalysis Enabled by Chiral Organocatalysts. *ChemCatChem.* **2022**, *14* (1), e202101292.
(419) Genzink, M. J.; Kidd, J. B.; Swords, W. B.; Yoon, T. P. Chiral Photocatalyst Structures in Asymmetric Photochemical Synthesis. *Chem. Rev.* **2022**, *122* (2), 1654−1716.
(420) Ávalos-Ovando, O.; Santiago, E. Y.; Movsesyan, A.; Kong, X.-T.; Yu, P.; Besteiro, L. V.; Khorashad, L. K.; Okamoto, H.; Slocik, J. M.; Correa-Duarte, M. A.; Comesaña-Hermo, M.; Liedl, T.; Wang, Z.; Markovich, G.; Burger, S.; Govorov, A. O. Chiral Bioinspired Plasmonics: A Paradigm Shift for Optical Activity and Photochemistry. *ACS Photonics* **2022**, *9* (7), 2219−2236.
(421) Wang, Z.; Cheng, F.; Winsor, T.; Liu, Y. Optical chiral metamaterials: a review of the fundamentals, fabrication methods and applications. *Nanotechnology* **2016**, *27* (41), 412001.
(422) Ishida, T.; Isawa, A.; Kuroki, S.; Kameoka, Y.; Tatsuma, T. All-plasmonic-metal chiral nanostructures fabricated by circularly polarized light. *Appl. Phys. Lett.* **2023**, *123* (6), No. 061111.
(423) Lee, S.; Fan, C.; Movsesyan, A.; Bürger, J.; Wendisch, F. J.; De S Menezes, L.; Maier, S. A.; Ren, H.; Liedl, T.; Besteiro, L. V.; Govorov, A. O.; Cortés, E. Unraveling the Chirality Transfer from Circularly Polarized Light to Single Plasmonic Nanoparticles. *Angew. Chem., Int. Ed.* **2024**, *63*, e202319920.
(424) Kim, J.-Y.; McGlothin, C.; Cha, M.; Pfaffenberger, Z. J.; Turali Emre, E. S.; Choi, W.; Kim, S.; Biteen, J. S.; Kotov, N. A. Direct-write 3D printing of plasmonic nanohelicoids by circularly polarized light. *Proc. Natl. Acad. Sci. U. S. A.* **2024**, *121* (11), e2312082121.
(425) Negrín-Montecelo, Y.; Movsesyan, A.; Gao, J.; Burger, S.; Wang, Z. M.; Nlate, S.; Pouget, E.; Oda, R.; Comesaña-Hermo, M.; Govorov, A. O.; Correa-Duarte, M. A. Chiral Generation of Hot Carriers for Polarization-Sensitive Plasmonic Photocatalysis. *J. Am. Chem. Soc.* **2022**, *144* (4), 1663−1671.
(426) Pedrueza-Villalmanzo, E.; Pineider, F.; Dmitriev, A. Perspective: plasmon antennas for nanoscale chiral chemistry. *Nanophotonics* **2020**, *9* (2), 481−489.
(427) Bainova, P.; Joly, J.-P.; Urbanova, M.; Votkina, D.; Erzina, M.; Vokata, B.; Trelin, A.; Fitl, P.; Audran, G.; Vanthuyne, N.; Vinklarek, J.; Svorcik, V.; Postnikov, P.; Marque, S. R. A.; Lyutakov, O. Plasmon-Assisted Chemistry Using Chiral Gold Helicoids: Toward Asymmetric Organic Catalysis. *ACS Catal.* **2023**, *13* (19), 12859−12867.
(428) Tang, Y.; Cohen, A. E. Enhanced Enantioselectivity in Excitation of Chiral Molecules by Superchiral Light. *Science* **2011**, *332* (6027), 333−336.
(429) Zhao, Y.; Saleh, A. A. E.; Dionne, J. A. Enantioselective Optical Trapping of Chiral Nanoparticles with Plasmonic Tweezers. *ACS Photonics* **2016**, *3* (3), 304−309.
(430) Solomon, M. L.; Saleh, A. A. E.; Poulikakos, L. V.; Abendroth, J. M.; Tadesse, L. F.; Dionne, J. A. Nanophotonic Platforms for Chiral Sensing and Separation. *Acc. Chem. Res.* **2020**, *53* (3), 588−598.
(431) Niinomi, H.; Sugiyama, T.; Cheng, A.-C.; Tagawa, M.; Ujihara, T.; Yoshikawa, H. Y.; Kawamura, R.; Nozawa, J.; Okada, J. T.; Uda, S. Chiral Optical Force Generated by a Superchiral Near-Field of a

https://doi.org/10.1021/acsnano.4c06192
ACS Nano XXXX, XXX, XXX−XXX

Plasmonic Triangle Trimer as Origin of Giant Bias in Chiral Nucleation: A Simulation Study. *J. Phys. Chem. C* **2021**, *125* (11), 6209−6221.

(432) Wei, X.; Liu, J.; Xia, G.-J.; Deng, J.; Sun, P.; Chruma, J. J.; Wu, W.; Yang, C.; Wang, Y.-G.; Huang, Z. Enantioselective photoinduced cyclodimerization of a prochiral anthracene derivative adsorbed on helical metal nanostructures. *Nature Chem.* **2020**, *12* (6), 551−559.

(433) Niinomi, H.; Sugiyama, T.; Tagawa, M.; Murayama, K.; Harada, S.; Ujihara, T. Enantioselective amplification on circularly polarized laser-induced chiral nucleation from a NaClO < sub > 3</sub> solution containing Ag nanoparticles. *CrystEngComm* **2016**, *18* (39), 7441−7448.

(434) Naaman, R.; Paltiel, Y.; Waldeck, D. H. Chiral molecules and the electron spin. *Nature Reviews Chemistry* **2019**, *3* (4), 250−260.

(435) Bhowmick, D. K.; Das, T. K.; Santra, K.; Mondal, A. K.; Tassinari, F.; Schwarz, R.; Diesendruck, C. E.; Naaman, R. Spin-induced asymmetry reaction—The formation of asymmetric carbon by electropolymerization. *Science Advances* **2022**, *8* (32), eabq2727.

https://doi.org/10.1021/acsnano.4c06192
ACS Nano XXXX, XXX, XXX−XXX